CHARACTERIZATION OF KIZILCAHAMAM GEOTHERMAL FIELD BY
TRACER TESTING

A THESIS SUBMITTED TO
THE GRADUATE SCHOOL OF NATURAL AND APPLIED SCIENCES
OF
MIDDLE EAST TECHNICAL UNIVERSITY

BY

TEVFİK KAYA

IN PARTIAL FULFILLMENT OF THE REQUIREMENT
FOR
THE DEGREE OF MASTER OF SCIENCE
IN
PETROLEUM AND NATURAL GAS ENGINEERING

SEPTEMBER 2005

Approval of Graduate School of Natural and Applied Sciences

_____

Prof. Dr. Canan Özgen
Director

I certify that this thesis satisfies all the requirements as a thesis for the degree of Master Science

_____

Prof. Dr. Birol Demiral
Head of Department

This is to certify that we have read this thesis and that in our opinion it is fully adequate, in scope and quality, as a thesis for the degree of Master of Science

_____   _____
Prof. Dr. Mahmut Parlaktuna   Assoc. Prof. Dr. Serhat Akın
        Co-Supervisor   Supervisor

Examining Committee Members

Prof. Dr. Şakir Şimşek   (HACETTEPE U-GEOE)   _____

Assoc. Prof. Dr. Serhat Akın   (METU-PETE)   _____

Prof. Dr. Mahmut Parlaktuna   (METU-PETE)   _____

Prof. Dr. Birol Demiral   (METU-PETE)   _____

Prof. Dr. Nilgün Güleç   (METU-GEOE)   _____

I hereby declare that all information in this document has been obtained and presented in accordance with academic rules and ethical conduct. I also declare that, as required by these rules and conduct, I have fully cited and referenced all material and results that are not original to this work.

Name, Last name : Tevfik Kaya

Signature :

ABSTRACT

CHARACTERIZATION OF KIZILCAHAMAM GEOTHERMAL FIELD BY
TRACER TESTING

Tevfik Kaya

M.S, Petroleum and Natural Gas Engineering Department

Supervisor   : Assoc. Prof. Dr. Serhat Akın

Co-Supervisor : Prof. Dr. Mahmut Parlaktuna

September 2005, 107 Pages

Kızılcahamam Geothermal Field which is 70 km far from Ankara, has been utilized for Geothermal District Heating System, 25 MWt, 2500 residences capacity, greenhouses heating, thermal facilities since 1994. The average production rate is $350m^3/h$ during the heating season , $150m^3/h$ during the summer season for hot water and yearly average reinjection rate is $114m^3/h$ from the field. The long term projections has been studied concerning on expected pressure decline by matching 10 years field history data which contain dynamic level and temperature data. The pressure decline is 140 kPa in the field between 1999 and 2005 with the existing reinjection rate, if the existing rates do not change, the additional pressure decline which is 120 kPa will be occurred up to 2011.

In order to get more information from the field, the fluorescein as tracer has been injected in to the MTA-1, and the samples were collected from the MTA-2, Fethi Bey, IHL-1 and IHL-3 for 3 months. The fluorescein concentration has been detected by using fluorimeter, and tracer concentration time plots were analyzed.

The fluoreiscein was detected in short breakthrough time in MTA-2 and Fethi Bey which are close to reinjection well, breakthrough time is longer in IHL-1 and IHL-3. The interpretation of tracer test shows that there is communication between all wells.

Tracer concentration time plots were compared with different mathematical models, the best match was obtained with multi-fractured model. These results show that Kızılcahamam field is not homogeneous field. It is expected that increasing the reinjection rate will decrease the pressure decline in the field.

Key Words; Kızılcahamam Geothermal Field, Geothermal Reservoir, Tracer Test

ÖZ

KIZILCAHAMAM JEOTERMAL SAHASININ TRACER TESTLE KARAKTERİZASYONU

Tevfik Kaya

Yüksek Lisans, Petrol ve Doğal Gaz Mühendisliği Bölümü

Tez Yöneticisi: Doç.Dr. Serhat Akın

Ortak Tez Yöneticisi: Prof. Dr. Mahmut Parlaktuna

Eylül 2005, 107 sayfa

Kızılcahamam Jeotermal Sahası Ankara'ya 70 km uzaklıkta olup, 25   MWt,   2500 konut jeotermal merkezi ısıtma, sera ısıtması, termal tesis ısıtması ve termalizm amaçlı olarak 1994 yılından beri işletilmektedir. Jeotermal saha özellikle konut ısıtılmasının yapıldığı kış aylarında 350 m^3/saat, yaz aylarında 150 m^3/saat ortalama debide çalıştırılmaktadır. Ortalama reenjeksiyon miktarı 114 m^3/saattir. Sahanın bilinen sıcaklık ve dinamik seviye değerlerini içeren 10 yıllık geçmiş tarihçesinin eğri çakıştırılması sonrasında, sahanın beklenen basınç düşüm tahminleri uzun dönemli olarak hesaplanmıştır. Halihazırdaki yapılan reinjeksiyon (geri basım) ile 1999 yılından 2005 yılına kadar jeotermal sahada 141 kPa basınç düşmesi olduğu ve mevcut durum değişmediği takdirde 2011 yılına kadar sahada tahmini olarak 120 kPa ilave basınç düşümü olacağı hesaplanmıştır.

Sahayı daha iyi tanıyabilmek için geribasım kuyusu olarak kullanılan MTA-1 kuyusundan izleyici (tracer) olarak fluorescein basımı yapılmış ve MTA-2, Fethi Bey, İHL-1 ve İHL-3 kuyularından 3 ay boyunca numuneler alınmıştır. Fluorimetre cihazı kullanılarak alınan numunelerdeki fluorescein derişimleri tespit edilerek derişim-zaman eğrileri elde edilmiştir. Geribasım kuyusunun yakınında bulunan

MTA-2 ve FethiBey kuyularına fluorescein çok kısa sürede ulaşmakta, ancak İHL-1 ve İHL-3 kuyularına ise belirli bir zaman sonrasında ulaşmaktadır. Yapılan tracer tesleri sonunda sahada bulunan tüm kuyular arasında bir etkileşim olduğunu göstermektedir.

Derişim-zaman verileri çeşitli matematiksel modellerle karşılaştırılmış ve her iki testte de çoklu çatlak modelinin en iyi çakışmayı sağladığı görülmüştür. Sonuç olarak sahanın homojen olmadığı görülmüştür. Üretilen suyun yeterli miktarının geri basımının basınç düşümünü azaltacağı anlaşılmaktadır.

Anahtar kelimeler: Kızılcahamam Jeotermal Sahası, Jeotermal Rezervuar, Tracer (İzleme) testi

ACKNOWLEDGMENTS

TABLE OF CONTENTS

LIST OF TABLES

LIST OF FIGURES

xiv

NOMENCLACTURE

h   = effective dispersion coefficient

μ = dissolver viscosity.

A = area (m^2)

b   = block size (m)

C =concentration (ppb)

C_{exp}= experimental concentration(ppb)

C_r = observed concentration (ppb)

C_t = total concentration (ppb)

D   = dispersion coefficient

 D_z =axial diffusion constant

D_z= axial dispersivity

e   = flow coefficient

a_f = rate of tracer interchange per unit fracture volume

I1 = Bessel's function of the 1st kind of order 1

J   = model parameter

L= distance between the wells (m)

a_m = rate of tracer interchange per unit matrix volume.

M =mass of the tracer chemical (kg)

a_m = rate of tracer interchange per unit matrix volume (l/s)

$n_{e:}$ =ϕ_f = porosity

n_f= α_f= fracture porosity

n_m = α_m = matrix porosity

p = Laplace transform parameter.

P_{bh}= Bottom Hole Pressure (kPa)

P_e = Peclet number

P_{wh}=Well head pressure (kPa)

Q =flow rate (l/s)

R_d =dimensionless dissolving factor,

t = time, space variable (hour)

t_b = response start time (hour)

T_{bh}=Bottom hole temperature (^{o}C)

t_f = matrix block fill up time (hour)

$t_{p,}$ = peek concentration time (hour)

t_r = mean arrival time (hour)

T_{wh} = Well head temperature(^{o}C)

u   = velocity (m/h)

w   = ratio of transport into the fractures to transport out of the fractures

CHAPTER 1

INTRODUCTION

Heat is a form of energy and geothermal energy is, literally, the heat contained within the Earth that generates geological phenomena on a planetary scale. The term 'Geothermal energy' is often used nowadays, however, to indicate that part of the Earth's heat that can, or could, be recovered and exploited by man, and it is in this sense that we will use the term from now on [1].

Three major types of geothermal energy systems are hot igneous, conduction-dominated, and hydrothermal systems. Although the first two systems may contain the largest amount of useful heat energy, the development of these systems requires advancements in extraction technologies in order to use the stored heat commercially. Therefore, hydrothermal energy systems are of prime concern at the present time.

Electricity generation is the most important form of utilization of high-temperature geothermal resources (> 150 °C). The medium-to-low temperature resources (< 150 °C) are suited to many different types of application specially district heating. Twenty-four countries generate power from geothermal resources with the total installed capacity of 8900 MW_e [2]. On the other hand, seventy-one countries report direct utilization of geothermal energy with an estimate of the installed thermal power for direct-use at the end of 2004 is 27,825 MW_t. The thermal energy used for direct-use is 261,418 TJ/year (72,622 GWh/yr). The distribution of thermal energy used by category is approximately 33% for geothermal heat pumps, 29% for bathing and swimming (including balneology), 20% for space heating (of which 77% is for district heating), 7.5% for greenhouse and open ground heating, 4% for industrial process heat, 4% for aquaculture pond and raceway heating, <1% for agricultural drying, <1% for snow melting and cooling, and <0.5% for other uses in 2005 [3].

In Turkey, more than 170 geothermal fields which can be useful at the economic scale and about 1500 hot and mineral water resources which have the temperatures ranged from 20-242 °C (spring discharge and reservoir temperature), have been determined. These manifestations are located mainly along the major grabens at the Western Anatolia, along the Northern Anatolian Fault Zone, Central and Eastern Anatolia volcanic regions. As a result of the geological, geophysical, geochemical surveys and the drillings carried out by General Directorate of Mineral Research and Exploration (MTA), the temperatures and the flow rates of thermal resources in geothermal fields have been increased very seriously.

The installed heat capacity is 1077 MW_t for direct-use and 20.4 MW_e for power production in Turkey with total production of 104.6 GWh/yr. A liquid carbon dioxide and dry ice production factory is integrated to the Kızıldere power plant with a 40000 tons/year capacity.

Most of the development is achieved in geothermal direct-use applications by 1077 MW_t. 750 MW_t (which equals to the heat requirement of 65000 residences equivalence[i]) of this potential is being utilized for geothermal heating including district heating, thermal tourism facilities heating and 635000 m^2 geothermal greenhouses heating. The remaining 327 MW_t of this potential is being utilized for balneological purposes (There exists 195 thermal facilities in Turkey).

The operational capacities of the city based geothermal district heating systems (GDHS) existing in Turkey are as the following: Gönen (Commissioned: 1987, 3400 residences, ~ 80 °C), Simav (1991, 3200 residences, ~120 °C), Kırşehir (1994, 1800 residences, ~57 °C), Kızılcahamam (1995, 2500 residences, ~ 80 °C), İzmir (1996, 10.000 residences, ~ 115 °C), Sandıklı (1998, 1600 residences, ~ 70 °C), Afyon (1996, 4000 residences, ~ 95 °C), Kozaklı (1996, 1000 residences, ~ 90 °C), İzmir-Narlıdere (1998, 1075 residences, ~ 98 °C), Diyadin (1999, 400 residences, ~70 °C), Salihli (2002, 3000 residences, ~94 °C), Edremit (2003, 1500 residences, ~60 °C), Sarıköy (2002, 1500 residences, ~130 °C) . Today, 40-45 °C temperature geothermal waters are being used for space heating in Turkey without heat-pump. [4]

The Kızılcahamam Geothermal Field is 70 km far from Ankara. The geothermal fluid produced with an average temperature of 70–80 °C, and a portion of it is reinjected with an average temperature of 42°C. The cumulative production is 21,435,470 m^3 between January 1995 and August 2005 (3865 day), the cumulative reinjection is 6,719,440 m^3 between December 1998 and August 2005 (2435 day). The average production rate is 231 m^3/h (64 l/s) and the average reinjection rate is 114 m^3/h (31 l/s) in Kızılcaham Geothermal Field. The geothermal water has been used in Başkent University Thermal Hotel, Asya Thermal Resorts, Ab-ı Hayat, District Heating and Hot Water Supply facilities which consists of 2500 residences and Municipality Hotels.

16 wells have been drilled in this field for thermal and mineral water. The geothermal district heating system which has been in operation since 1995 with a capacity of 2500 residences (20 MW$_t$) is fed by 6 production wells (MTA-2, Fethi Bey, IHL-1, IHL-2, IHL-3, KHD-1) and one re-injection well (MTA-1).

The main concern for Kızılcahamam Geothermal District Heating System (GDHS) is the depletion of reservoir pressure as a result of higher production rate and the use of GDHS effluent after heat exchanger in the thermal facilities instead of reinjection. More reinjection of wastewater to underground seems the best solution to solve the problems of pressure depletion.

Reinjection schemes must be engineered carefully because of the danger of early fluid and/or thermal breakthrough of injected fluid. Reservoir characterization and modeling studies are the effective tools to describe the flow of energy and fluid in porous media.

It is aimed in this study to utilize these tools to understand the behavior of Kızılcahamam Geothermal Field with the help of existing production data, and tracer test.

*One residence equivalence is assumed to be 100 m^2 floor area.

CHAPTER 2

GEOTHERMAL ENERGY

Dickson and Fanelli [1] define geothermal energy in the broadest sense as the heat contained within the Earth that generates geological phenomena on a planetary scale. However, the term 'Geothermal energy' is often used nowadays, to indicate that part of the Earth's heat that can, or could, be recovered and exploited by man.

The increase in temperature with depth in the Earth's crust is defined as geothermal gradient. The average geothermal gradient is about 2.5-3 °C/100 m down to the depths accessible by drilling with modern technology, i.e. over 10,000 m. For example, if the temperature within the first few meters below ground-level, which on average corresponds to the mean annual temperature of the external air, is 15 °C, then we can reasonably assume that the temperature will be about 65°-75 °C at 2000 m depth, 90°-105 °C at 3000 m and so on for a further few thousand meters. There are, however, in some 'geothermal areas' the gradient which is more than ten times the average value of 2.5-3 °C/100 m.

The difference in temperature between deep hotter zones and shallow colder zones generates a conductive flow of heat from the former towards the latter, with a tendency to create uniform conditions, although, as often happens with natural phenomena, this situation is never actually attained. The mean terrestrial heat flow of continents and oceans is 65 and 101 mWm^{-2}, respectively, which, when areally weighted, yield a global mean of 87 mWm^{-2} [1]. These values are based on 24,774 measurements at 20,201 sites covering about 62% of the Earth's surface.

Our planet consists of a *crust*, which reaches a thickness of about 20-65 km in continental areas and about 5-6 km in oceanic areas, a mantle, which is roughly 2900 km thick, and a core, about 3470 km in radius (Figure 2.1).

4
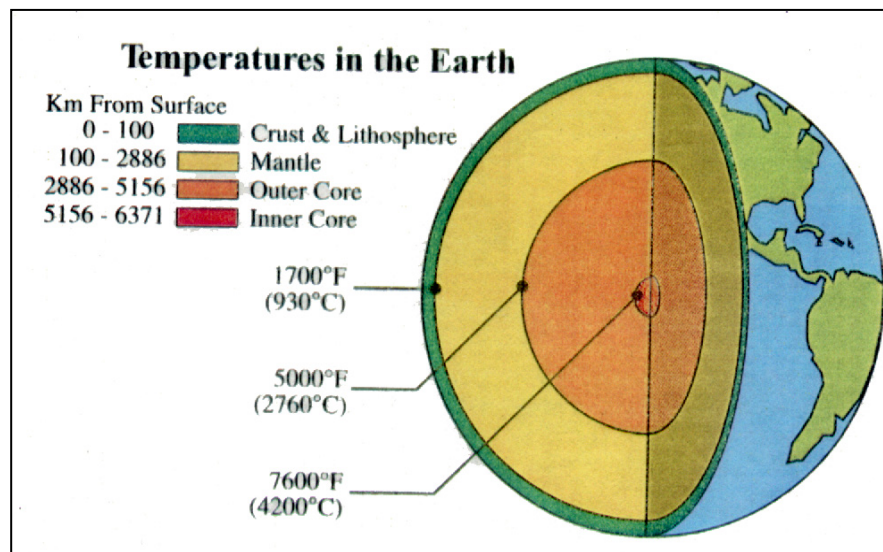
Figure 2.1 Planet Earth depth and temperature [1]

The physical and chemical characteristics of the crust, mantle and core vary from the surface of the Earth to its centre. The outermost shell of the Earth, known as the lithosphere, is made up of the crust and the upper layer of the mantle. Ranging in thickness from less than 80 km in oceanic zones to over 200 km in continental areas, the lithosphere behaves as a rigid body. Below the lithosphere is the zone known as the asthenosphere, 200-300 km in thickness, and of 'less rigid' or 'more plastic' behavior. In zones where the lithosphere is thinner, and especially in oceanic areas, the lithosphere is pushed upwards and broken by the very hot, partly molten material ascending from the asthenosphere, in correspondence to the ascending branch of convective cells. It is this mechanism that created and still creates the spreading ridges that extend for more than 60,000 km beneath the oceans, emerging in some places (Azores, Iceland) and even creeping between continents, as in the Red Sea. A relatively tiny fraction of the molten rocks upwelling from the asthenosphere emerges from the crests of these ridges and, in contact with the seawater, solidifies to form a new oceanic crust. Most of the material rising from the asthenosphere, however, divides into two branches that flow in opposite directions beneath the lithosphere. The continual generation of new crust and the pull of these two branches

5

in opposite directions have caused the ocean beds on either side of the ridges to drift apart at a rate of a few centimeters per year. Consequently, the area of the ocean beds (the oceanic lithosphere) tends to increase. The ridges are cut perpendicularly by enormous fractures, in some cases a few thousand kilometers in length, called transform faults.

These phenomena lead to a simple observation: since there is apparently no increase in the Earth's surface with time, the formation of new lithosphere along the ridges and the spreading of the ocean beds must be accompanied by a comparable shrinkage of the lithosphere in other parts of the globe. This is indeed what happens in subduction zones, the largest of which are indicated by huge ocean trenches, such as those extending along the western margin of the Pacific Ocean and the western coast of South America. In the subduction zones the lithosphere folds downwards, plunges under the adjacent lithosphere and re-descends to the very hot deep zones, where it is "digested" by the mantle and the cycle begins all over again. Part of the lithospheric material returns to a molten state and may rise to the surface again through fractures in the crust. As a consequence, magmatic arcs with numerous volcanoes are formed parallel to the trenches, on the opposite side to that of the ridges. Where the trenches are located in the ocean, as in the Western Pacific, these magmatic arcs consist of chains of volcanic islands; where the trenches run along the margins of continents the arcs consist of chains of mountains with numerous volcanoes, such as the Andes. Figure 2.2. illustrates the phenomena that was just described.
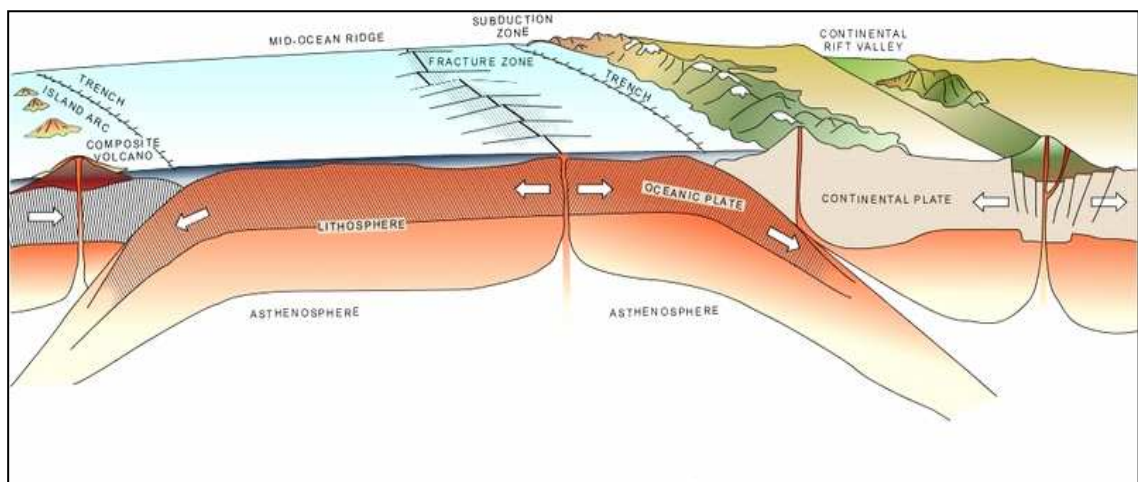
Figure 2.2 Schematic cross-section showing plate tectonic processes [1]

6

Spreading ridges, transform faults and subduction zones form a vast network that divides our planet into six immense and several other smaller lithospheric areas or plates (Figure 2.3). Because of the huge tensions generated by the Earth's thermal engine and the asymmetry of the zones producing and consuming lithospheric material, these plates drift slowly up against one another, shifting position continually.

The margins of the plates correspond to weak, densely fractured zones of the crust, characterized by an intense seismicity, by a large number of volcanoes and, because of the ascent of very hot materials towards the surface, by a high terrestrial heat flow. As shown in Figure 2.3, the most important geothermal areas are located around plate margins.
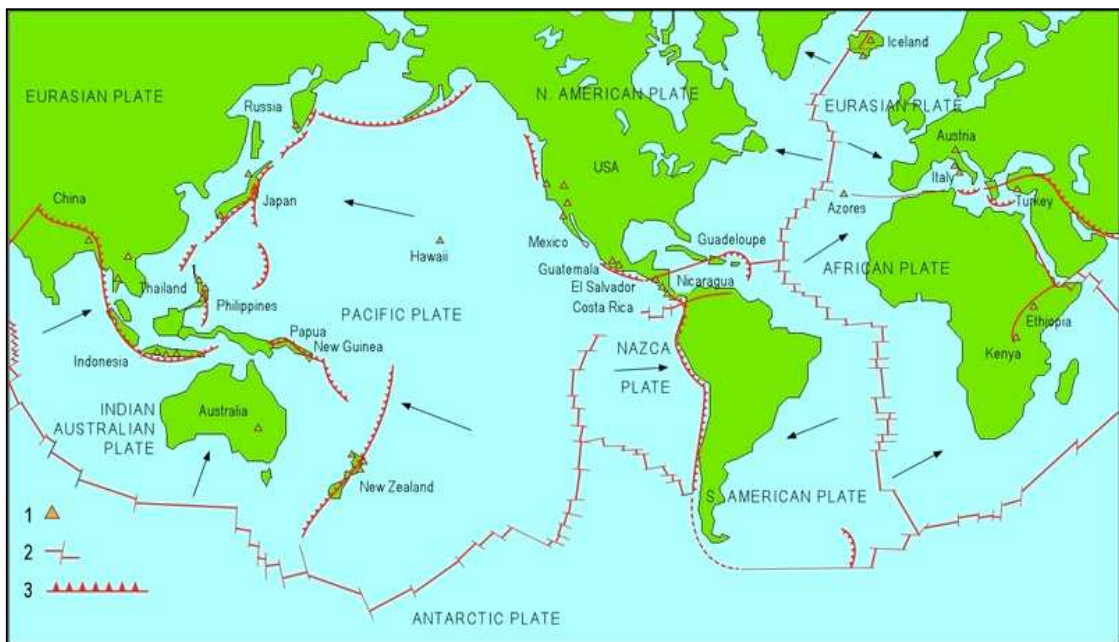
Figure 2.3 World pattern of plates, oceanic ridges, oceanic trenches, subduction zones, and geothermal fields [1]

(Arrows show the direction of movement of the plates towards the subduction zones. (1) Geothermal fields producing electricity; (2) mid-oceanic ridges crossed by transform faults (long transversal fractures); (3) subduction zones, where the subducting plate bends downwards and melts in the asthenosphere).

2.1. Geothermal Systems

Geothermal systems can therefore be found in regions with a normal or slightly above normal geothermal gradient, and especially in regions around plate margins where the geothermal gradients may be significantly higher than the average value. What is a geothermal system and what happens in such a system? It can be described schematically as convecting water in the upper crust of the Earth. A geothermal system is made up of three main elements: *a heat source*, *a reservoir* and *a fluid*, which is the carrier that transfers the heat. The heat source can be either a very high temperature (> 600 °C) magmatic intrusion that has reached relatively shallow depths (5-10 km) or, as in certain low-temperature systems, the Earth's normal temperature, which, as it was explained earlier, increases with depth. The reservoir is a volume of hot permeable rocks from which the circulating fluids extract heat. The reservoir is generally overlain by a cover of impermeable rocks and connected to a recharge area through which the meteoric waters can replace or partly replace the fluids that escape from the reservoir through springs or are extracted by boreholes.

The geothermal fluid is water, in the majority of cases meteoric water, in the liquid or vapor phase, depending on its temperature and pressure. This water often carries with it chemicals and gases such as CO_2, H_2S, etc. Figure 2.4 is a greatly simplified representation of an ideal geothermal system.

The mechanism underlying geothermal systems is by and large governed by fluid convection. Figure 2.5 describes schematically the mechanism in the case of an intermediate-temperature hydrothermal system. Convection occurs because of the heating and consequent thermal expansion of fluids in a gravity field; heat, which is supplied at the base of the circulation system, is the energy that drives the system. Heated fluid of lower density tends to rise and to be replaced by colder fluid of high density, coming from the margins of the system. Convection, by its nature, tends to increase temperatures in the upper part of a system as temperatures in the lower part decrease. Geothermal systems also occur in nature in a variety of combinations of geological, physical and chemical characteristics, thus giving rise to several different types of system.
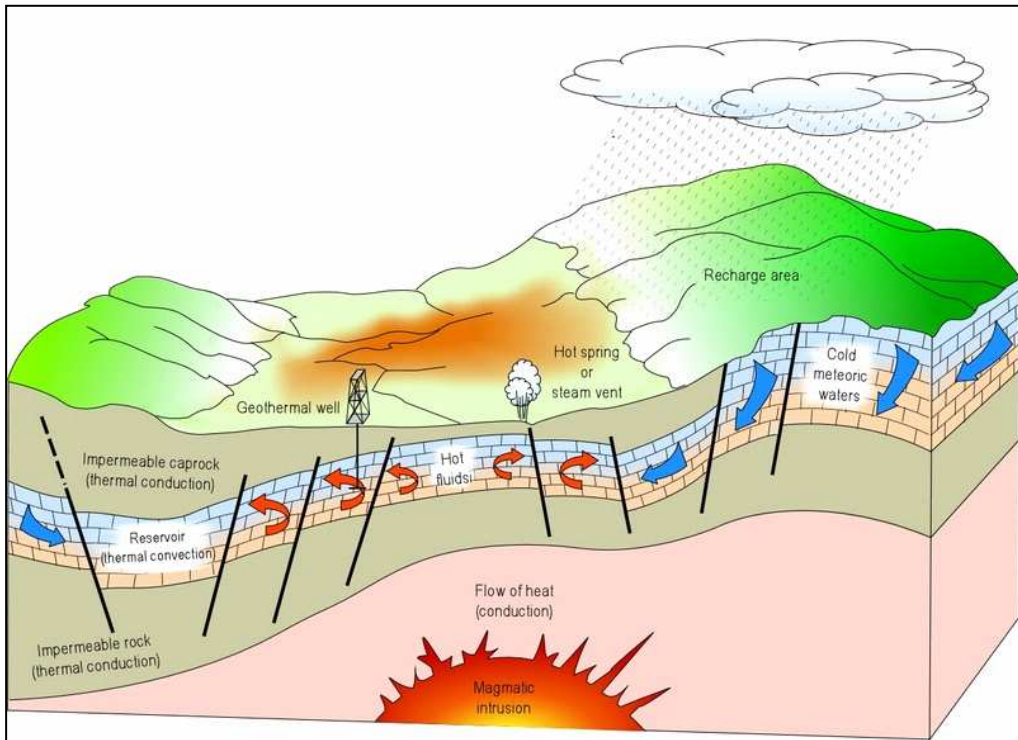
Figure 2.4 Schematic representation of an ideal geothermal system [1]
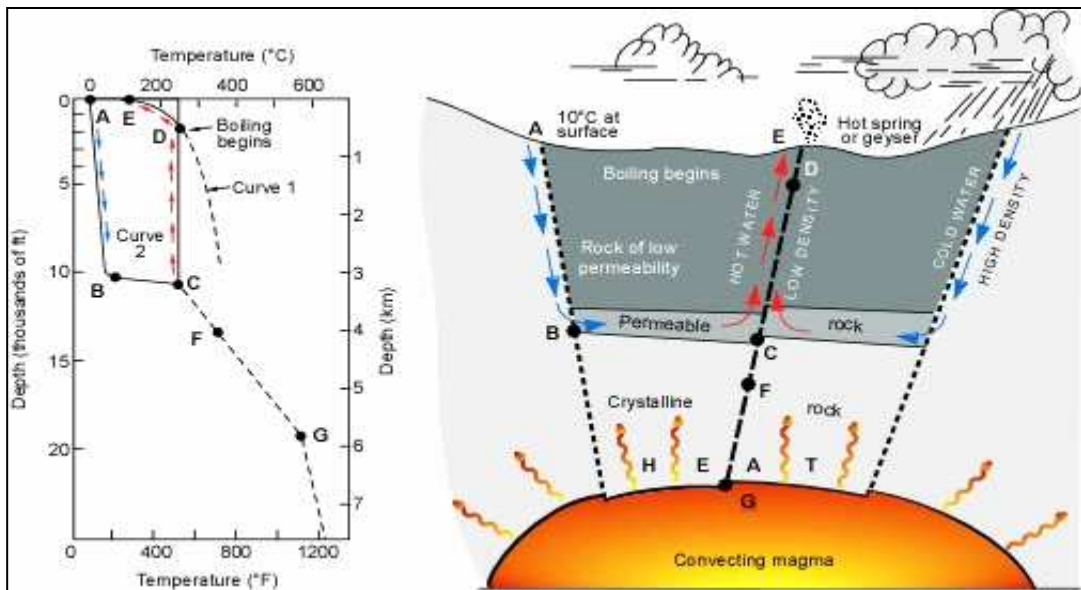
Figure 2.5 Model of a geothermal system. [1]
(Curve 1 is the reference curve for the boiling point of pure water. Curve 2 shows the temperature profile along a typical circulation route from recharge at point A to discharge at point E)

Of all the elements of a geothermal system, the heat source is the only one that needs to be natural. Providing conditions are favorable, the other two elements could be

9

'artificial'. For example, the geothermal fluids extracted from the reservoir to drive the turbine in a geothermal power-plant could, after their utilization, be injected back into the reservoir through specific injection wells. In this way the natural recharge of the reservoir is integrated by an artificial recharge. For many years now re-injection has also been adopted in various parts of the world as a means of drastically reducing the impact on the environment of geothermal plant operations.

Artificial recharge through injection wells can also help to replenish and maintain 'old' or 'exhausted' geothermal fields. For example, in The Geysers field in California, USA, one of the biggest geothermal fields in the world, production began to decline dramatically at the end of the 1980s because of a lack of fluids. The first project of this type, the Southeast Geysers Effluent Recycling Project, was launched in 1997, to transport treated wastewater for 48 km to the geothermal field. This project has led to the reactivation of a number of power plants that had been abandoned because of a lack of fluids.

In the so-called Hot Dry Rock (HDR) projects, which were experimented for the first time at Los Alamos, New Mexico, USA, in 1970, both the fluid and the reservoir are artificial. High-pressure water is pumped through a specially drilled well into a deep body of hot, compact rock, causing its hydraulic fracturing. The water permeates these artificial fractures, extracting heat from the surrounding rock, which acts as a natural reservoir. This 'reservoir' is later penetrated by a second well, which is used to extract the heated water. The system therefore consists of (i) the borehole used for hydraulic fracturing, through which cold water is injected into (ii) the artificial reservoir, and (iii) the borehole used to extract the hot water. The entire system, complete with surface utilization plant, could form a closed loop [5].

The Los Alamos project was the forerunner for other similar projects in Australia, France, Germany, Japan and the UK. The European HDR project has been implemented over a number of phases, including the drilling of two wells, one of which has reached bottom-hole at 5060 m. Very promising results have been obtained from their geophysical surveys and hydraulic tests, and the European Project seems, for the moment, to be the most successful.

In the framework of the one of HDR project is Soultz project (France), the recent drilling of the wells (GPK2, GPK3, GPK4) at 5 km depth, where the bottom hole temperature reaches 200°C, allows to revisit the deep-seated geology of the granite reservoir. The deep geology of the reservoir was studied from cutting observation and well logging data (spectral gamma-ray, caliper, drilling parameters). By using a fine resolution image log, the Ultrasonic Borehole Imager, the fracture network was evaluated in terms of fracture density and orientation between 1500 to 5100 m depth [6].

2.2 Utilization of Geothermal Resources

Type of utilization of geothermal energy mainly depends on the fluid temperature. The classical Lindal diagram [7], which shows the possible uses of geothermal fluids at different temperatures, still holds valid (Table 2.1), derived from the original Lindal diagram, with the addition of electricity generation from binary cycles.

Electricity generation is the most important form of utilization of high-temperature geothermal resources (> 150 °C). The medium-to-low temperature resources (< 150 °C) are suited to many different types of application specially district heating. Table 2.2 lists the countries with their installed geothermal generating capacities for the years 1995, 2000 and 2005 [2].

Fluids at temperatures below 20 °C are rarely used and in very particular conditions or in heat pump applications. The Lindal diagram emphasizes two important aspects of the utilization of geothermal resources [7]: (a) with cascading and combined uses it is possible to enhance the feasibility of geothermal projects and (b) the resource temperature may limit the possible uses.

Table 2.1 Approximate temperature requirements of geothermal fluids for various applications [7]

	Temperature (°C)	Application	
SATURATED STEAM	200		CONVENTIONAL ELECTRIC GENERATION
	190		
	180	Evaporation of highly concentrated solutions Refrigeration by ammonia absorption Digestion in paper pulp (Kraft)	
	170	Heavy water via hydrogen sulphide process Drying of diatomaceous earth	
	160	Drying of fish meal Drying of timber	
	150	Alumina via Bayer's process	
	140	Drying farm products at high rates Canning of food	
	130	Evaporation in sugar refining Extraction of salts by evaporation and crystallization Fresh water by distillation	BINARY FLUID ELECTRIC GENERATION
	120	Most multi-effect evaporation. Concentration of saline solution	
HOT WATER	110	Drying and curing of light aggregate cement slabs	
	100	Drying of organic materials, seaweeds, grass, vegetables etc. Washing and drying of wool	
	90	Drying of stock fish Intense de-icing operations	
	80	Space-heating (buildings and greenhouses)	
	70	Refrigeration (lower temperature limit)	
	60	Animal husbandry Greenhouses by combined space and hotbed heating	
	50	Mushroom growing Balneology	HEAT PUMP APPLICATIONS
	40	Soil Warming	
	30	Swimming pools, biodegradation, fermentations Warm water for year-round mining in cold climates De-icing	
	20	Hatching of fish. Fish farm	

Existing designs for thermal processes can, however, be modified for geothermal fluid utilization in certain cases, thus widening its field of application.

Table 2.2 Installed geothermal generating capacities world-wide from 1995, 2000, 2005 [2]

Country	Installed capacity [MW]			Increase [MW]	Increase (%)
	1995	2000	2005	2005-2000	
Australia	0.2	0.2	0.2	0	Stable
Austria	0	0	1	1	New Entry
China	29	29	28	-1	Stable
Costa Rica	55	143	163	20	14
El Salvador	105	161	151	-10	Stable
Ethiopia	0	7	7	0	Stable
France	4	4	15	11	275
Germany	0	0	0.2	0.2	New Entry
Guatemala	0	33	33	0	Stable
Iceland	50	170	202	2	19
Indonesia	310	590	797	207	35
Italy	632	785	790	5	1
Japan	414	547	535	-12	Stable
Kenya	45	45	127	82	182
Mexico	753	755	953	198	16
New Zealand	286	437	435	-2	Stable
Nicaragua	35	70	77	7	10
Papua New Guinea	0	0	6	6	New Entry
Philippines	1227	1909	1931	22	1
Portugal	5	16	16	0	Stable
Russia	11	23	79	56	244
Thailand	.3	.3	.3	0	Stable
Turkey	20	20	20	0	Stable
USA	2817	2228	2544	316	3
TOTAL	**6 797**	**7 947**	**8 912**	**938**	**12**

Direct heat use is one of the oldest, most versatile and also the most common form of utilization of geothermal energy. Bathing, space and district heating, agricultural applications, aquaculture and some industrial uses are the best known forms of utilization, but heat pumps are the most. There are many other types of utilization, on a much smaller scale, some of which are unusual. Geothermal (ground-source) heat pumps have the largest energy use and installed capacity, accounting for 33.2% and

56.5% of the word-wide use and capacity. The installed capacity is 15,723 MWt and the annual energy use is 86,673 TJ/yr with a capacity factor of 0.17 (in the heating mode) [3].

As regards non-electric applications of geothermal energy, Table 2.3 and Figure 2.6 gives the installed capacity (27,825 MW_t) and energy use (261,418 TJ/yr) world-wide for the years 1995 and 2005 [3]. During that year 71 countries reported direct

Table 2.3 Summary of the various worldwide direct-use categories, 1995-2005 [3]

	Capacity,MW_t			UtilizationTJ/yr			Capacity Factor		
	2005	2000	1995	2005	2000	1995	2005	2000	1995
Geothermal heat pumps	15723	5275	1854	86673	23275	14617	0.17	0.14	0.25
Space heating	4158	3263	2579	52868	42926	38230	0.40	0.42	0.47
Greenhouse heating	1348	1246	1085	19607	17864	15742	0.46	0.45	0.46
Aquaculture pond heating	616	605	1097	10969	11733	13493	0.56	0.61	0.39
Agricultural drying	157	74	67	2013	1038	1124	0.41	0.44	0.53
Industrial uses	489	474	544	11068	10220	1012	0.72	0.68	0.59
Bathing and swimming	4911	3957	1085	75289	79546	15742	0.49	0.64	0.46
Cooling snow melting	338	114	115	1885	1063	1124	0.18	0.30	0.31
Others	86	137	238	1045	3034	2249	0.39	0.70	0.30
Total	**27825**	**15145**	**8664**	**261418**	**190699**	**112441**	**0.30**	**0.40**	**0.41**
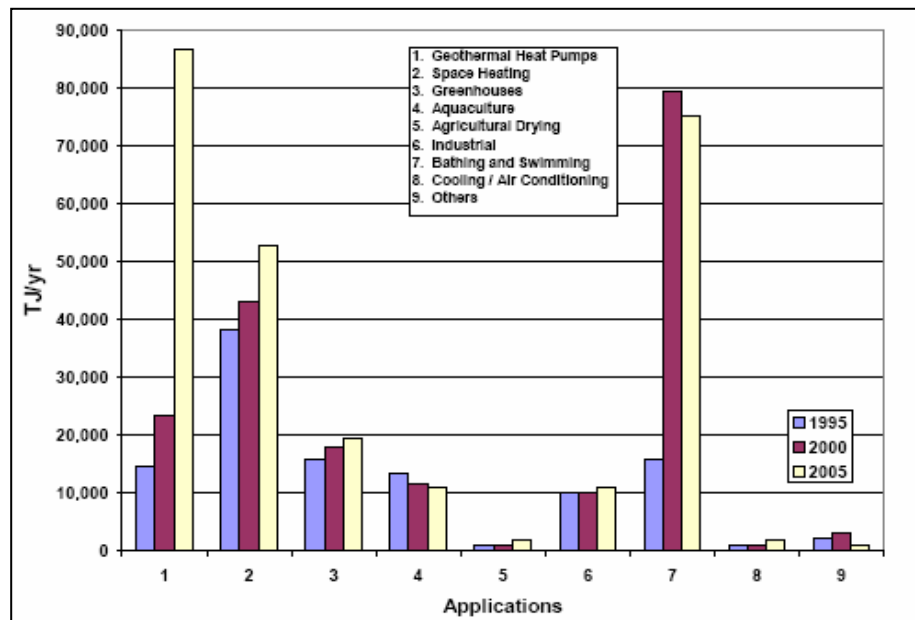
Figure 2.6 Comparison of worldwide energy use in TJ/yr for 1995, 2000 and 2005 [3]

14

uses, compared to 58 in 2000, 28 in 1995 and 24 in 1985. The number of countries with direct uses has very likely increased since then, as well as the total installed capacity and energy use.

The most common non-electric use world-wide (installed capacity) is heat pumps (33%),followed by bathing (29%), space-heating (20%), greenhouses (7.50%), aquaculture (4%), industrial processes (4%) and 2,5 % for other uses in 2005 [3].

Non-electric uses of geothermal energy in the world (2005): installed thermal power 27.824.8 MW$_t$ and energy use 261.418.0 TJ/yr [3]. Table 2.4 lists the countries with their non-electrical use of geothermal energy for the year 2005.

Table 2.4 Non-electric applications of geothermal energy [3]

Country	Capacity MWt	Use TJ/yr	Use GWh/yr	Capacity Factor
Albania	9.6	8.5	2.4	0.03
Algeria	152.3	2417.0	671.4	0.50
Argemina	149.9	609.1	169.2	0.13
Armenia	1.0	15.0	4.2	0.48
Australia	109.5	2968.0	824.5	0.86
Austria	352.0	352.0	2.229.9	0.20
Belarus	1.0	13.3	3.7	0.42
Belgium	63.9	431.2	119.8	0.21
Brazil	360.1	6622.4	1839.7	0.58
Bulgaria	109.6	1671.5	464.3	0.48
Canada	461.0	2546.0	707.3	0.18
Canbbean Islanda	0.1	2.8	0.8	0.89
Chile	8.7	131.1	36.4	0.48
China	3.687.0	45.373.0	12.604.6	0.39
Columbia	14.4	287.0	79.7	0.63
Costa Rica	1.0	21.0	5.8	0.67
Croatia	114.0	681.7	189.4	0.19
Czech Republic	204.5	1220.0	338.9	0.19
Denmark	821.2	4.360.0	1.211.2	0.17
Ecuador	5.2	102.4	28.4	0.62
Egypt	1.0	15.0	4.2	0.48
Ethiopia	1.0	15.0	4.2	0.48
Finland	260.0	1.950.0	541.7	0.24
France	308.0	5.195.7	1.443.4	0.53
Georgia	250.0	6.307.0	1.752.1	0.80
Germany	504.6	2.909.8	808.3	0.18

Table 2.4 Continued

Greece	74.8	567.2	157.6	0.24
Guatemala	2.1	52.5	14.6	0.79
Hondiuras	0.7	17.0	4.7	0.77
Hungary	694.2	7.939.8	2.205.7	0.36
Iceland	1.791.0	23.813.0	6.615.3	0.42
India	203.0	1.606.3	446.2	0.25
Indonesia	2.3	42.6	11.8	0.59
Iran	30.1	752.3	209.0	0.79
Ireland	20.0	104.1	28.9	0.17
Isreal	82.4	2.193.0	609.2	0.84
Italy	606.6	7554.0	2098.5	0.39
Japan	413.4	5161.1	1433.8	0.40
Jordan	153.3	1.540.0	427.8	0.32
Kenya	10.0	79.1	22.0	0.25
Korea(South)	16.9	175.2	48.7	0.33
Lithuania	21.3	458.0	127.2	0.68
Macedonia	62.3	598.6	166.3	0.30
Mexico	164.7	1.931.8	536.7	0.37
Mongolia	6.8	213.2	59.2	0.99
Nepal	2.1	51.4	14.3	0.78
Netherlands	253.5	685.0	190.3	0.09
New Zealand	308.1	7086.0	1968.5	0.73
Norway	450.0	2.314.0	642.8	0.16
Papua New Guinea	0.1	1.0	0.3	0.32
Peru	2.4	49.0	13.6	0.65
Philippines	3.3	39.5	11.0	0.38
Poland	170.9	838.3	232.9	0.16
Portugal	30.6	385.3	107.0	0.40
Romania	145.1	2.841.0	789.2	0.62
Russia	308.2	6.143.5	1.706.7	0.63
Serbia	88.8	2.375.0	659.8	0.85
Slovak Republic	187.7	3.034.0	842.8	0.51
Slovenia	48.6	712.5	197.9	0.46
Spain	22.3	347.2	96.5	0.49
Sweden	3840.0	36000.0	10000.8	0.30
Switzerland	581.6	4229.3	1174.9	0.23
Thailand	1.7	28.7	8.0	0.54
Tunisia	25.4	219.1	60.9	0.27
Turkey	1077.0	19.623.1	5.451.3	0.53
Ukraine	10.9	118.8	33.0	0.35
United Kinedom	10.2	45.6	12.7	0.14
United States	7817.4	31239.0	8678.2	0.13
Venezuela	0.7	14.0	3.9	0.63
Vietnam	30.7	80.5	22.4	0.08
Yemen	1.0	15.0	4.2	0.48
GRAND TOTAL	**27824.8**	**261418.0**	**72621.9**	**0.30**

Geothermal district heating systems are capital intensive. The main costs are initial investment costs for production and injection wells, down-hole and transmission pumps, pipelines and distribution networks, monitoring and control equipment, peaking stations and storage tanks. Operating expenses, however, are comparatively lower than in conventional systems and consist of pumping power, system maintenance, control and management. A crucial factor in estimating the initial cost of the system is the thermal load density or the heat demand divided by the ground area of the district. A high heat density determines the economic feasibility of a district heating project since the distribution network is expensive. Some economic benefit can be achieved by combining heating and cooling in areas where the climate permits. The load factor in a system with combined heating and cooling would be higher than the factor for heating alone and the unit energy price would consequently improve [9].

Geothermal space conditioning (heating and cooling) has expanded considerably since the 1980s following on the introduction and widespread use of heat pumps. The various systems of heat pumps available permit us to economically extract and utilize the heat content of low-temperature bodies such as the ground and shallow aquifers. ponds etc. [10] (see for example Figure 2.7).
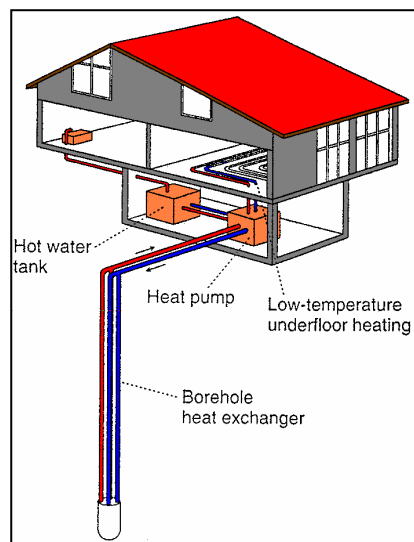
Figure 2.7 Typical application of ground-coupled heat pump system [10]

As engineers already know, heat pumps are machines that move heat in a direction opposite to that in which it would tend to go naturally i.e. from a cold space or body to a warmer one. A heat pump is effectively nothing more than a refrigeration unit [11]. Any refrigeration device (window air conditioner, refrigerator, freezer, etc.) moves heat from a space (to keep it cool) and discharges that heat at higher temperatures. The only difference between a heat pump and a refrigeration unit is the desired effect, cooling for the refrigeration unit and heating for the heat pump. A second distinguishing factor of many heat pumps is that they are reversible and can provide either heating or cooling in the space. Ground-coupled and ground-water heat pump systems have now been installed in great numbers in at least 32 countries. Geothermal (ground-source) heat pumps have the largest energy use and installed capacity, accounting for 33.2% and 56.5% of the word-wide use and capacity respectively. The installed capacity is 15,723 MWt and the annual energy use is 86,673 TJ/yr with a capacity factor of 0.17 (in the heating mode). Almost all of the installations occur in North American and Europe, increasing from 26 countries in 2000 to 2005. 32 countries. The equivalent number of installed 12-kWt units (typical of US and western European homes) is approximately 1.3 million over double the number of units reported for 2000 [3].The agricultural applications of geothermal fluids consist of open-field agriculture and greenhouse heating. Thermal water can be used in open-field agriculture to irrigate and/or heat the soil. The main advantages of temperature control in open-field agriculture are: (a) it prevents any damage ensuing from low environmental temperatures, (b) it extends the growing season, increases plant growth and boosts production and (c) it sterilises the soil [12].

The most common application of geothermal energy in agriculture is, however, in greenhouse heating which has been developed on a large scale in many countries. The cultivation of vegetables and flowers out-of-season or in an unnatural climate can now draw on a widely experimented technology. Various solutions are available for achieving optimum growth conditions based on the optimum growth temperature of each plant (Figure 2.8). Exploitation of geothermal heat in greenhouse heating can considerably reduce their operating costs which in some cases account for 35% of the product costs (vegetables, flowers, house-plants and tree seedlings).
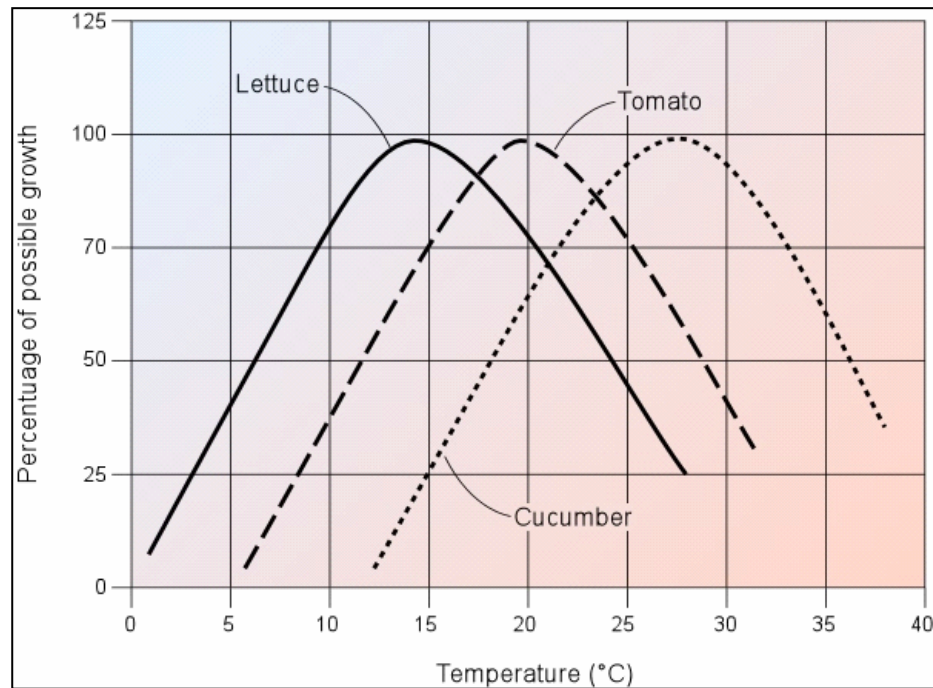
Figure 2.8 Growth curves for some crops [14]

Farm animals and aquatic species as well as vegetables and plants can benefit in quality and quantity from optimum conditioning of their environmental temperature. In many cases geothermal waters could be used profitably in a combination of animal husbandry and geothermal greenhouses. The energy required to heat a breeding installation is about 50% of that required for a greenhouse of the same surface area so cascade utilization could be adopted. Breeding in a temperature-controlled environment improves animal health and the hot fluids can also be utilized to clean, sanitize and dry the animal shelters and waste products [12]. Aquaculture, which is the controlled breeding of aquatic forms of life, is gaining world-wide importance nowadays due to an increasing market demand. Control of the breeding temperatures for aquatic species is of much greater importance than for land species as can be seen in Figure 2.9, which shows that the growth curve trend of aquatic species is very different from that of land species. By maintaining an optimum temperature artificially we can breed more exotic species improve production and even in some cases double the reproductive cycle [12].

19
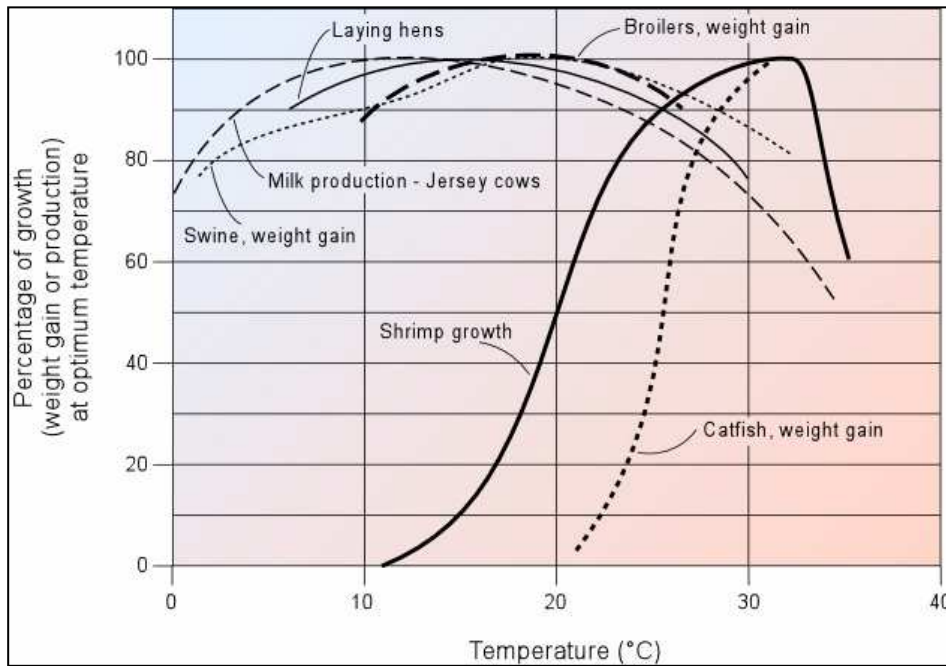
Figure 2.9 Effect of temperature on growth or production of food animals [14]

The species that are typically raised are carp, catfish, bass, tilapia, mullet, eels, salmon, sturgeon, shrimp, lobster, crayfish, crabs, oysters, clams, scallop, mussels and abalone.

The entire temperature range of geothermal fluids whether steam or water can be exploited in industrial applications as shown in the Lindal diagram (Table 2.1). The different possible forms of utilization include process heating, evaporation, drying, distillation, sterilization, washing, de-icing, and salt extraction. This is a category that has applications in 15 countries in 2005, down from 19 in 2000, where the installations tend to be large and energy consumption high. Examples include: concrete curing (Guatemala and Slovenia), bottling of water and carbonated drinks (Bulgaria, Serbia and the United States), milk pasteurization (Romania), leather industry (Slovenia and Serbia), chemical extraction (Bulgaria, Russia and Poland), CO_2 extraction (Iceland and Turkey), mushroom growing and laundry use (Mexico and the United States), salt extraction and diatomaceous earth drying (Iceland), pulp and paper processing (New Zealand), iodine and salt extraction (Vietnam), borate

and boric acid production (Italy) and timber (New Zealand, Romania. and Mexico). A zinc extraction plant in the Imperial Valley of southern California in the United States did start operation but was shut down about a short period due to economic and technical problems. The use of geothermal energy has increased slightly since 2000, with an installed capacity of 489 MWt and 11,068 TJ of energy used annually, with the highest capacity factor of all uses of 0.72 [3].

One of the main usage of thermal water is Bathing and Swimming. Almost every country has spas and resorts with swimming pools (including balneology) but many allow the water to flow continuously regardless of use (Figure 2.6). As a result, the actual use and capacity figures may be high. In some cases, where use was reported, no flows and temperature drops were known, thus a figure of 0.35 MWt and 7.0 TJ/yr were applied to estimate the capacity and energy use for a typical installation. In addition to the 59 countries (up from 48 in 2000) that reported bathing and swimming use, there are known developments in Malaysia, Mozambique, South Africa and Zambia, but no information was available from these countries. The installed capacity has increased 24% over the past five years.

CHAPTER 3

GEOTHERMAL ENERGY IN TURKEY

Turkey is located on the Alpine-Himalayan orogenic belt, which have high geothermal potential. The first geothermal researches and investigations in Turkey started by MTA in 1960's. MTA discovered 170 geothermal fields where 95% of them are low-medium enthalpy fields and suitable mostly for direct-use applications. In addition about 1500 hot and mineralized natural springs and wells exist in Turkey. Figure 3.1 shows the locations of those 170 geothermal fields which can be useful at the economic scale and about 1500 hot and mineral water resources which have the temperatures ranged from 20-242 °C (spring discharge and reservoir temperature) [4]. These manifestations are located mainly along the major grabens at the Western Anatolia, along the Northern Anatolian Fault Zone, Central and Eastern Anatolia volcanic regions.

Figure 3.1 Main neotectonic lines and hot spring distribution of Turkey [4]

With the existing springs (600 MW$_t$) and geothermal wells (2693 MW$_t$), the proven geothermal capacity calculated by MTA is 3293 MW$_t$ (discharge temperature is assumed to be 35 °C). The geothermal potential, on the other hand, is estimated as 31,500 MW$_t$ [14]. The distributions of proven geothermal potential according to the geographic regions are given at Figure 3.2.

The installed heat capacity is 1077 MW$_t$ for direct-use and 20.4 MW$_e$ for power production in Turkey with total production of 104.6 GWh/yr. A liquid carbon dioxide and dry ice production factory is integrated to the Kızıldere power plant with a 40000 tons/year capacity.

The total number of wells drilled today for geothermal energy is about 700 of which 500 are exploration and production wells and 200 gradient wells. The deepest well is 2398 m. Most of these wells have been drilled by MTA and financed by the Governorships, Municipalities and their companies, which constitutes 66.2 % and followed by MTA with 16.5 % and Private with 11.7 % [15]. In order to utilize the geothermal energy potential of Turkey, the number of wells drilled should be increased.
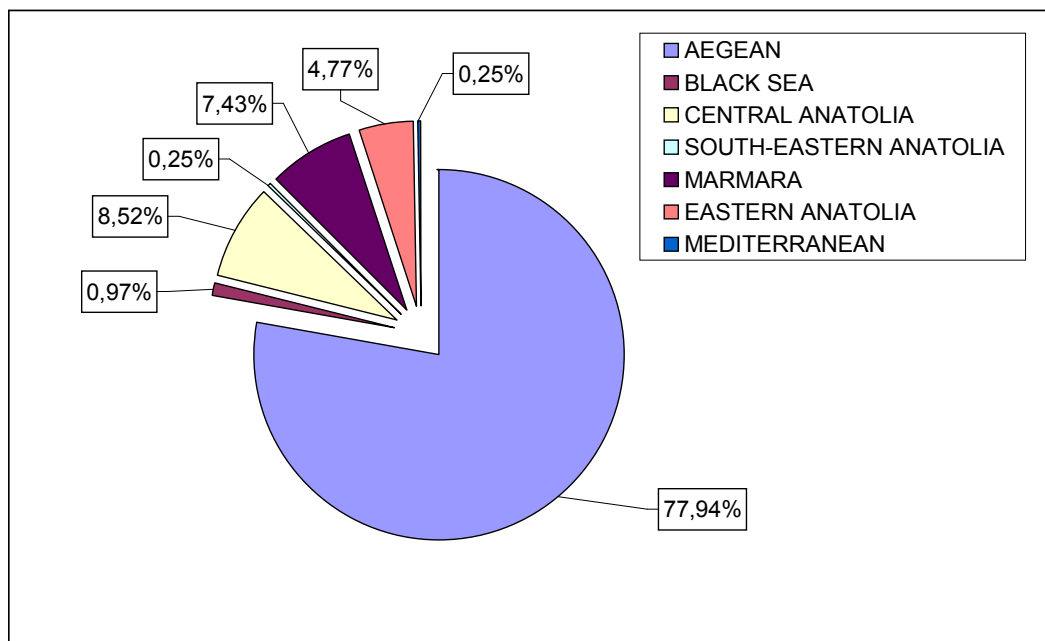
Figure 3.2 Proven geothermal potentials of regions in Turkey [4]

On the other hand, studies on Hot Dry Rock (HDR) systems which develop at zones included high temperature formations at shallow depths are continued very successfully. If the studies on the management of these systems will be economic, the geothermal potential of Turkey will grow up rapidly. From this point of view, especially in Central Anatolia the region of Acigol and the young volcanic fields of Eastern Anatolia are the positive fields.

Most of the development in Turkey is achieved in geothermal direct-use applications with 65,000 residences equivalence using geothermal heating (750 MW_t) including district heating, thermal facilities and 635,000 m^2 geothermal greenhouse heating. Geothermal water is being used in nearly 195 spas for balneological purposes (327 MW_t). Engineering design of over 300,000 residences equivalence of geothermal district heating has been completed. By summing up all these geothermal utilizations, the geothermal direct use installed capacity is 1077 MW_t in Turkey in October 2004.

The electricity generation has been increased from 90 GWh to 108 GWh in Kızıldere geothermal power plant which is the only existing geothermal power plant of Turkey. Besides electricity generation at Kızıldere, the separated CO_2 from the steam in the condenser is partly supplied to the liquefied CO_2 and dry ice factory installed next to the plant and about 120,000 t/year dry ice and liquefied CO_2 is produced for Turkey's beverage industry.

The estimated geothermal heating potential of Turkey is 31,500 MWt (5 million residences equivalence geothermal heating) [14]. According to today's technical and economical conditions, the total geothermal heating potential is 1 million residences equivalency [15].

3.1 Geothermal District Heating Systems

Today 13 cities are heated partially with geothermal in Turkey. These geothermal district heating systems have been constructed since 1987 and many developments have been achieved in technical and economical aspects. The rapid development of geothermal district heating systems in Turkey is mostly depending on [17];

- construction of suitable geothermal district heating systems according to Turkey's conditions,

24

- participation of the consumers to the GDHS investments by about 50-60% without any direct financing refund, called "Turkish Financing System"

- geothermal heating is about 50-70 % cheaper than natural gas heating.

The existing geothermal district heating systems including Dokuz Eylül University Campus heating are given in Table 3.1.

Table 3.1. The existing geothermal district heating systems in Turkey [17]

Name	Residences	Start-up date	Geoth. Water T. (°C)	Investor
Dokuz Eylül University.Campus	1500	1983	115-60	Rectorship of Univ.
Gönen	3400	1987	80	*
Simav	3200	1991	137	Municipality
Kırşehir	1800	1994	57	**.
Kızılcahamam	2500	1995	80	*.
Balçova	12500	1996	137	******
Afyon	4500	1996	95	**
Kozaklı	1000	1996	90	**
Narlıdere	1500	1998	125	***
Sandıklı	3200/5000	1998	70	*
Diyadin	400	1999	70	****
Salihli	3000/24000	2002	94	Municipality
Sarayköy	1500/5000	2002	140	*
Edremit	500/7500	2003	60	*****

 * Joint Stock Company (JSC), shares mainly belong to Municipality,
 ** JSC, shares belong mainly to Governorship (some shares belong to Municipality)
 *** Limited Company (LC), Governorship mainly holds the shares,
 **** JSC, main share holder is Governorship,
 ***** LC, shares mainly belong to Municipality,
 ****** LC, Governorship mainly holds the shares.

Some other low temperature geothermal thermal facilities heating are as follows:

- Afyon-Oruçoğlu Thermal Facilities, 48 °C

- Bolu-Karacasu Thermal Facilities, 44 °C

- Rize-Ayder Curing Center, 55 °C

- Hatay-Kumlu Thermal Facilities, floor heating with 37 °C

- Samsun-Havza Thermal Facilities, 54 °C

- Çankırı-Çavundur Thermal Facilities, 54 °C

Also, a mosque in the town of Haymana is heated by floor heating with 45 °C geothermal water.

3.2 Thermal Facilities and Balneological Applications in Turkey

Turkey is one of the rare countries, where combining sea/sun/cultural tourism with thermal tourism and balneological applications are possible. The main advantage of this combination is the increase of the variety and number of the tourists and the extension of the high tourism season to the whole year, instead of limiting it to 4-5 months which is mostly the case by the sea/sun/cultural tourism. This will bring an important economical development to these regions. Some of the regions that are suitable for sea and thermal tourism combination are towns of Bodrum, Kuşadası, Datça and Edremit which are located at the Aegean and Mediterranean Seas. In Çeşme (town of İzmir), thermal water is transported to the hotels for balneological utilization and this combination is applied there with a great success.

A possible producible potential flow rate of geothermal water (~40°C) that has been estimated for the balneological use in Turkey is 50,000 l/sec. This equals to the benefit of 8 million people per day from thermal waters in spas in Turkey [18]. The number annually expected local thermal curists is around 7 million and the number of the foreign thermal curists is around 10,000 in Turkey [15].

The foreign curist target number is 1 million and the local curist target number is 30 million for the year 2020 [15].

3.3 Greenhouse Heating

The geothermal greenhouse heating capacity has been increased to 145 MW$_t$, especially due to additional construction of total 190,000 m^2 greenhouses in Dikili (town of İzmir) and other places. The existing geothermal greenhouses in Turkey are as shown in Table3.2.

A 100 m^2 geothermal heat pump assisted greenhouse project in the city of Erzurum is approved by UNDP Energy for Sustainable Development Thematic Trust Funds Standing Committee in June 2002.

Table 3.2 Existing geothermal greenhouses in Turkey [15]

LOCATION	AREA (m²)	CAPACITY (MW$_t^*$)	LOCATION	AREA (m²)	CAPACITY (MW$_t^*$)
Şanlıurfa	106000	24.5	Dikili	190000	38
Simav	120000	33	Gölemezli	1000	0.2
Sındırgı	2000	0.4	Seferihisar	6000	1.06
Afyon	5500	1.5	Bergama	2000	0.4
Kızıldere	10750	2.4	Germencik	500	0.1
Balçova	100000	17.6	Edremit	49620	8.7
Kestanbol	2000	0.4	Ezine	1500	0.3
Saraykent	2000	0.6	Niksar	500	0.14
Tekkehamam	8000	1.8	Kızılcahamam	5000	1.45
Yalova	600	0.12	Gediz	8500	2.1
Kozaklı	4000	1.2	Çanakkale-Tuzla	50.000	9

*Load factor is 0.6

3.4 Geothermal Electricity Production

Geothermal electricity production is advantageous because of the relatively low installation and operational cost as well as being more environmentally benign, in comparison to the conventional thermic and hydraulic power plants. At present, ten of the geothermal fields of Turkey are of high enthalpy and are appropriate for the geothermal electric energy generation by binary cycle or by flashing cycle. These fields are [4]:

1. Denizli-Kızıldere (242 °C)

2. Aydın-Germencik-Ömerbeyli (232 °C)

3. Manisa-Salihli-Göbekli (182 °C)

4. Çanakkale-Tuzla (174 ° C)

5. Aydın-Salavatlı (171 °C)

6. Kütahya-Simav (162 °C)

7. Manisa-Salihli-Caferbey (150 °C)

8. İzmir-Seferihisar (153 °C)

9. İzmir-Balçova (142°C)

10. Aydın-Yılmazköy (142 °C)

At present there is only one operating geothermal power plant in Kızıldere. A geothermal power plant in Aydın-Germencik geothermal field is expected to be constructed in the very near future. It has been estimated that Aydın-Germencik geothermal field would have 100 MW_e power production capacities [15].

3.4.1 Kızıldere geothermal power plant

The plant operates on single flash with condensing cycle. Geothermal steam and brine mixture of about 12 % steam quality with 150 °C well head temperature and 15 bar pressure is separated to dry steam and brine at 147 °C and 3.5 bar. The dry steam is supplied to a turbine which drives an electric generator and a compressor.

In 2002 electricity generation has been increased from 90 GWh to 108 GWh in Kızıldere geothermal power plant, due to the drilling of a new well with 242 °C downhole temperature and connecting it to the system. 25 % of the produced geothermal brine is reinjected back to the reservoir.

3.4.2 Germencik geothermal power plant

At Germencik 25 MW_e B.O.T. project is underway. It is planned to utilize the field with 5 production and 3 reinjection wells. Total flow rate of geothermal fluid is 1434 t/h with a temperature of 210 °C and well head pressure of 15-18 bar. The foundation has not been realized yet [15].

3.5 Mineral recovery

The yearly production of 120000 tons of liquid CO_2 and dry ice production is continuing from the factory connected to the Kızıldere power plant.

CHAPTER 4

KIZILCAHAMAM GEOTHERMAL FIELD

Kızılcahamam Geothermal Field is located at the city center of Kızılcahamam town of Ankara. Kızılcahamam is in the north-west of Ankara at a distance of 70 km (Figure 4.1). The main use of Kızılcahamam geothermal fluid, with an average temperature of 70-80 °C and flow rate of 80 l/sec, is district heating which comprises 2500 residences. After transferring the energy of geothermal fluid to the cold-end fluid at the central heating stations by means of heat exchangers, about half of the geothermal fluid is used in Başkent University Thermal Hotel, Asya Thermal Resorts, Ab-ı Hayat, District facilities and Municipality hotels.

Figure 4.1 Location map of Kızılcahamam

The remaining half is reinjected from the well MTA-1. The outlet temperature of geothermal fluid from the heat exchangers is about 42 °C [20].

4.1 Geologic and hydrogeologic setting of the field

The investigation area is highlands with deep valleys. Koca Stream flowing in the direction of N-S which is formed by the union of Perçin and Sey streams (Figure 4.2). This area forms the main drainage system which consists of the temporary and permanent dry streams [21].

The high hills in the field do not show a regular arrangement and they are dispersed in an irregular way with various heights according to their lithology. The main hills in the field are; Taşavur Tepe (1311m), Gevrekdoruktepe (1319m), Sivritepe (1343m), Ortadede Tepe (1427m), Taşlık Tepe (1438m), Karadağ Tepe (1826m), Büyüktepecik (1218m), Geleviz Tepe (1473m), Dedepam Tepe (1457m). Briefly, the valleys are outcropped valleys and their abrasion surfaces belong to end of Miocene and they are represented by limited plains which are preserved [21].

Kızılcahamam geothermal field is located within the Tertiary Galatian Volcanic Complex which consists of lava flows, tuffs and agglomerates intercalated with lacustrine sediments. The basement beneath the complex consists of Paleozoic schist and Permo-Triassic limestones. The Mesozoic, development mainly in Lower Cretaceous limestone and Upper Cretaceous flysch facies, comes over the Paleozoic basement and is overlain by the Galatian Volcanic Complex. The volcanic activity which built up this complex is reported to have started at the end of the Upper Cretaceous, but reached its climax during the Miocene. Quternary alluvium uncomfortably covers the Galatian Volcanic Complex. The complex is cut across by faults which strike dominantly in ENE-WSW direction [36].

The volcanic activity seems to have started with the lava flows of dacitic-andesitic composition, followed by and locally intercalated with the pyroclastic products of (tuffs and agglomerates), and ended with andesitic-basaltic lava flows (Figure 4.2 (A)) [37].

The general hydrogeologic setting of the Kızılcahamam area is summarized by Koçak (1977) [23], Gevrek and Aydın (1988) [38], Özbek (1988) [20]. The area is

drained by the Koca Stream which flows southwards. Groundwater is recharged through the fractures in the volcanics and emerges, at the elevation of about 1000 m, as both hot and cold springs through these fractures, tuff contacts and fault zones (Figure 4.2 (B)) which, on a regional scale, are associated with an E-W trending graben the presence of which has been revealed by gravimetric as well as geological studies (Kutman and Şamilgil, 1975, Şimşek and Okandan 1990). Being accompanied by various anthitetic and synthetic faults, the master fault in Kızılcahamam area strikes approximately E-W direction (Figure 4.2 (B)) in conformity with the general trend of faults cutting across the Galatian Volcanic Complex [36].

Stratigraphic columns determined from MTA-1 and KHD-1 wells are displayed in Figure 4.3 and 4.4, respectively. Size and depths of casings of those wells are also reported in these figures to indicate the completion designs. In the Kızılcahamam geothermal field, Middle-Upper Miocene volcanics, Pliocene sediments and Quaternary alluviums exist. The volcanics called as a group name of Kızılcahamam Volcanites, are separated into four formations. Starting from the bottom, Akyarlar formation is the main unit and consists of tuff. The Çakal formation consists of pyroclastics, while the Gevrekdoruk formation is formed by andesitic and the Taşlıca formation is formed by basaltic lavas [22].

In 1998, MTA carried out an extensive geophysical study. According to result of this study; an anomaly of 500 m long to the east of the field and 800 meter wide from North to South was determined. After this study IHL series well locations were determined and wells were drilled. The geothermal area is 1.5 m^2 with respect to resistivity studies [22].
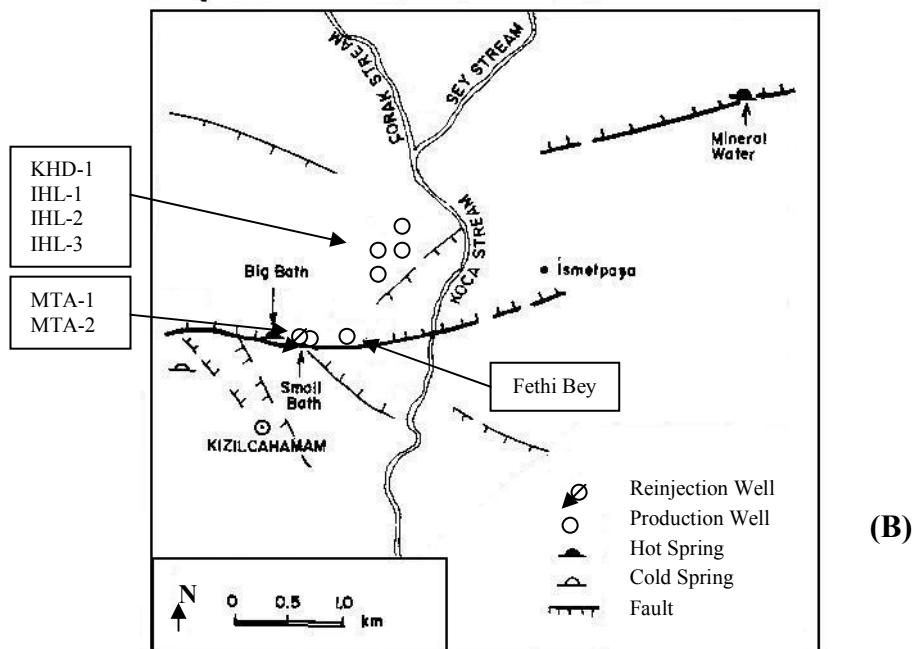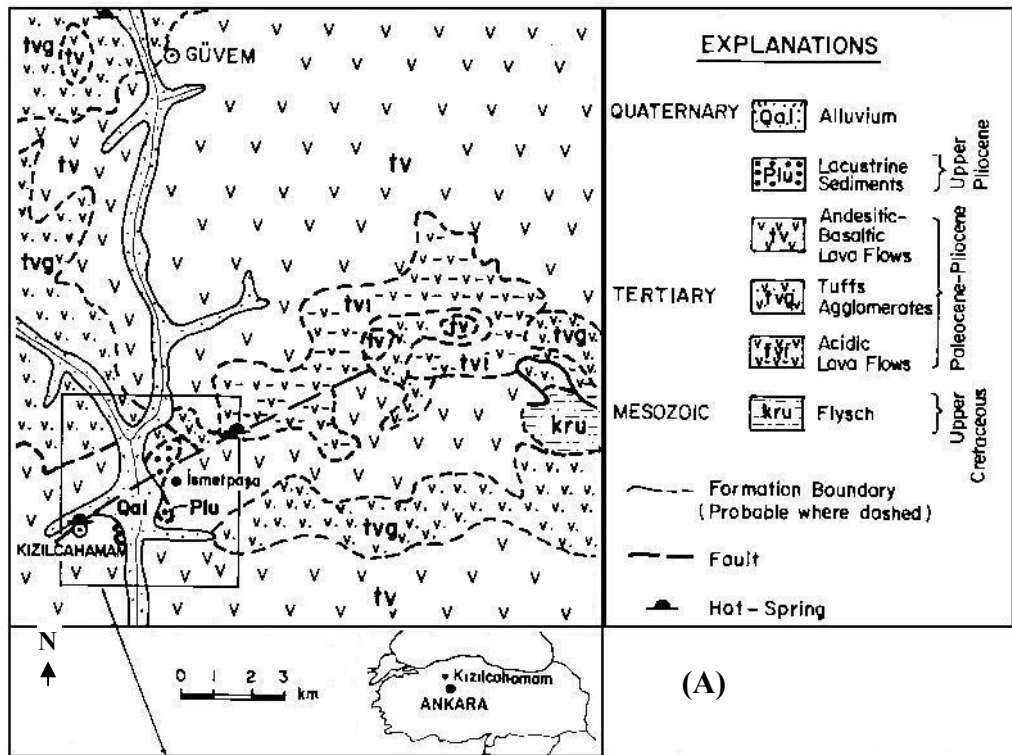
Figure 4.2 (A) Geological map of Kızılcahamam area (Erol, 1955), (B) Location of wells in Kızılcahamam Geothermal Field (Revised from Özbek, 1988).
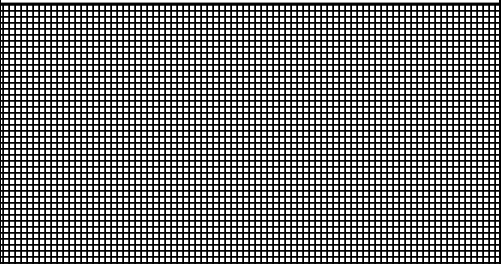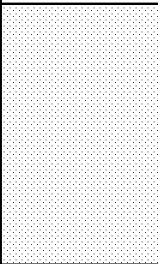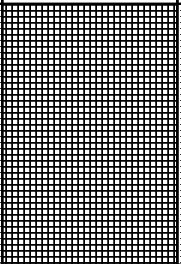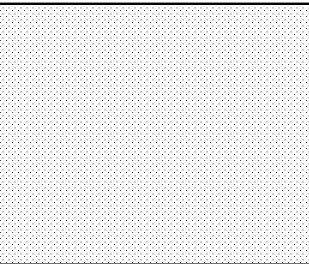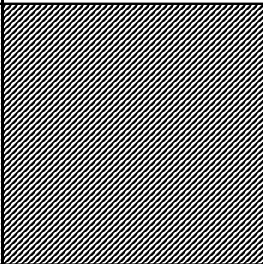
		Depth (m)	Formation	Casing Size and setting depth
		23	BASALT	13 3/8" 20 m
		60	TUFF	
		76	ANDESITE	8 5/8" 62.5m
QUATERNARY		100	TUFF	
TERTIARY	MIOCENE	179	ANDESITE	6 5/8" 178.5 m Liner

Era: CENEZOIC
System: TERTIARY — QUATERNARY
Series: MIOCENE
Lithology

Figure 4.3 Stratigraphic column and well completion design of MTA-1 [22].

Log Temperature (°C)	Depth(m)	Lithology	Casing size and setting depth
39	20	Alluvium (Andesite, Basalt, Tuff Grave)	16 3/4 " 50 m
51	80	Tuff (Grey and Red diffused Basalt)	
		Andesite (Grey, Pink with Tuff Alteration)	
52	130	Tuff (Grey and Red diffused Basalt)	
	160		
55		Andesite	
58	300	Tuff (Grey and Red diffused Basalt)	
62	360	Aglomera (Andesite, Basalt Gravel)	11 3/4" 390 m
64	380	Andesite (with Tuff)	
	400	Tuff (Grey and Red diffused Basalt)	
	420	Andesite	
66	440	Tuff (White and Light Grey)	
	460	Andesite	
69	500	Tuff (Light Green and more Silica)	
	580	Andesite (Hematite, Chlorite, Calcite Pink Color)	
68	640	Basalt (Black Color with Silica)	
70	680	Tuff (Chlorite)	
72	700	Andesite (Hematite, Chlorite Pyrite)	
	720	Tuff (Andesite Particules)	
74	790	Andesite (Dark Brown Color, fracture Calcite)	
75	760	Riyolitic Tuff (White Yellow with Mafic Mineral)	
76	940	Andesite-Tuff Ardalanması	5 3/4" 750 m
77	1000	Andesite (Silica and Chlorite)	
	1060	Rhyolitic	
77	1100	Tuff(Rhyolitic Andesite, Agglomerate Hematic, Chlorite,Calcite)	
	1140	Rhyolitic (more Silica)	
	1180	Andesite (Quartz, Calcite and Olivine Mineral)	
78	1220	Rhyolitic Tuff (Light Grey and Brown Pyrite, Calcite)	
79	1300	Rhyolitic(Fractured with Calcite and Silica with Grey Color)	
84	1340	Rhyolitic Porphyroid	
86	1400	Andesite (Red, Grey with Silica)	5 3/4" 1420 m Liner
87	1420	Rhyolitic Porphyroid	
	1500	Conglomerate (Volcanic Rock with Grave and Calcite Cement)	
105	1560	Andesite	1538 m

8 5/8" 390 m

Figure 4.4 Stratigraphic column and well completion design of KHD-1 [22].

4.2 The natural springs and wellbores

There are several discharging natural springs as well as wellbores in the gothermal field of Kızılcahamam. Some of the natural springs were dried out after the drilling of wellbores in the field.

4.2.1 Natural Springs

There are four main natural springs in the Kızılcahamam area:

1. Big thermal spring: This spring was in Kızılcahamam center and it had 50 °C temperature and flowrate of 2 l/s. It is dry nowadays, because of the production wells drilled in the field.

2. Small thermal spring: It was also in Kızılcahamam center with temperature of 51 °C and flowrate of 0.8 l/s, unfortunately, this spring was also dried out after the drilling of production wells.

3. Acısu spring (Kızılcahamam mineralwater): It is 4 km far to the town and contains with a flowrate of 8 l/s. It is rich in CO_2 content and more than 80000 bottles (200 ml each) are filled daily as mineral water. The bottling of the mineral water is made by Municipality of Kızılcahamam and As - Koop Mineralwater Business Enterprise. The mineralwater is useful not only for stomach, liver and gall bladder but also for blood circulation, heart diseases and fatigue [20]

4. Sey Bath: It is 18 km far from Kızılcahamam along the Çerkeş road. It has a temperature of 43 °C and flowrate of 17 l/s. It contains bicarbonate, sodium, calcium, CO_2 and fluorite. It is suitable for drinking and house cures. It is said to be useful for diseases of respiratory system, circulation system and heart, digestive system, kidney and urethra.

    The usage right of the bath and thermal water belongs to General Management of Foundations. The old bath building and its pool were restored. It has two in-door pools, one for women and one for men. There exists a motel for accommodation with a capacity of 30. Also additional motels exist in the field. The facilities are elementary [21].

4.2.2 Wellbores

The wellbores of Kızılcahamam geothermal field are mainly drilled in the center of Kızılcahamam and along the Ankara – İstanbul highway. Six wells exist in the field for thermal and heating purposes. Some of them are production wells, some of them are reinjection wells:

1. MTA-1: This is the first production well drilled in the field. The well had a first production temperature of 75,5^{o}C and artesian flow of 60 l/s. After 4 months and stabilization of pressure, the artesian flow dropped to 30 l/s [21, 22]. The well has a depth of 179. 60 m and it is currently used for reinjection with a rate of 40 l/s.

2. MTA-2: It is only 40 m away from MTA-1 and has a depth of 310 m. The well has a flowrate of 30 l/s, temperature of 77 °C and pump was set at 90m depth. The geothermal fluid produced from this well is used for district heating and in the baths of Municipality hotels.

3. KHD-1: This well was drilled by MTA to a depth of 1556.6 m. The initial measured production parameters of the well were 32 l/s artesian flow with wellhead temperature of 85.5 °C and bottomhole temperature of 88 °C. The present values; flowrate: 10 l/s, temperature 78°C and depth of pump 45 m.

4. IHL-3: It was drilled at a location close to KHD-1 to a depth of 673 m because of the decrease in the flowrate of KHD-1. The flowrate of IHL-3 is 20 l/s with the temperature of 76 °C and the depth of the pump is 70 m.

5. IHL-1: This well is not in use because of low fluid temperature, 45 °C although it has a flowrate of 30 l/s. Most probably, there is a cold water entry into the wellbore. The depth of the well is 590 m.

6. IHL-2: It has the least gas ratio among the wells drilled in the field. The depth of the pump is 70 m, the temperature is 77 °C and the flowrate is 20 l/s. The depth of the well is 670 m.

7. Fethibey: This wellbore is in the residential area of Kızılcahamam field and has a flowrate of 15 l/s, temperature of 78 °C and the depth of the pump is 68 m. The depth of the well is 592 m

8. MTA-2 (Old Well): This well has no production and it has a bottomhole temperature of 38 °C, because of drilling failure this well was not completed.

9. MTA-3: This wellbore was completed as a dry hole with a bottomhole temperature of 38 °C.

10. MTA-4: It wellbore was drilled along Sey stream and resulted with a bottomhole temperature of 53 °C but no water.

11. MTA-5: Another dry well which was drilled at the entry OF Kızılcahamam.

12. MTA-6: Although it has a high bottomhole temperature of 85 °C it does not have geothermal fluids. It was drilled in the residential area. [24]

The geothermal resources are not only used in thermal hotels and baths but also in the geothermal heating center established for heating 2500 houses, with a power capacity of 25 MW$_t$.

The six of the eight successful wells drilled in Kızılcahamam, are production wells and the remaining two are reinjection wells (Table 4.1). The distance between two outermost wellbores (MTA-1 and IHL-1) is nearly 1400m (Figure 4.5).

Table 4.1 Production and reinjection wells present in August 2004

Well Name	Well Depth (m)	Flow Rate (l/s)	Wellhead Temp. (°C)	Dynamic Level (m)	Pump Setting Depth(m)	Use
MTA-1	179	40	42	0	0	Re-injection
MTA-2	310	30	77	20	90	Production
KHD-1*	1556	15	42	0	0	Re-injection
IHL-1	590	20	45	30	70	Production
IHL-2	670	20	77	30	70	Production
IHL-3	673	20	76	20	70	Production
Fethibey	592	20	76	25	65	Production
Asya Finans*	600	20	65	25	50	Production

*This well was operated as reinjection well during the 2004-2005 winter, the production characteristics of the well are: flowrate rate of 10 l/s, temperature of 78 °C with a pump depth of 45 m.

** Asya Finans geothermal well was drilled by private company and it has been operated by Asya Finans Termal Facility, so this well is not used for the evaluation in this study.
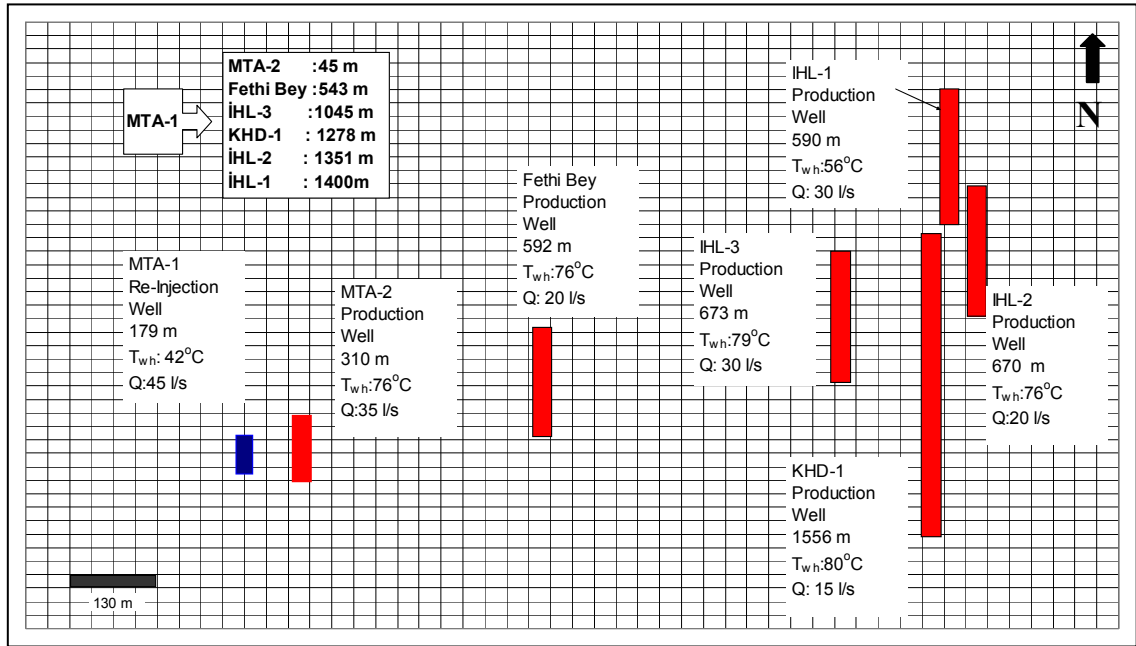
Figure 4.5 Locations of the Production and Reinjection Wells

4.3 Chemical Properties of Geothermal Fluids

The Kızılcahamam thermal water has temperature of 44-86.5 °C and pH of 7, contains bicarbonate, chlorite, sodium, carbon dioxide and arsenic. The water is suitable for bath cures and useful for rheumatism, heart and circulation system, neural and muscle exhaustion, neural diseases, liver and gall bladder, articulation and calcification and malnutrition. Kızılcahamam thermal water has solution mineral value is between 2675.2-3117.63 mg/l. Chemical analysis of MTA-2 are given in Table 4.2 [26].

Table 4.2 Chemical Analysis of MTA-2 [26]

pH	7.20	Cl	273 mg/I
Conductivity	2600 μmho/cm	SiO_2	58 mg/l
Na	720 mg/l	B	7 mg/l
K	58 mg/l	SO_4	120 mg/l
Ca	48 mg/l		
Mg	11 mg/l		
HCO_3	1586 mg/l		

According to chemical analysis, Kızılcahamam region waters are sodium bicarbonated, The reservoir temperatures according to SiO_2 geothermometers is 134 °C [26].

4.4 Geological Models of the Kızılcahamam Geothermal Field

Two geological models for Kızılcahamam geothermal field were proposed by Gevrek and Aydin [38] and Özbek [20]. (Figure 4.6 and Figure 4.7). Both models define the field with a main fault zone from which the hot water is ascending. High hills of the Kızılcahamam area are the recharge zones of the field where the meteoric cold water is fed into the geothermal field.
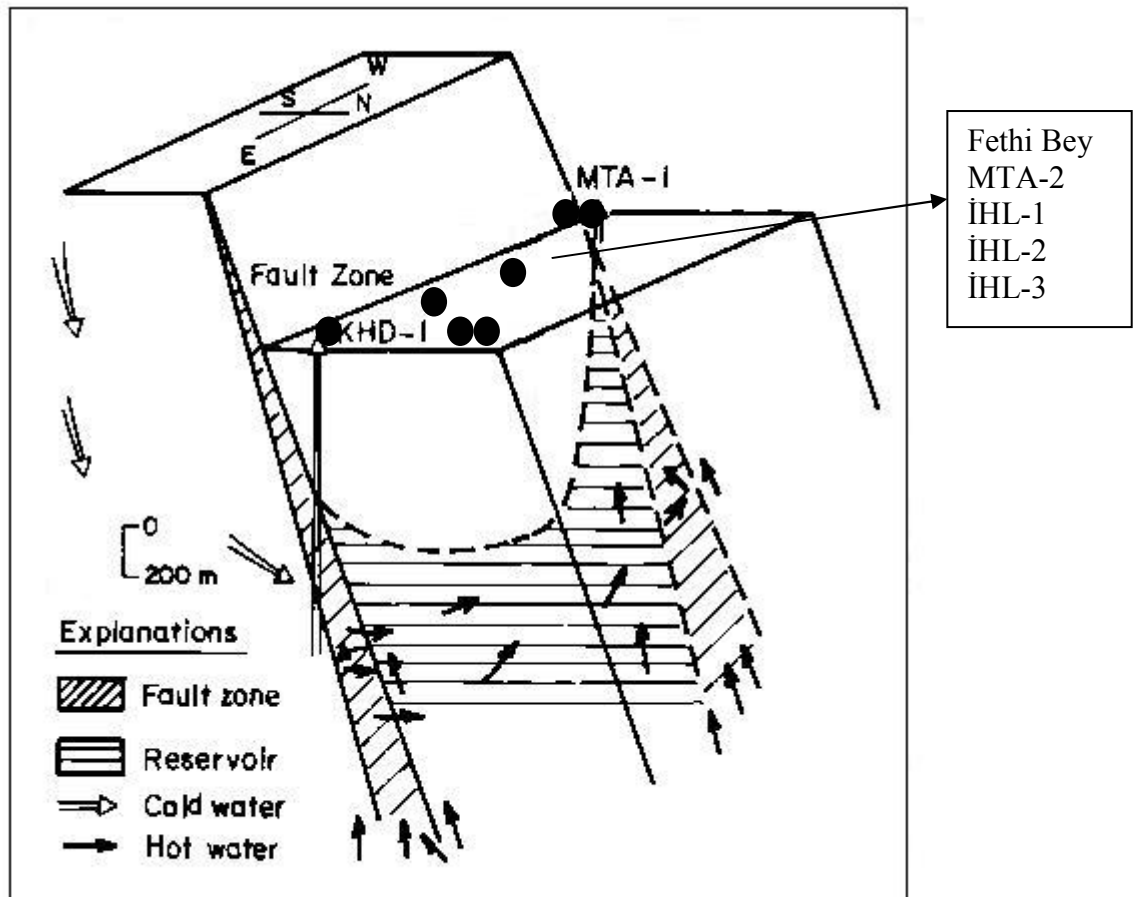
Figure 4.6 A simplified schematic model for the geothermal system in the Kızılcahamam geothermal field [38]
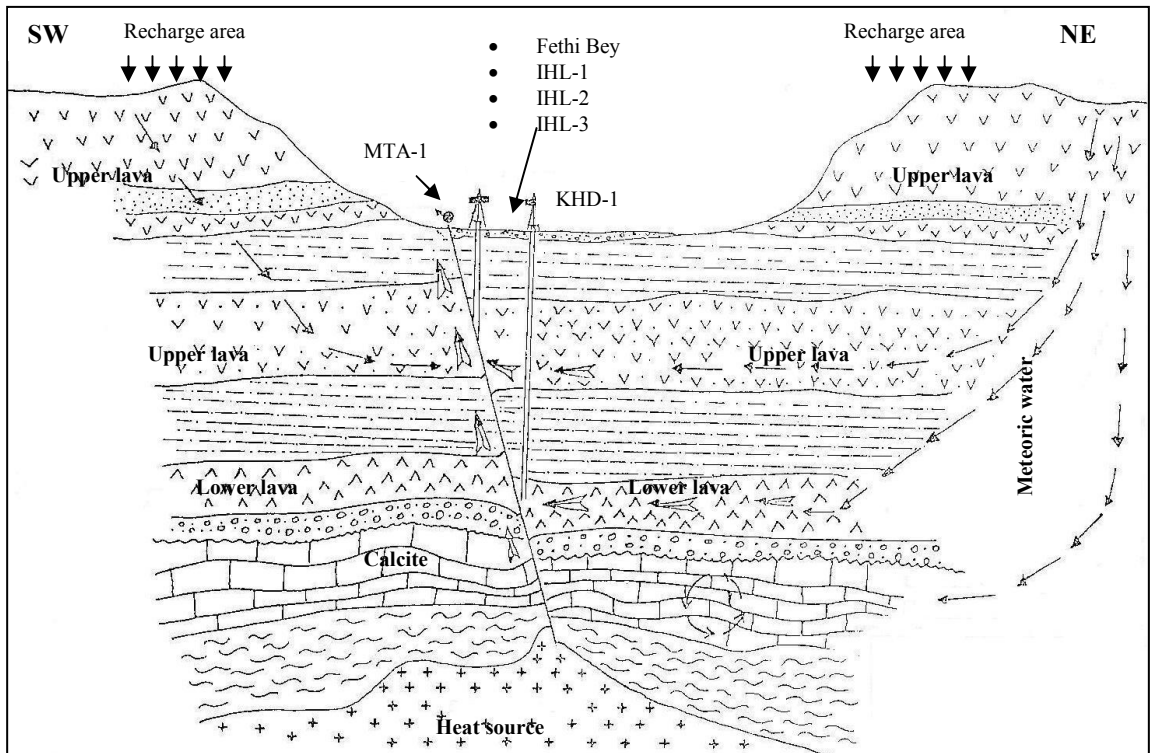
Figure 4.7 Conceptual Model of the Kızılcahamam Geothermal Field [20]

CHAPTER 5

STATEMENT OF THE PROBLEM

Reinjection is the integrated part of almost all geothermal fluid production schemes. The main two reasons of reinjection are the reservoir pressure maintenance and the disposal of environmentally harmful geothermal water. On the other hand, reinjection schemes must be engineered carefully because of the danger of early fluid and/or thermal breakthrough of the injected fluid. Reservoir characterization and modeling studies are the effective tools to describe the flow of energy and fluid in porous and/or fractured media. Tracer tests are one of the effective tools to understand the flow characteristics of injected fluid in the reservoir.

The purpose of this study is to characterize and re-evaluate Kızılcahamam geothermal field by means of tracer test analysis and historical well data which are well head-bottom hole temperatures, dynamic-static levels, bottom hole pressures and flow rates. In order to reach this goal tracer test(s) will be designed, conducted and interpreted.

CHAPTER 6

INTERPRETATION OF TRACER TESTS

The flow of tracer between an injection and a production well pair has been described both analytically and numerically by a number of authors [27]. In this study, six different models were considered: multi-fracture model [28], fracture-matrix model [29], uniform porous model [30], double porosity slabs model, double porosity cubes model, and double porosity pseudo steady state model [29]. In each model it is assumed that there is a good connection between the injection and production wells along a streamline which is surrounded by a stream tube of constant cross section. The tracer is injected as a slug from the injection well and the response is recorded in the observation well. The description of each model is given below.

6.1. Multi-Fracture Model

This model, as reported by Fossum and Horne (1982) [28], assumes a single/multi fracture system, joining the injection and observation wells. Dispersion is due to the high velocity profile across the fracture and molecular diffusion, which moves tracer particles between streamlines (Taylor dispersion) (Figure 1). The transfer function C_t is given by the following expression:

$$C_t = \sum_{i=1}^{n} e_i C_r (R_i / u_i, P_{ei})$$

(6.1)

Here n is number of flow channels in the fracture system, e_i is the flow contribution coefficient, R_i is the apparent fracture length, u_i is the velocity, and P_{ei} is the Peclet number of the ith flow channel. Therefore if "n" is taken as one then only a single (foult)

fracture is present. It should be noted that for all practical purposes, a multi fracture system must be represented with at least two fractures, since the value of the transfer function, C_t does not change much as "n" increases [29].

The form of C_r for each of the paths for a mass of tracer concentrated at point x=0 at time=0 is

$$C_r = L \frac{1}{\sqrt{t}} \frac{2t_m}{t} Exp\left(\frac{-P_e(t-t_m)^2}{4t_m t} \right) \qquad (6.2)$$
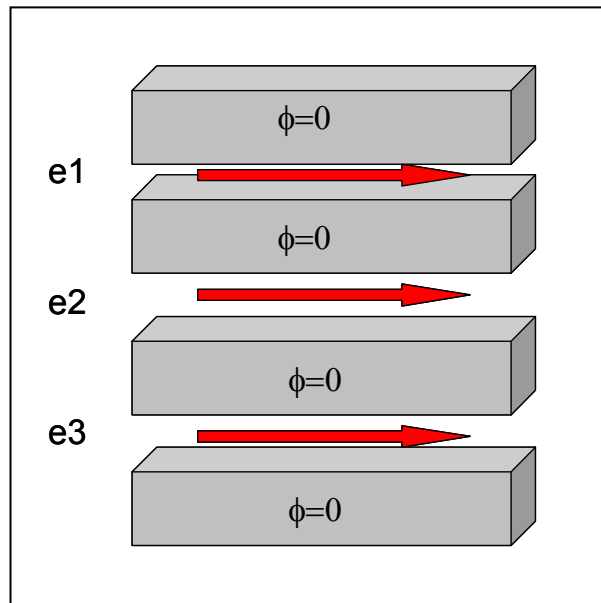
Figure 6.1 Schematic drawing of the multi fracture model

Here P_e is a Peclet number corresponding to the ratio of tracer transport by advection to tracer transport by diffusion, t_m is the mean arrival time (seconds) and L is a model parameter. Using the above model and by knowing the distance between the injector and producer, R, it is possible to obtain m, the mass of tracer entering the stream tube,

43

the dispersion coefficient for each flow channel by using the following definition:

$$D_{tr} = \frac{R^2}{P_e t_m}$$

(6.3)

It should be noted that the above model could also be used together with other models presented in this thesis. [29].

6.2. Fracture-Matrix Model

In this model, as reported by Bullivant and O'Sullivan (1989), there is a large fracture with micro fracturing in the rock matrix on either side (Figure 6.2). Tracer particles leave the main fracture and enter the micro fracture network (there is a small amount of fluid exchange), stay for a while, and then return to the main fracture.
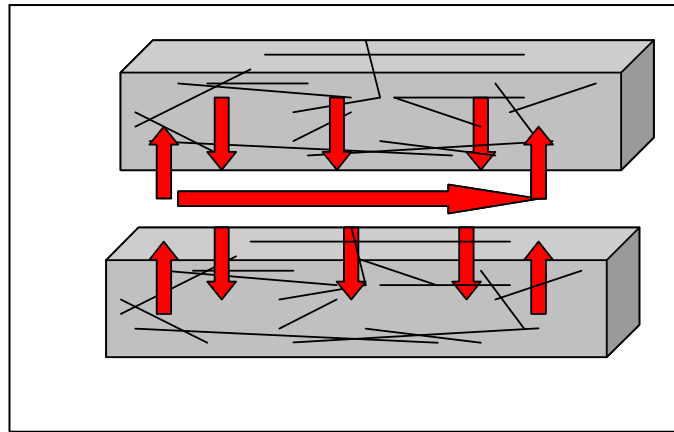
Figure 6.2 Schematic drawing of the fracture matrix model

Longitudinal dispersion due to the velocity profile across the fracture is ignored in order to give a clear distinction from the single fracture model. A fracture with fluid velocity constant across the thickness and with diffusion perpendicular to the fracture into an infinite porous medium is used in this model. The solution is in the following form:

$$C_r = JU(t - t_b)^{-1/2} Exp \frac{-t_b}{w(t - t_b)}$$

(6.4)

Here U is the Heaviside step distribution, w is a ratio of transport along the fracture to transport out of the fracture, t_b is the response start time, and J is a model parameter w is peclet number[29].

6.3. Uniform Porous Model

In the uniform, homogeneous porous model, it is assumed that a slug of tracer is instantaneously injected into a system with constant thickness (Figure 6.3). It is also assumed that, the flow is rapid allowing the kinematic dispersion components to be predominant (For purely hydrodispersive transfer the solution for one-dimensional flow as reported by Sauty (1980) is,

$$C_r = \frac{K}{\sqrt{t_r}} Exp(-\frac{P_e}{4t_r}(1-t_r)^2)$$

(6.5)

where

$$K = \sqrt{t_{rm}} Exp(\frac{P_e}{4t_{rm}}(1-t_{rm})^2)$$

(6.6)

$$t_{rm} = \sqrt{1+P_e^{-2}} - P_e^{-1}$$
(6.7)
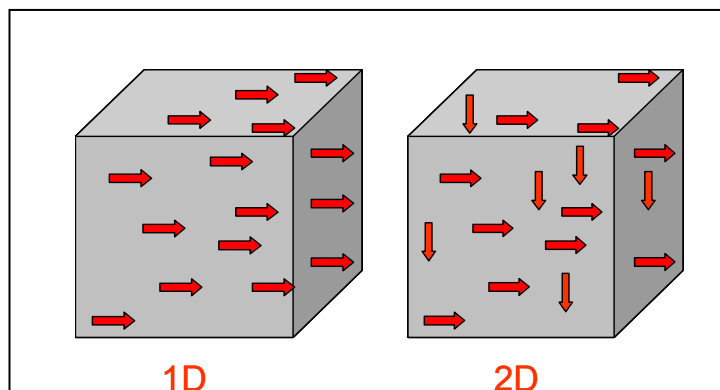
Figure 6.3 Schematic drawing of the uniform porous model

In the above equations P_e is the dimensionless Peclet number and t_r is the mean arrival time, K is model parameter. Similarly, Sauty (1980) also reported an analytical expression for the slug injection of a tracer solution into a two dimensional field. The solution on the flow axis can be obtained similar to the one-dimensional form as shown below. [29].

$$C_r = \frac{K}{t_r} Exp(-\frac{P_e}{4t_r}(1-t_r)^2)$$

(6.8)

where

$$K = t_{rm} Exp(\frac{P_e}{4t_{rm}}(1-t_{rm})^2)$$

(6.9)

$$t_{rm} = \sqrt{1+4P_e^{-2}} - 2P_e^{-1}$$

(6.10)

6.4. Double Porosity Slabs Model

The double-porosity slabs model has parallel fractures with constant thickness a, separated by slabs of the rock matrix giving a constant separation b (Bullivant and O'Sullivan, 1989) (Figure 6.4).

Tracer movement in slabs is modeled by diffusion perpendicular to the fractures. If the ratio of transport along the fracture to transport out of the fracture, w, the response start time, t_b, the matrix block fill up time, t_f, and the model parameter, J, and the injection rate, Q are known, the mass of tracer, m , p is laplace inversion parameters and the ratio of fracture porosity, ϕ_f to matrix porosity ϕ_m can be estimated using the equation given below. [29].

46
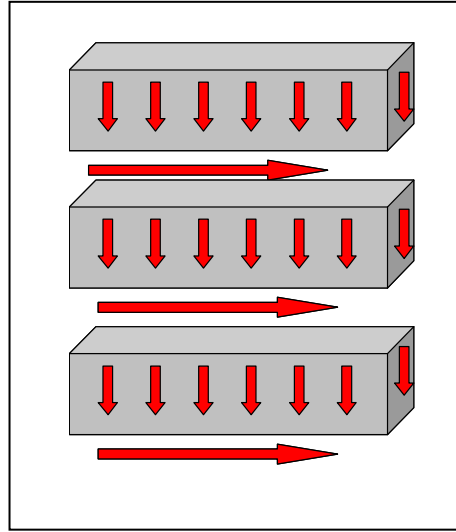
Figure 6.4 Schematic drawing of the double porosity slab model

The solution is given by the following equation: [29] Here p is the Laplace transform parameter.

$$C_r = JExp(-t_b(2\sqrt{\frac{p}{wt_b}}\tanh(\frac{t_f}{2}\sqrt{\frac{p}{wt_b}})+p))$$

(6.11)

6.5. Double Porosity Cubes Model

In the double-porosity cubes model as reported by Bullivant and O'Sullivan (1989), it is assumed that the rock matrix consists of cubic blocks of side b separated by high permeability fractures of aperture "a" (Figure 6.5).

The double-porosity cubes model differs from the double-porosity slabs model because for the cubes model, the area of the surface a distance b/2+z from the nearest fracture is proportional to the square of z, whereas for the slabs model the area of the surface a distance b/2-z from the nearest fracture does not vary with z. This affects the way tracer diffuses into the block.
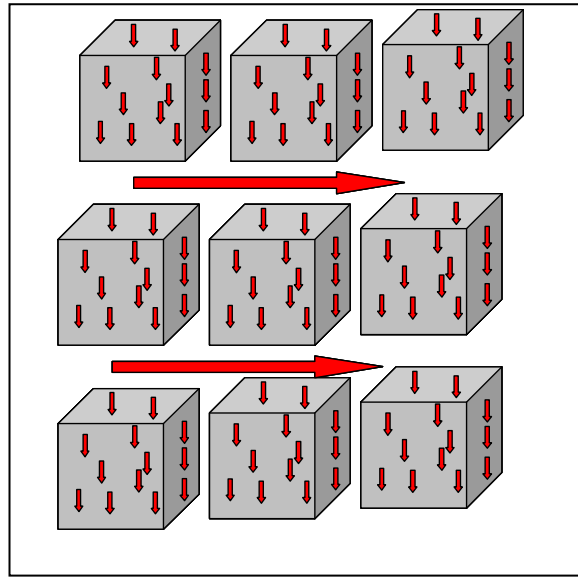
Figure 6.5 Schematic drawing of the double porosity cubes model

Tracer movement in the blocks is modeled by diffusion perpendicular to the nearest face. The solution is given by the following equation: [29]

$$C_r = JExp(-t_b(2\sqrt{\frac{p}{wt_b}}\coth(\frac{t_f}{2}\sqrt{\frac{p}{wt_b}})-\frac{4}{t_f}+p)) \qquad (6.12)$$

6.6. Double Porosity Pseudo Steady State Model

For this model, the reservoir contains uniformly distributed high permeability micro fractures which divide the reservoir into low permeability blocks that consist of unswept pores by the fluid flow (Figure 6.6).

Similar to the mechanism defined for the fracture-matrix model, the tracer leaves the micro fractures and then returns again. However the effect is different, such that the

blocks may be filled with tracer. Longitudinal dispersion due to the movement of fluid

into the micro fracture network is neglected. The solution for this case is reported by O'Sullivan and Bullivant (1989) and given below. In this equation, α_m matrix porosity, and α_f is fracture veloncity.
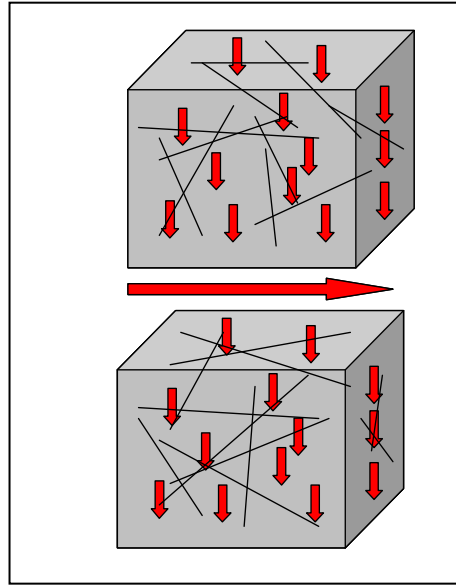
Figure 6.6 Schematic drawing of the double porosity

pseudo state model

$$C_r = JExp(-\alpha_m t)U(t-t_b)^{1/2}I_1(2(t_b \alpha_f \alpha_m(t-t_b))^{1/2}) \tag{6.13}$$

In the above equation a_f is the rate of tracer interchange per unit fracture volume and a_m is the rate of tracer interchange per unit matrix volume. [29].

CHAPTER 7

METHOD OF SOLUTION

In this first part of this chapter tracer test design, modifications conducted on wellhead of MTA-1 (reinjection well), collection of pressure, temperature, flow rate and tracer data will be given.

7.1. Tracer Test Design

In order to determine the amount of tracer, fluoreiscein was used as the tracer for this study to be mixed in the geothermal fluid in reinjection well, a literature survey was done and 33 design methods were determined. Most of the methods are empirical equations that depend on the chemicals used in the tracer test, the lithology of the formation of injection (karst, sandstone etc.) and fractured or not and the permeability of the formation. In these methods, the main aim is to determine the amounts of the chemicals used in injection fluid. For example, Kilpatrick [31] offered to use the equation M (mass) = V(volume) / 200 in order to determine the mass of the tracer. The methods examined by Field [32], are applicable for only one chemical like fluorescein or in fractured and karstic formations. The design equations are functions of flowrate, the distance between the wells and time.

The most complex part of the tracer test is the determination of the sampling frequency in the investigation well. To determine the sampling frequency two basic methods are offered; the methods depend on the samples of the tracer tests, the sampling frequencies are hours, days and weeks (at most 1-2 weeks); the methods calculated by using the travel distance and time of the tracer chemical. It was reported that the quantitative

methods gave wrong results by different studies. One of the quantitative methods is the one offered by Kirkpatrick and Wilson [33]. In this method, by using the equation below, t_p, the time of the peak concentration of the tracer is determined. The sampling frequency is determined by dividing the test time by 30.

$$t_p = 2.78x10^{-4} \frac{L}{v_p}$$

(7.1)

where L is the distance between the wells and υ_p is the velocity.

The amount of the chemical and the sampling frequency used in this project was determined by EHTD method offered by Field [32] This method depends on the solution of the equation 7.2 shown below.

$$R_d \frac{\partial C}{\partial t} = D_z \frac{\partial^2 C}{\partial z^2} - \upsilon \frac{\partial C}{\partial z} - \mu z$$

(7.2)

where R_d dimensionless dissolving factor, C is concentration, t is time, z is space variable, D_z axial diffusion constant, υ is the average velocity, μ is dissolver viscosity. In this equation, the assumptions are such that the tracer is injected as a slug and it is assumed that no reaction takes place. For the other boundary conditions such as continuous injection, Field [32] offered different solutions [7.3].

$$f(x*) = C_p - \frac{M}{An_e\sqrt{4\pi D_z t_p}}$$

(7.3)

In order to use the equation above the mass of the tracer chemical, M, flow rate Q, porosity, n_e, axial dispersivity D_z, area A and the peak concentration time, t_p, should be known. Field[32] used the functional dependence of these parameters on flow rate and travel time in order to determine the tracer concentration, tracer mass and

axial dispersivity by using the tank reactor mixing continuously. For the unknown parameters, correlations were used.

Using EHTD method (Appendix A) assuming that fluoreiscein will be injected from reinjection well (MTA – 1) with a flowrate of 40 l/s, 1.53 kg tracer chemical should be used for a 50 m thickness reservoir formation with 8 % porosity. It is further assumed that production well (MTA-2) is approximately 100 m away from the injection well. Although the surface distance between the two wells is 40 m, because of the different depths of two wellbores (MTA-1 is 179.6 m and MTA-2 is 310 m) the actual distance differs from the surface distance (Figure 7.1).
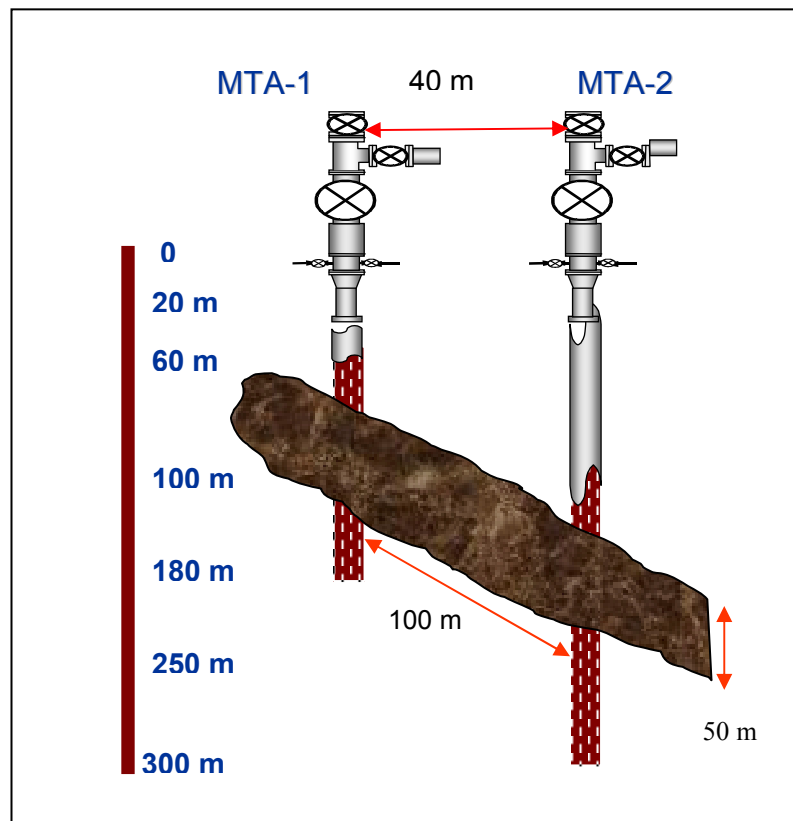
Figure 7.1 Schematic drawing of the reinjection and production wells

It was assumed that the tracer will be injected for 4 hours. The expected values of chemical concentration and sampling frequency (circles) graph for MTA-2 is shown in Figure 7.2.
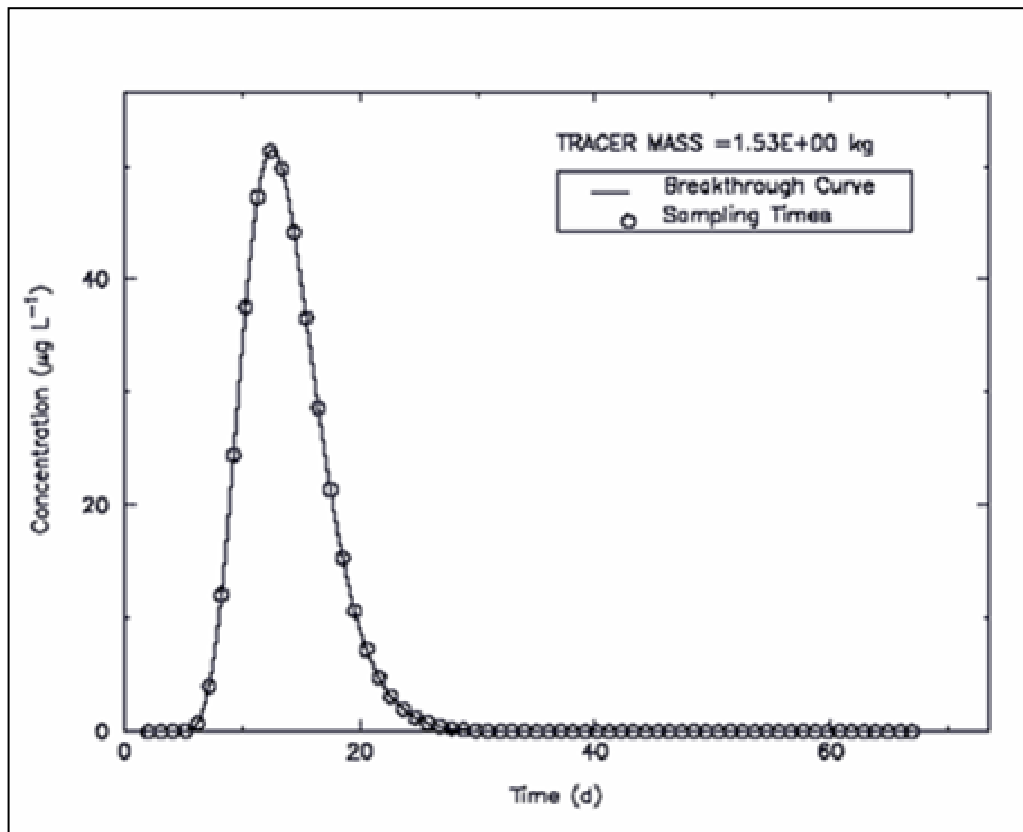
Figure.7.2 The expected values of chemical concentration and sampling frequency

7.2 Implementation of Tracer Test

The flow rate, temperature and dynamic level measurements were made in production and re-injection wells (Figure. 7.3). Flow rates were measured using a Danfoss 3000 magnetic flow meter. Temperatures were measured using a thermometer. Static and dynamic levels in production wells were measured using nitrogen injection

lines. Wellhead of MTA-1 was modified for tracer test. All production well heads were prepared for sample collection purposes. ½" and 1" valves were installed to all production wells between the pump discharge head and control valves (Figure 7.3).
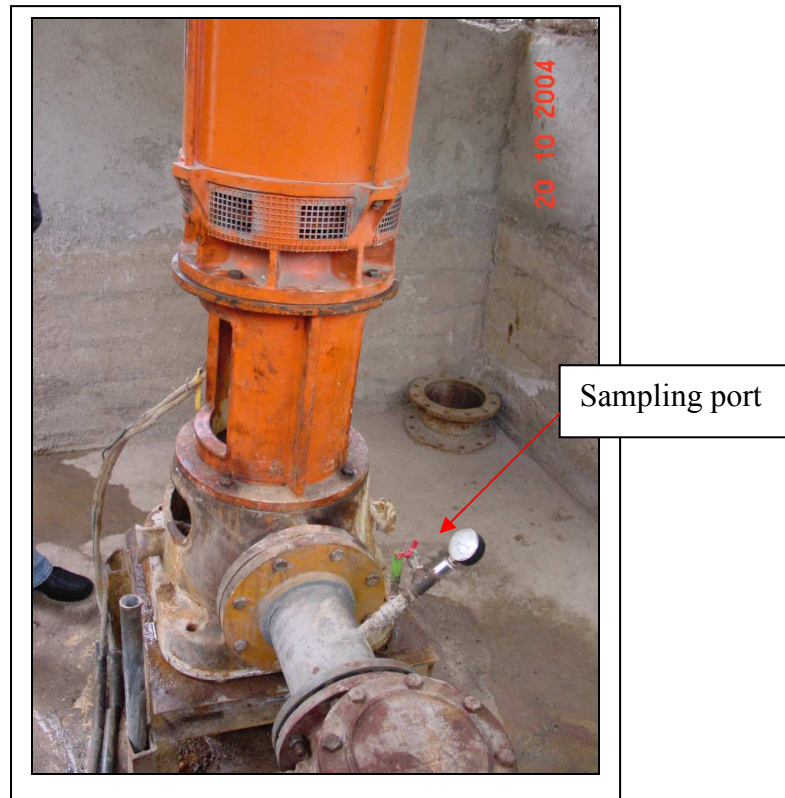
Figure 7.3 Well Head for sample collection (MTA-2)

Well data which are well head temperature, dynamic level of the wells, flow rate of the production and re-injection wells have been collected every day. The well head of the MTA-1 well was prepared by installing DN 50 pipe as spool line (Figure 7.4). The tracer which is 1.53kg Fluorescein was mixed with 20 kg water and then injected into MTA –1 well in nearly 6 minutes (Figure 7.5). The concentration is 7,65%. Prior to the tracer tests calibration samples were collected from each well.
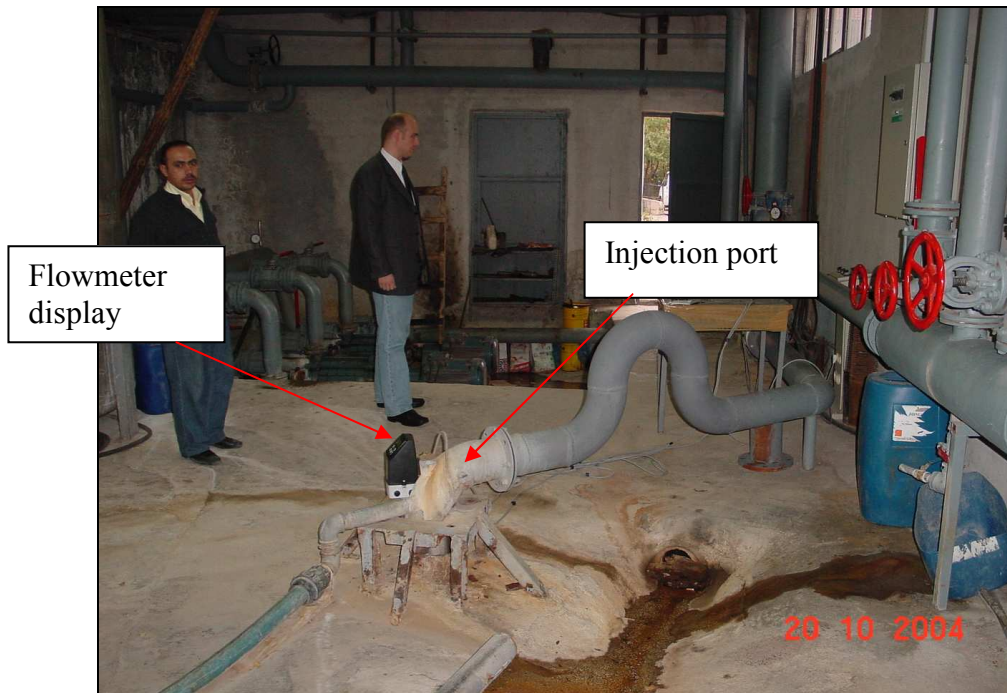
Figure 7.4 Flow Rate Measurement

Figure 7.5 Tracer (Fluorescein) injection to MTA-1 well

After that according to program which is given in Table 7.1, samples (680 bottles) were collected in 0.5 liter sample bottles for 72 days. The fluorescein concentration was detected by using Turner Quantech Fluorimeter. Samples were placed in 3.5 ml

Suprasil quartz cuvettes and a 490 nm narrow band excitation filter was used in measurements. First a calibration fluid is prepared for different concentrations (i.e. 1, 2, 4, 8, 10, 20, 30, 40 and 50 ppb). Following that a calibration run is conducted. A regression constant, larger than 0.9, was used in all measurements. Following that samples were placed in 3.5 ml cuvettes and measurements were conducted. Calibration was repeated each day as the fluorimeter required re-calibration once the device is turned off.

Table 7.1 Sampling program

Well Name	Number of Samples/day	Sampling time
MTA-1	1	08:00
MTA-2	4	08:00-14:00-20:00-02:00
FETHİBEY	2	08:00-20:00
IHL-1	1	08:00
IHL-3	1	08:00

Tracer test data measured was analyzed using multi fracture, single fracture, uniform porous (1-D and 2-D), fracture-matrix, double porosity pseudo steady state, double porosity cubes and double porosity slabs models described in chapter 6. The models were matched to field data using non-linear-least-squares approximation. Microsoft Excel Solver uses the Generalized Reduced Gradient (GRG2) nonlinear optimization code developed by Lasdon and Waren (Fylstra et al. 1998). By minimizing the following objective function R, the parameters of the proposed analytical transfer functions can be estimated [34].

$$R = \sum_{i=1}^{n} w_i (C_{model} - C_{experiment})^2$$

(7.4)

Here w_i' s are the inverses of the variances of the experimental measurement errors, which will give the maximum-likelihood/minimum-variance estimates of the parameters [35].

In nonlinear parameter estimation or curve fitting, it is important to have good initial estimates for the model parameters. The peak time and response start time can be

easily found from the test data. However, initial estimates for the nonlinear parameters (i.e. Peclet number) should be carried out in trial and error fashion. The methodology can be summarized as follows. First, the problem is defined by specifying the target cell (R), changing cells (P_e, w, etc.), and the constraints ($P_e > 0$, etc.). At this stage plotting abilities of the spreadsheet software can be used to find reasonable initial estimates for the unknown parameters. Following that, the solution time, number of iterations, and the precision of constraints that control the solution process are defined. Then the method used by the "Solver" is input. At this point, the estimation technique (tangent or quadratic), the method for calculating derivatives (central difference equation or forward difference equation), and finally the search method (quasi-Newton or conjugate) must be defined.

After the solver has found a solution, to specify the goodness of the estimate, confidence intervals of the changing parameters were found. Using 95 % confidence intervals to evaluate the goodness of fit of a nonlinear regression analysis of tests, it was observed that an acceptable estimate was the one with a confidence interval that is at least 10 % of the value itself. If the confidence interval of one of the changing parameters exceeds the aforementioned value, initial estimates of the changing parameters were readjusted and/or the search direction and the estimates were changed until a reasonable value was achieved. It should be noted that, the confidence interval is a function of noise in the data, as well as the number of data points, and the degree of correlation between the unknowns.

CHAPTER 8

RESULTS and DISCUSSION

In this part of thesis the flow rate, temperature and dynamic level measurements, tracer test results will be given and interpreted.

8.1. Temperature and Pressure Data

Since all the production wellbores are equipped with pumps, it is only possible to measure the temperature at the wellhead as well as to measure the dynamic fluid level in the wellbore. Those two measurements should be converted to bottomhole values. Equation 8.1 is used to estimate the bottomhole temperature with the help of wellhead temperature measurements. The average gradient temperature is taken 0.5 ^{o} C/100 m in Kızılcaham Geothermal Field according to drilled gradient geothermal wells.

$$T_{bh} = T_{wh} + \frac{0.5°C}{100m} \times Depth$$

$$(8.1)$$

On the other hand, the bottomhole pressure values were obtained by using the dynamic fluid level data and well depth with the use of Equation 8.2.

$$p_{bh} = \rho \times g \times h$$

(8.2)

$$h = welldepth - dynamiclevel$$

(8.3)

where ρ = 979.38 kg/m^3 at T_{av}=70° C, g: gravitational constant 9.81 m/s^2

8.2. Production Analysis

Figure 8.1 and 8.2 gives the cumulative production and reinjection for each well and

for the Kızılcahamam geothermal field as hole respectively. Detailed production plots are given in Figure 8.3 through 8.10. As can be seen from these Figures MTA-1 was a producer up to July 98 and then converted to be an injector to reinject the geothermal fluid as of heating season of 98-99. During summers only MTA-2 operates and that's why flat production is observed in other wells. Total production to reinjection ratio was found as 3.2 (Figure. 8.2). This ratio is relatively high for a low temperature geothermal field and this shows that pressure decline is more than it should be (See for example Figure. 8.18). Thus, this ratio has to be reduced to a smaller number (for example 1.5) for good pressure support and efficient management of the field.
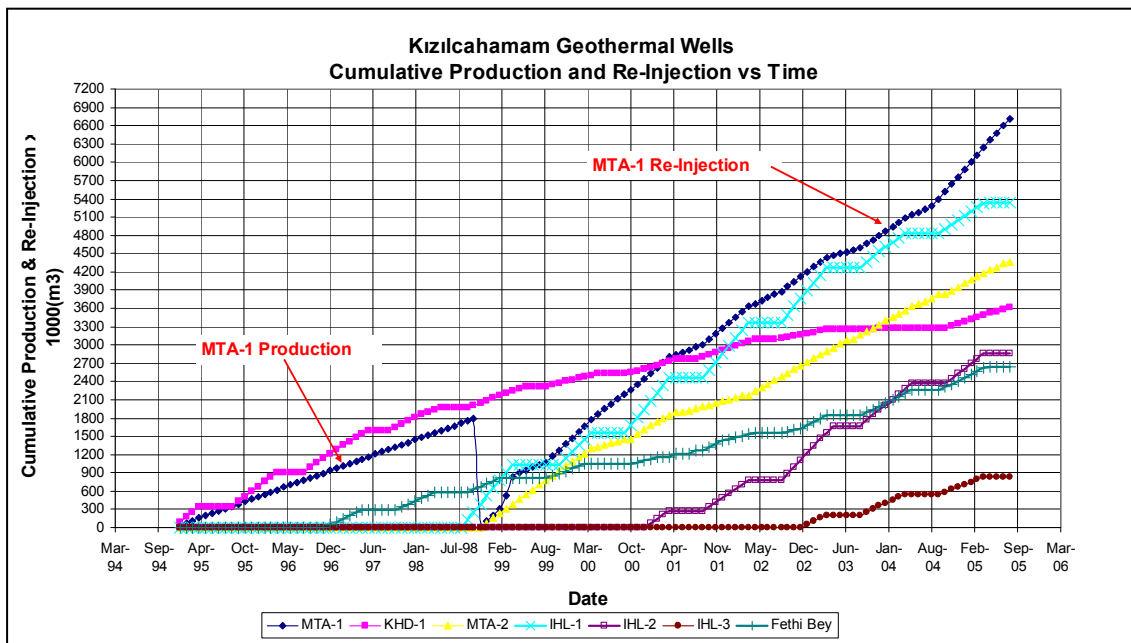
Figure 8.1 Production and re-injection flow rate of Kızılcahamam Geothermal Wells

The cumulative production is 21.435.470 m³ between January 1995 and August 2005 (3865 day), the cumulative reinjection is 6.719.440 m³ between December 1998 and August 2005 (2435 day). The average production is 231 m³/h (64 l/s) and the average reinjection is 114 m³/h (31 l/s).

59
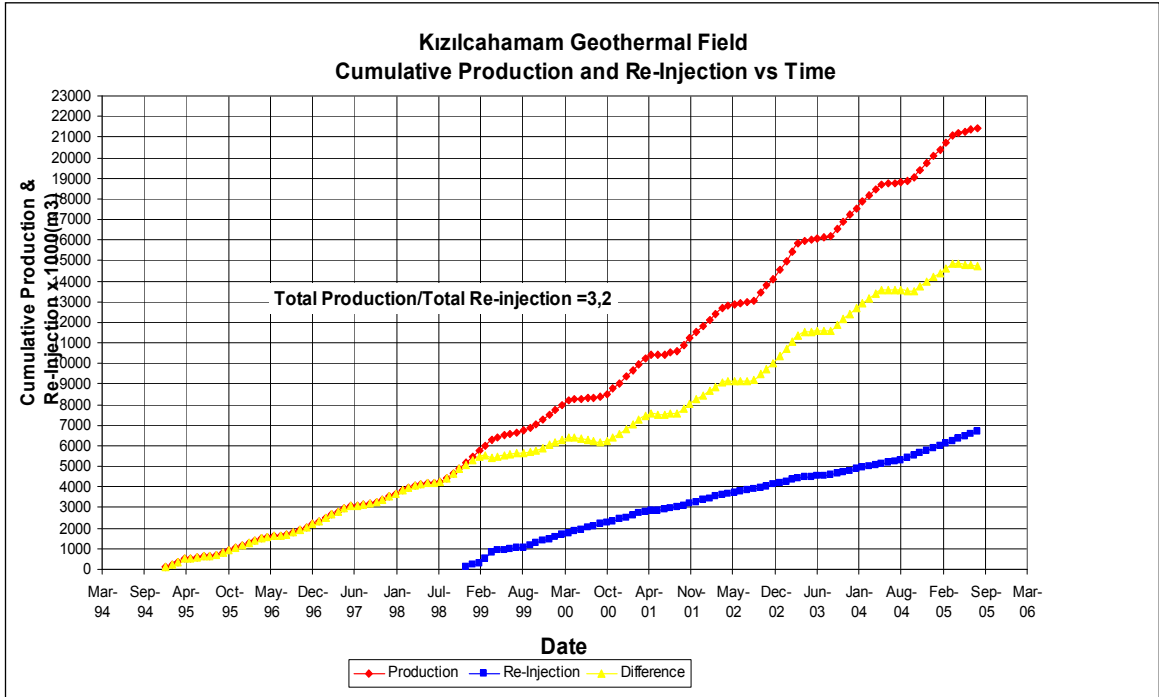
Figure 8.2 Cumulative production and re-injection rates
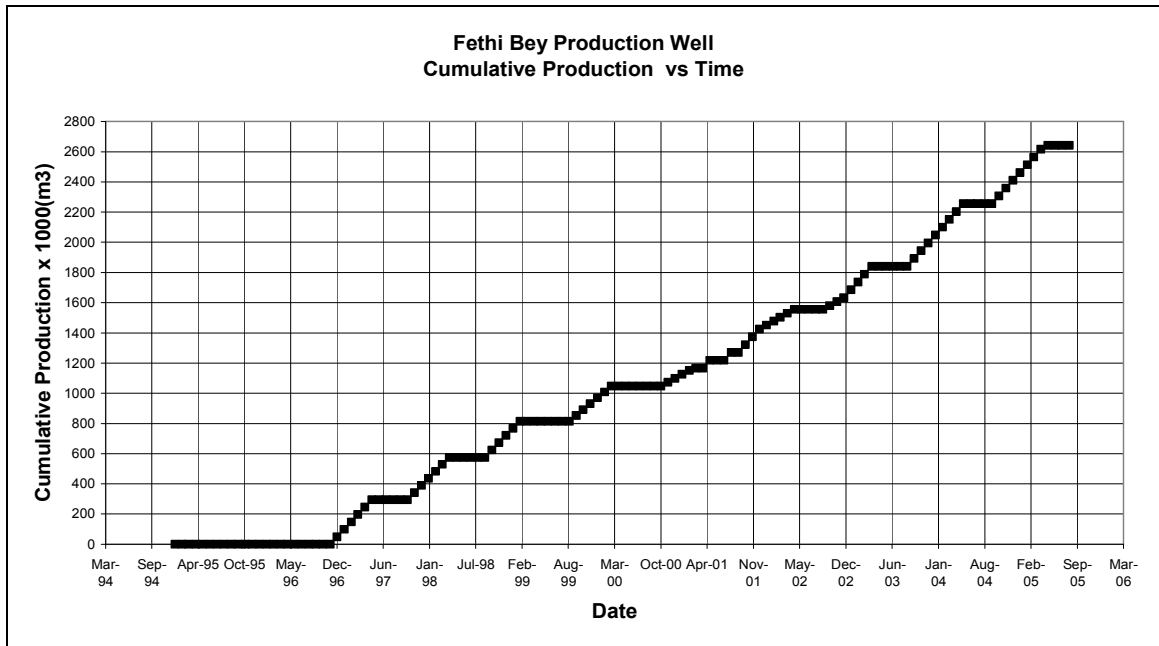
Figure 8.3 Cumulative production history of Fethibey Geothermal Well

60
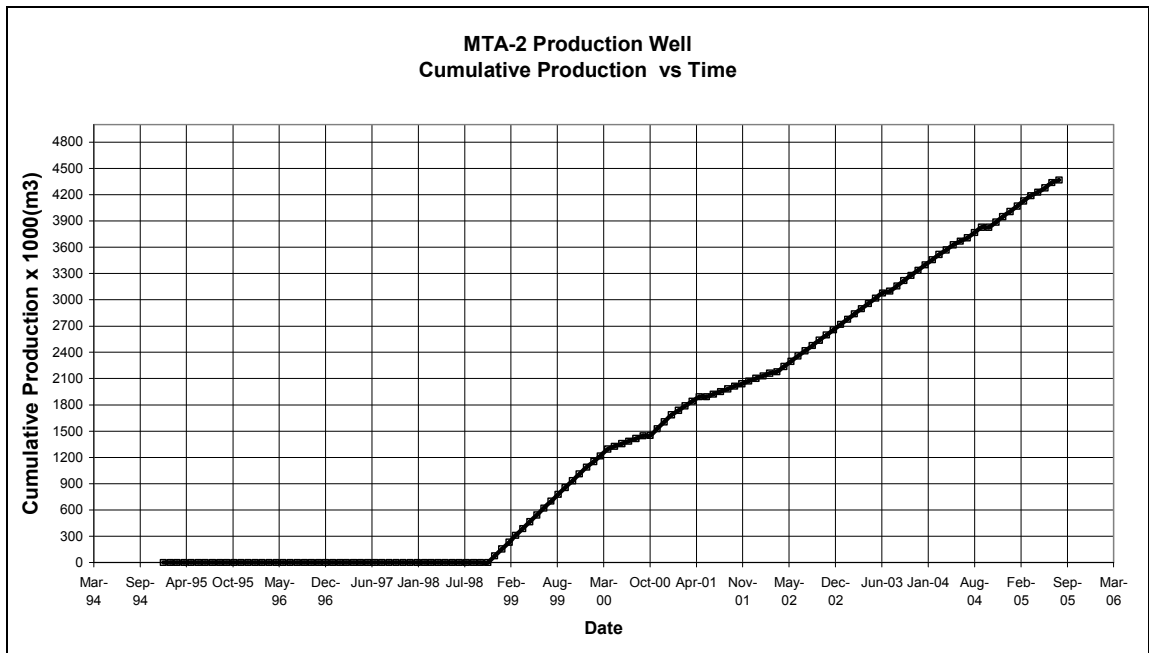
Figure 8.4 Cumulative production history of MTA-2 Geothermal Well
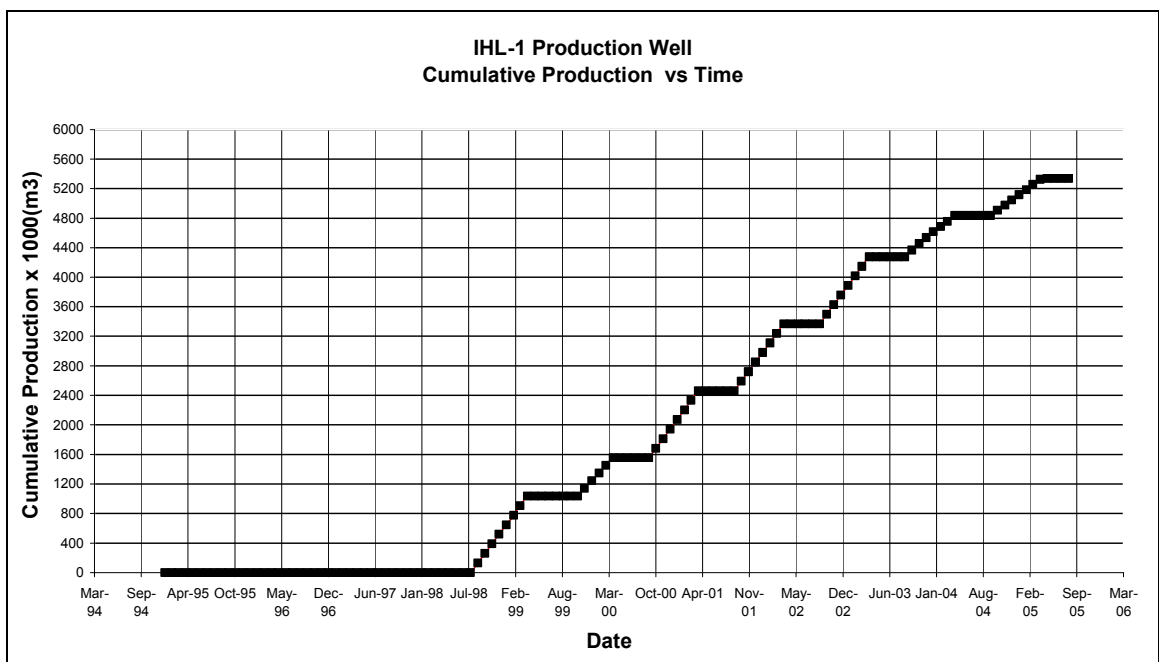
Figure 8.5 Cumulative production history of IHL-1 Geothermal Well
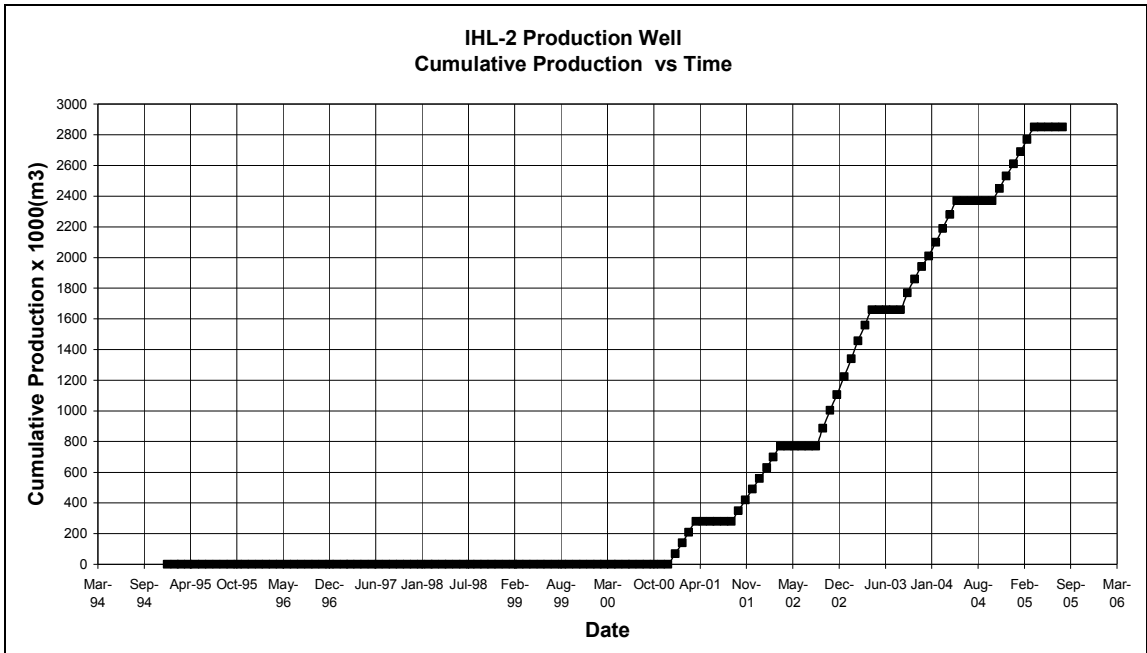
Figure 8.6 Cumulative production history of IHL-2 Geothermal Well
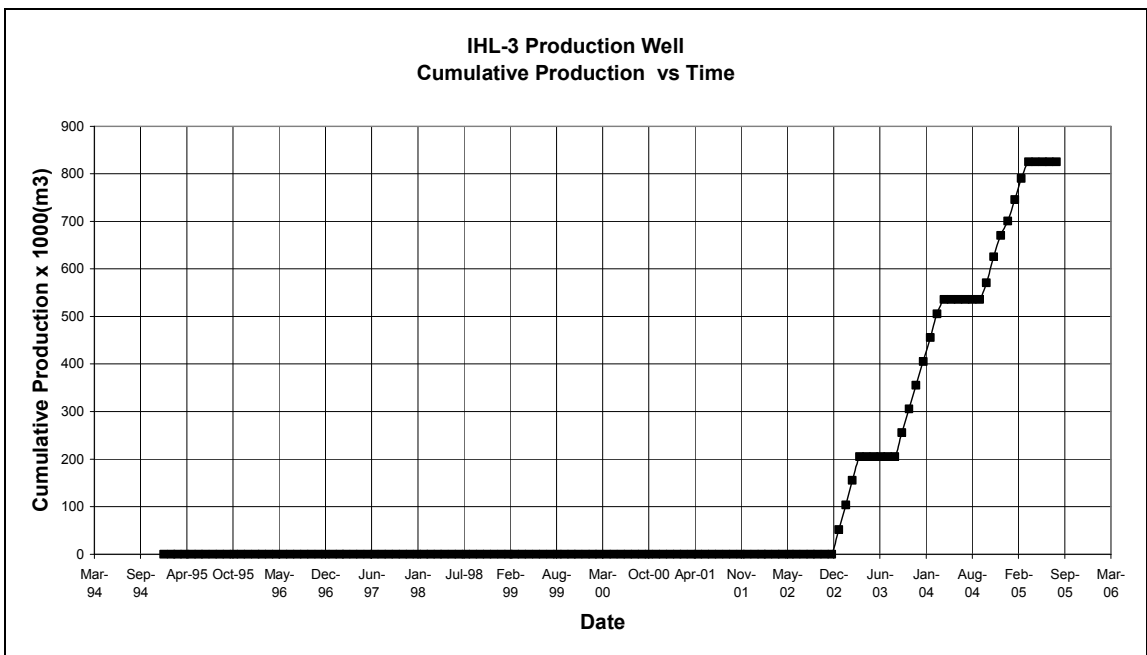
Figure 8.7 Cumulative production history of IHL-3 Geothermal Well

62
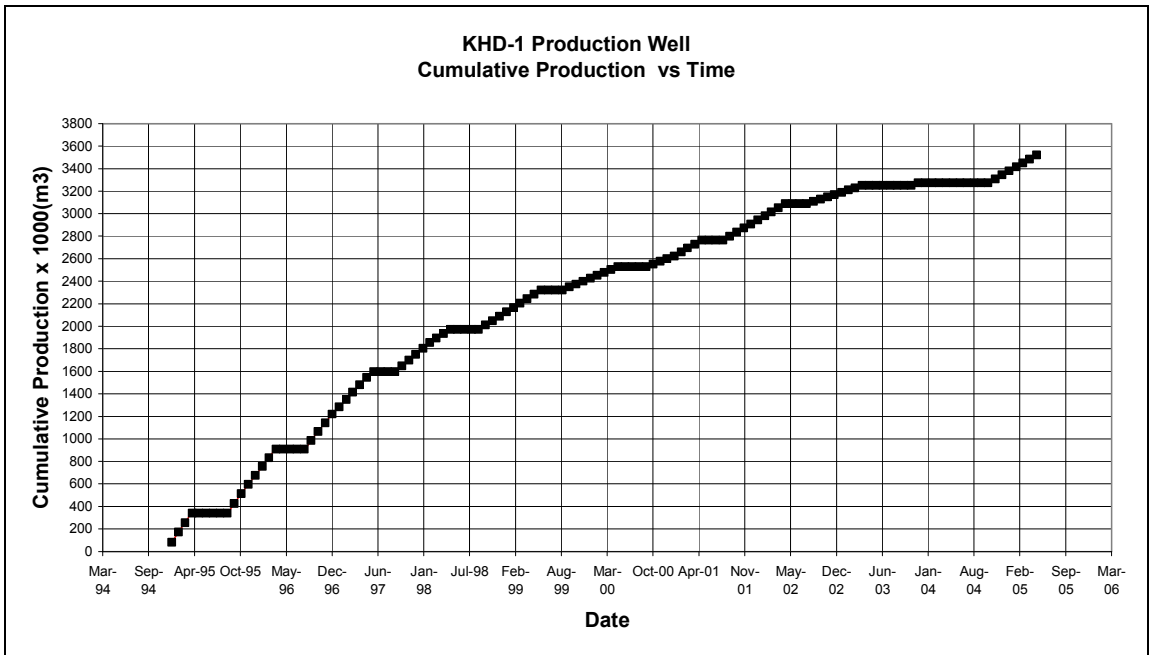
Figure 8.8 Cumulative production history of KHD-1 Geothermal Well
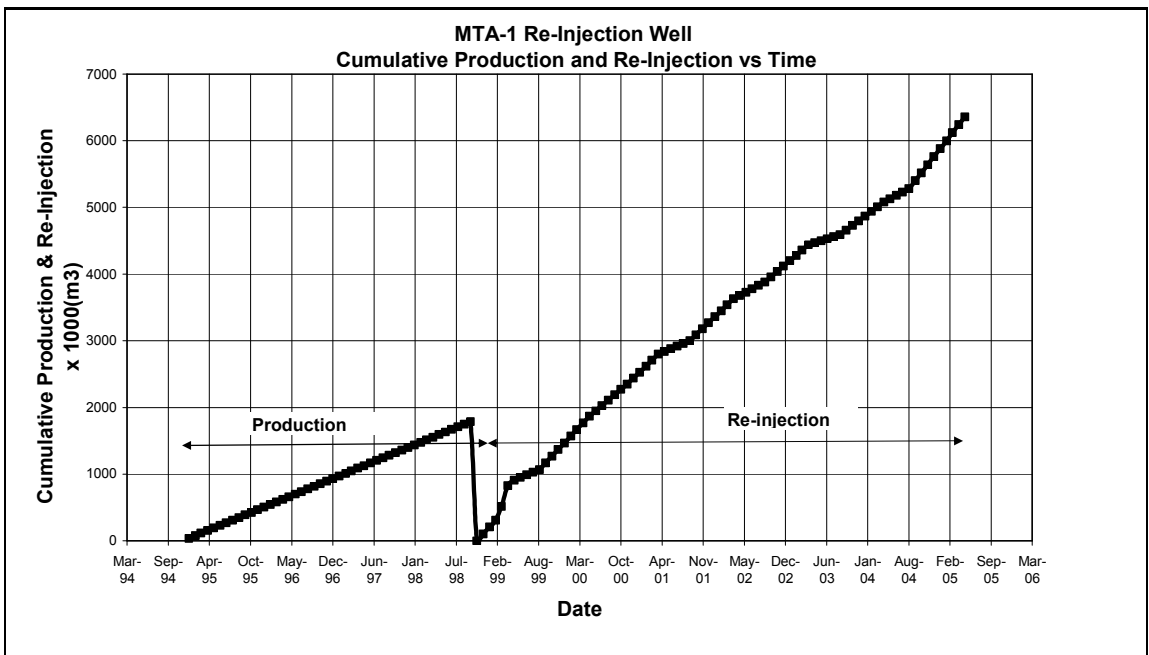
Figure 8.9 Cumulative production history of MTA-1 Geothermal Well

63

8.3. Temperature Analysis

Temperature measurements of the wells are given in Figure 8.10 through 8.17. MTA-1 was used as production well up to July 98 after this date re-injection started. The well head temperature was 75-80 °C before the start of reinjection but dropped to 42°C after re-injection. It can be observed that temperature increased when a well was shut-in during summer seasons. Temperature of the field seems to be not affected by re-injection with the exception of IHL-1 and MTA-1. MTA-1 is a re-injection well so it is expected. On the other hand, there is a sudden drop in temperature of IHL-1 which is a producer relatively far from the reinjection well. Such drop in temperature may occur a result of fresh and cold water intrusion into the well possibly due to a mechanical failure such as cement bond or casing / liner failure(s).
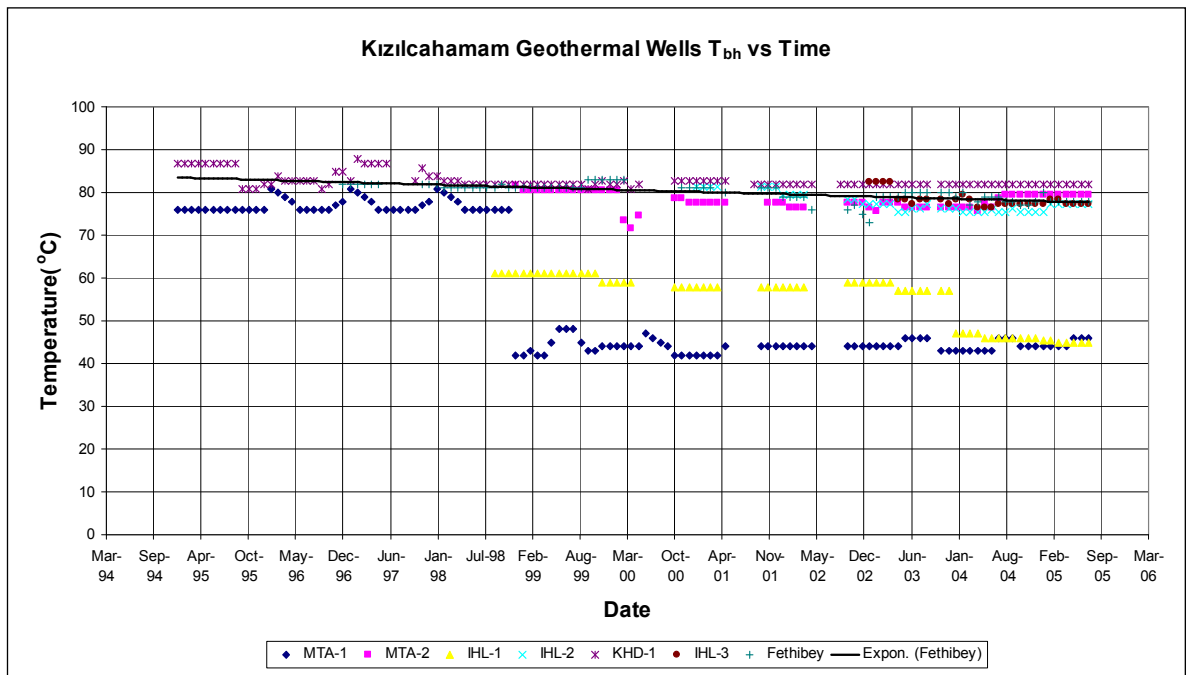
Figure. 8.10 Kızılcahamam Geothermal Well Bottom Hole Temperature History
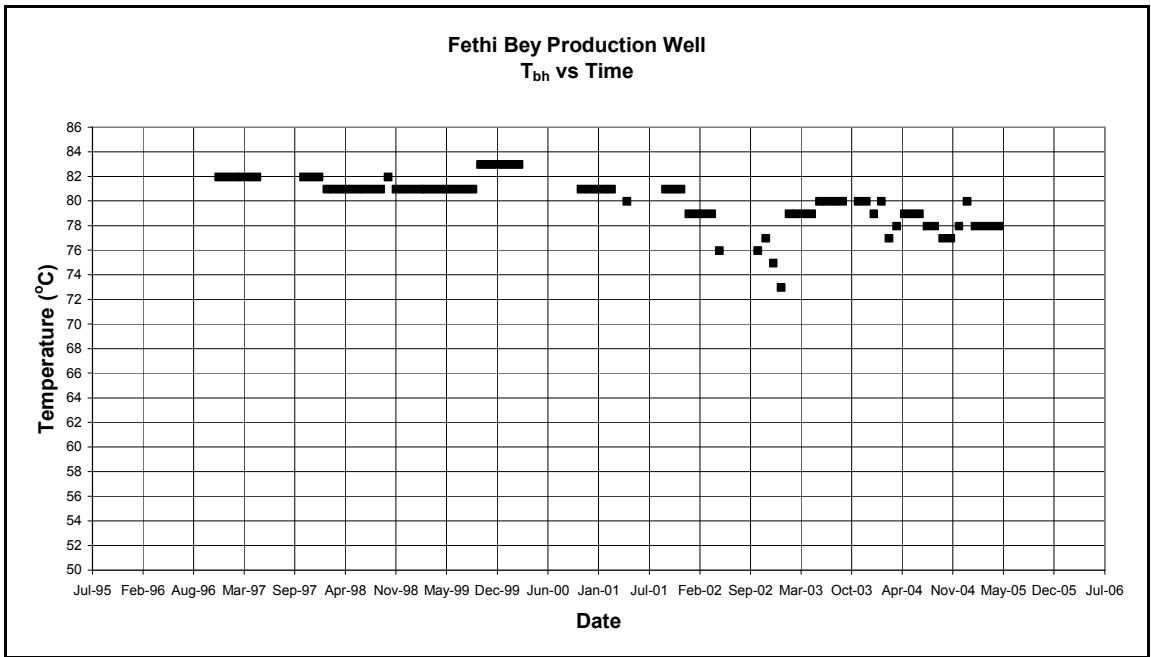
Figure 8.11 Fethi Bey Production Well Bottom Hole Temperature History
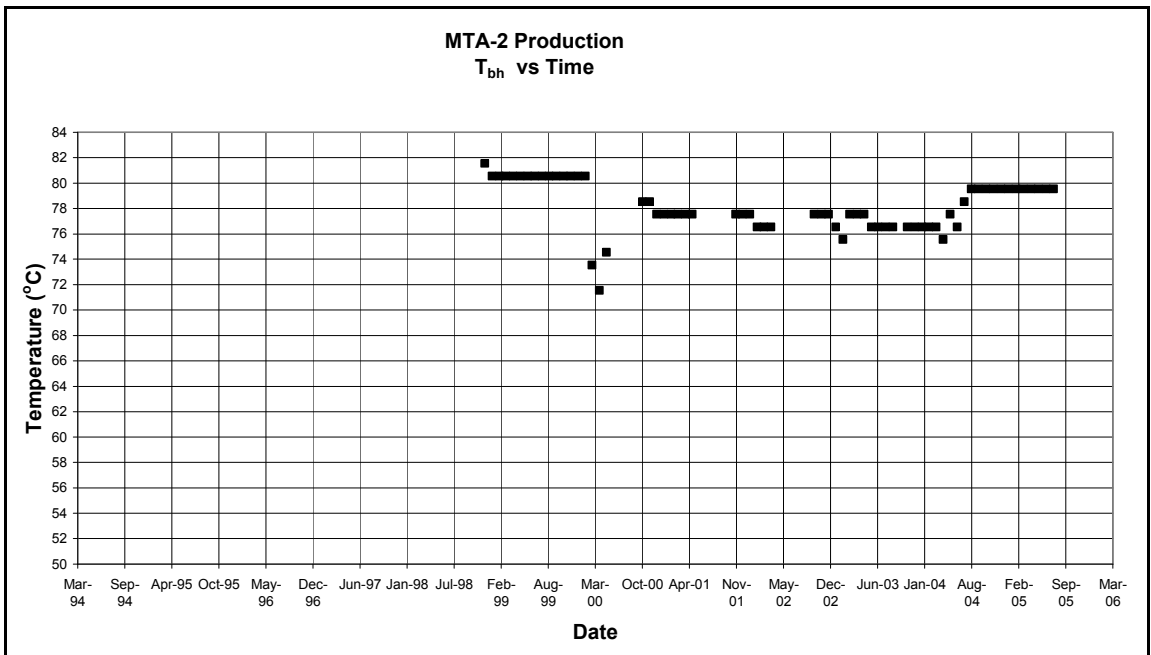
Figure 8.12 MTA-2 Production Well Bottom Hole Temperature History
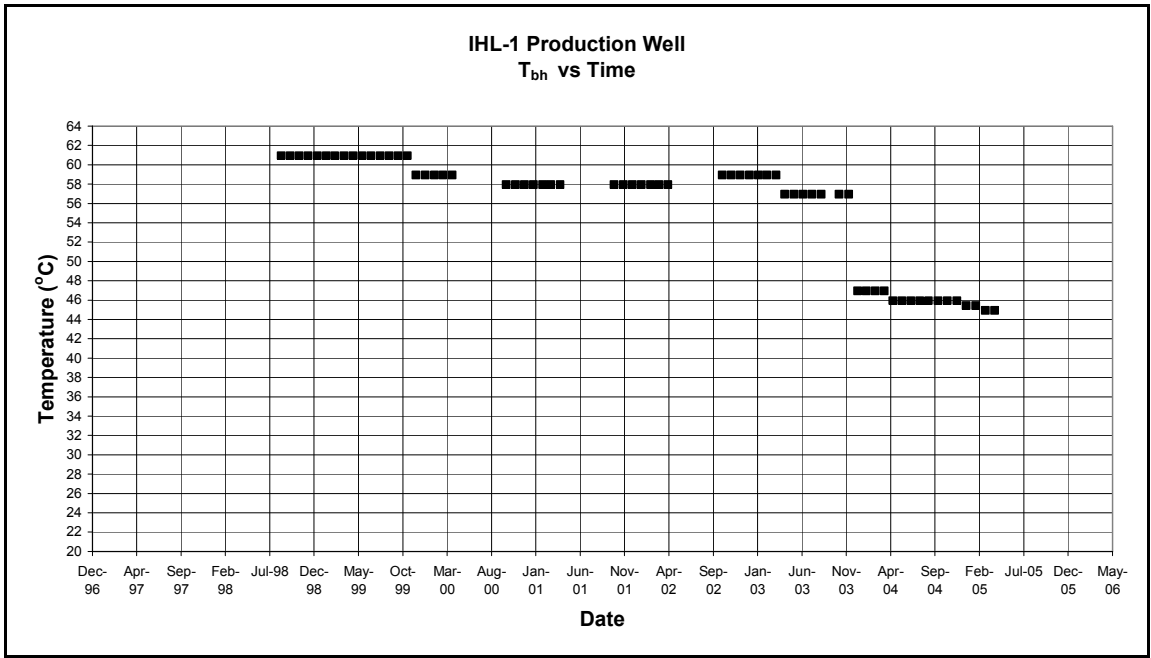
Figure 8.13 IHL-1 Production Well Bottom Hole Temperature History
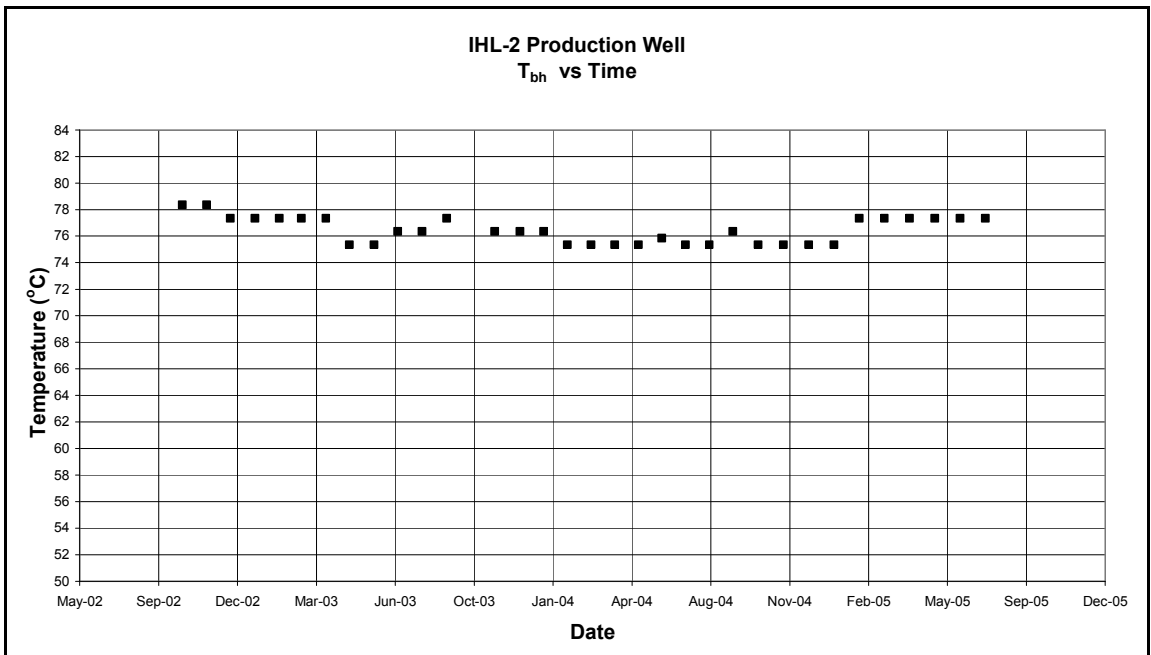
Figure 8.14 IHL-2 Production Well Bottom Hole Temperature History
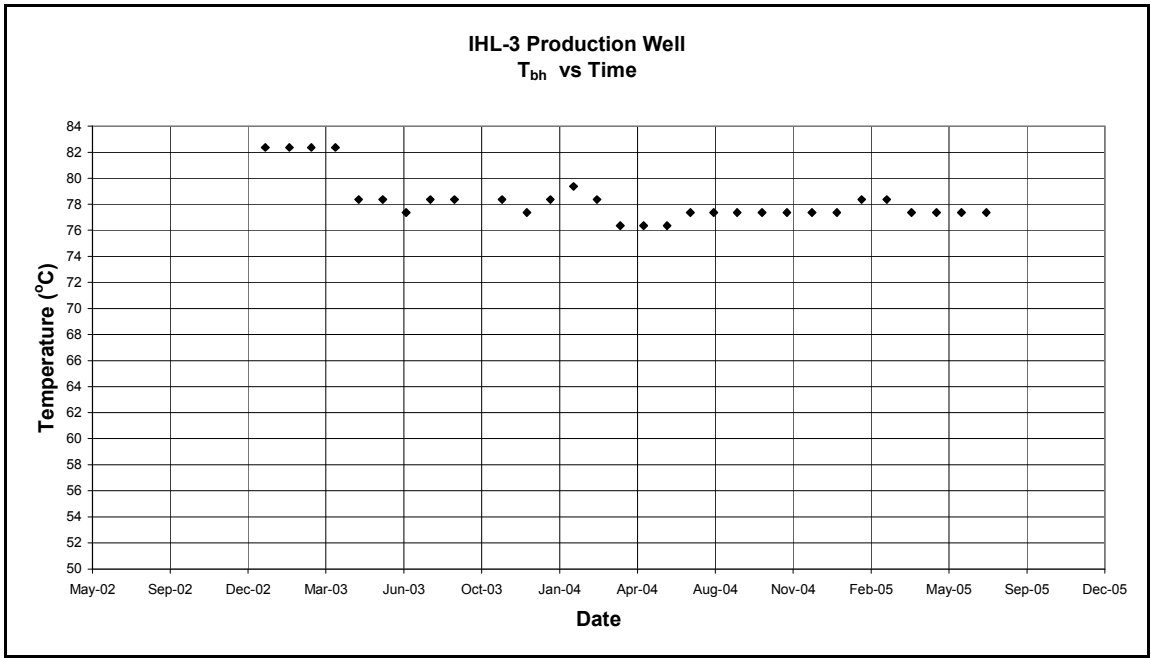
Figure 8.15 IHL-3 Production Well Bottom Hole Temperature History
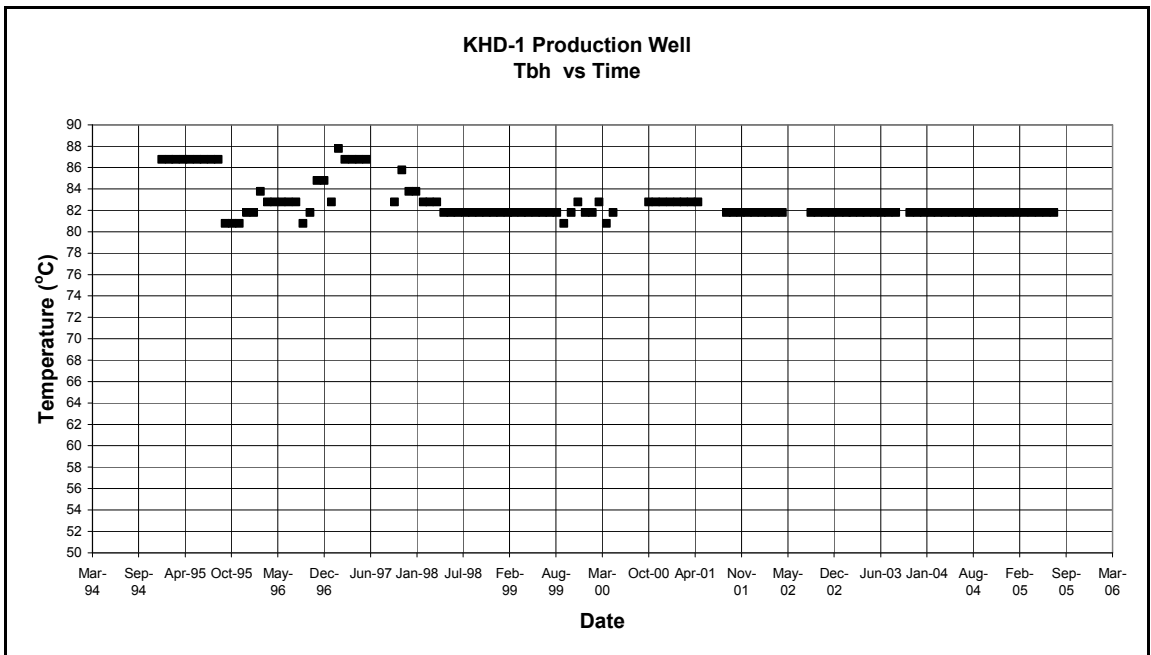
Figure 8.16 KHD-1 Production Well Bottom Hole Temperature History

67
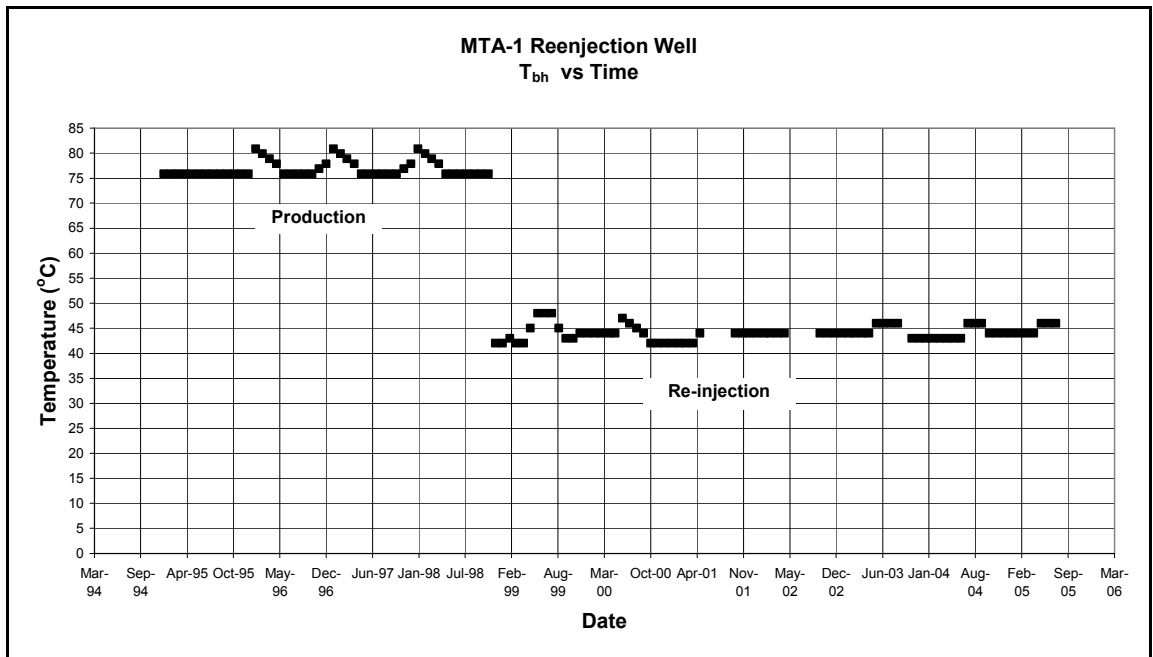
Figure 8.17 MTA-1 Re-injection Well Bottom Hole Temperature History

8.4. Pressure Analysis

Pressure decline is more pronounced than temperature decline. For that reason pressure analyses and evaluation is more important for the Kızılcahamam Geothermal Field.

A regression analysis was conducted to quantify the decline. Results are given in Figure 8.18 through 8.24 and Table 8.1. From these slopes it is possible to calculate the dynamic level in the coming years. Table 8.2 gives the expected dynamic levels that will be reached in 2011 .It will be seen that the lowest level be in well IHL-1 well as 80 meter in 2011.

Table 8.1 Bottom Hole Pressure (kPa) vs Years

	MTA-2	KHD-1	IHL-1	IHL-2	IHL-3	Fethibey
Jan-95		16089				
Jan-96		16039				
Jan-97		15867				
Jan-98		15766				
Jan-99	2613	15746	5450	6262	6343	5088
Jan-00	2575	15736	5410	6255	6340	5058
Jan-01	2575	15726	5380	6240	6325	5097
Jan-02	2546	15665	5370	6220	6320	5017
Jan-03	2546	15615	5310	6195	6301	4998
Jan-04	2517	15867	5300	6180	6270	4998
Jan-05	2498	15867	5290	6150	6241	4969

Table 8.2 Dynamic Level vs Year

Well Name	1999 Dyn. Level (m)	2005 Dyn. Level (m)	2011 Dyn. Level (m)
Fethi Bey	40	53	75
MTA-2	49	63	75
IHL-1	50	65	80
IHL-2	50	60	71
IHL-3	46	56	64
KHD-1	8	11	41
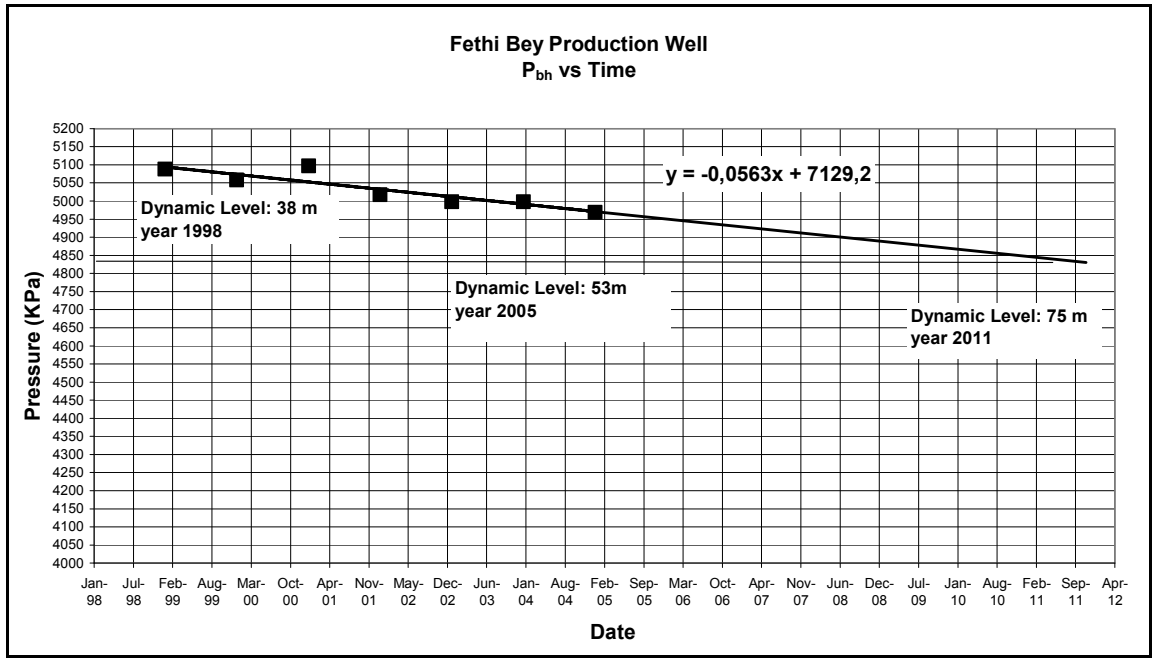
Figure 8.18 Fethi Bey Production Well Bottom Hole Pressure History
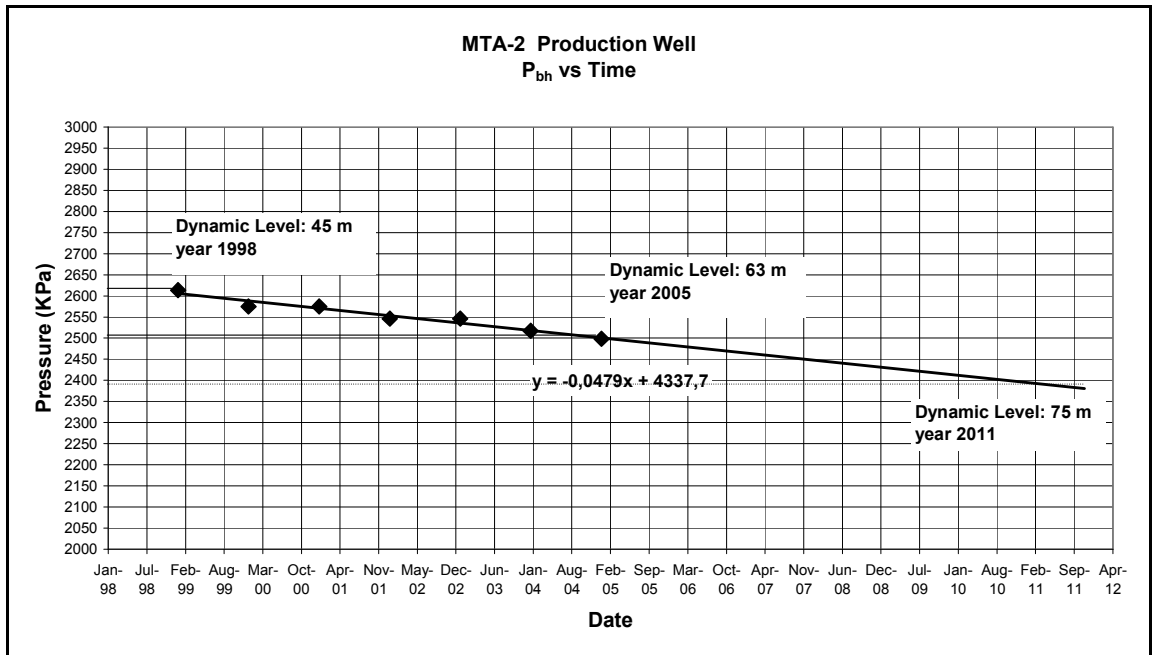
Figure 8.19 MTA-2 Production Well Bottom Hole Pressure History

70
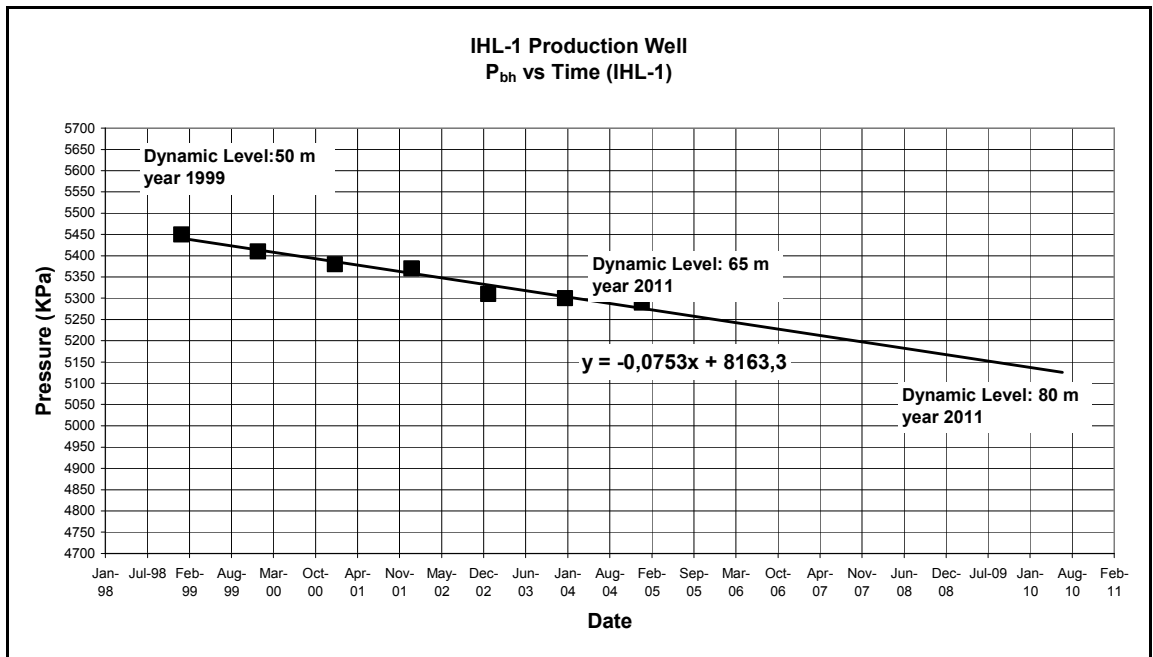
Figure 8.20 IHL-1 Production Well Bottom Hole Pressure History
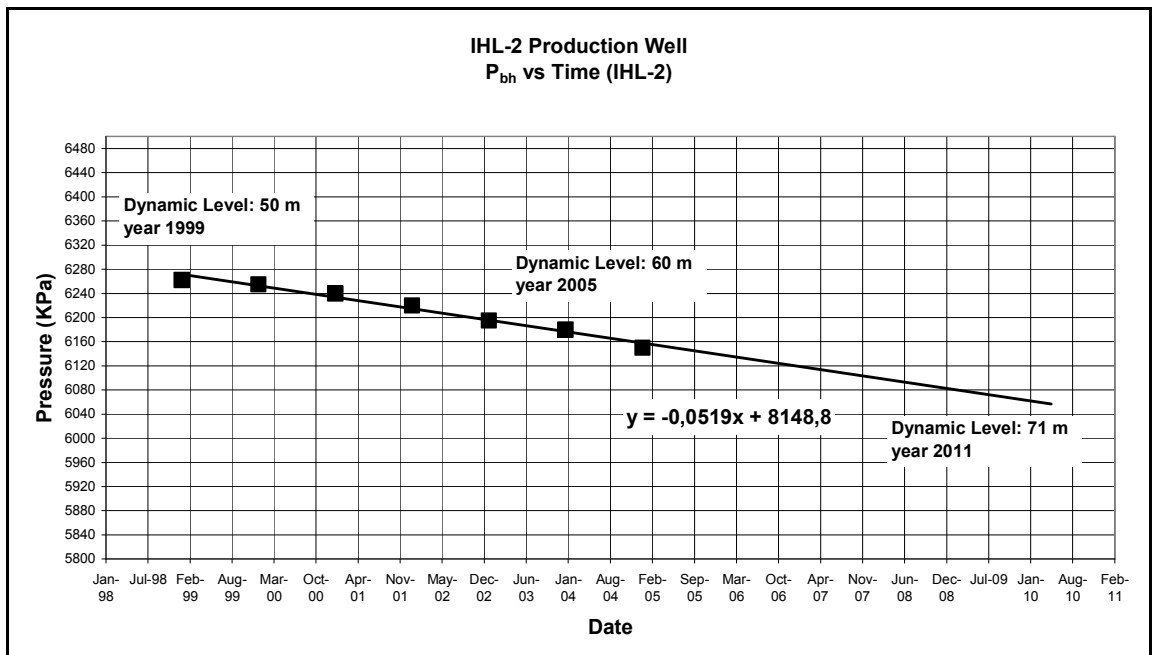
Figure 8.21 IHL-2 Production Well Bottom Hole Pressure History
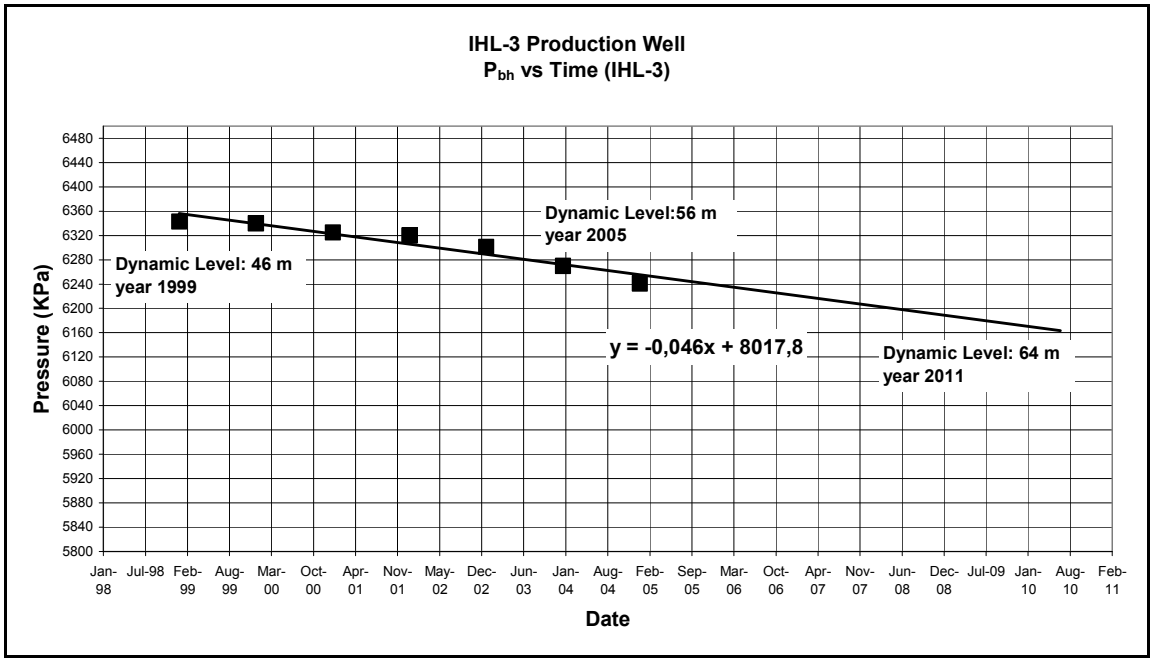
Figure 8.22 IHL-3 Production Well Bottom Hole Pressure History
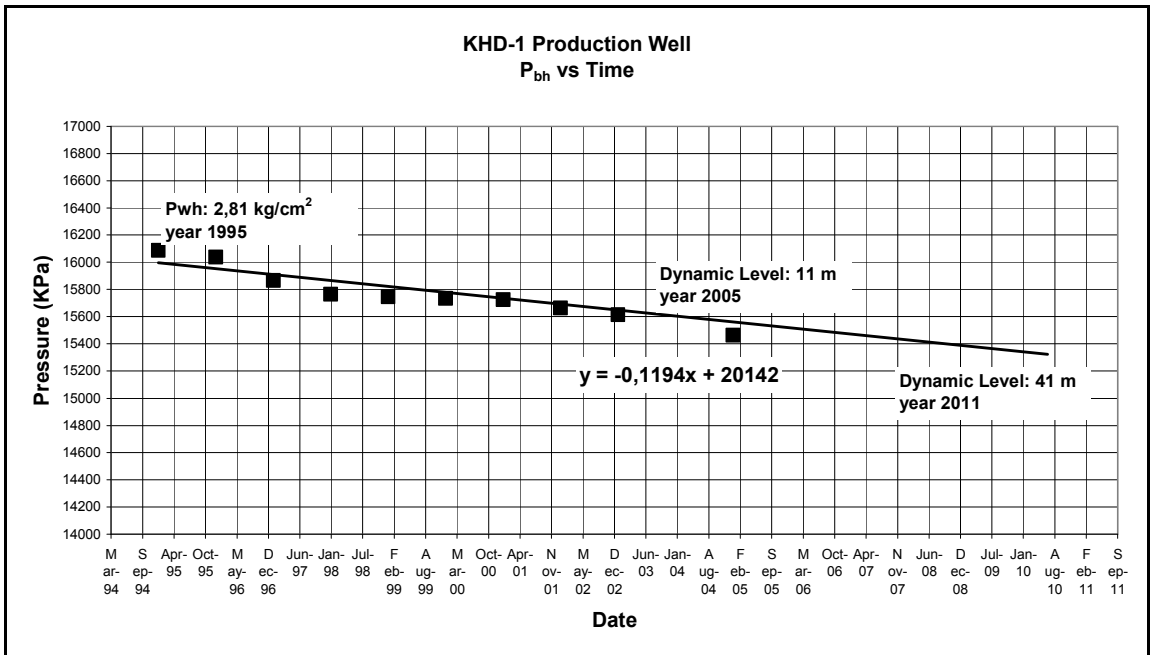
Figure 8.23 KHD-1 Production Well Bottom Hole Pressure History
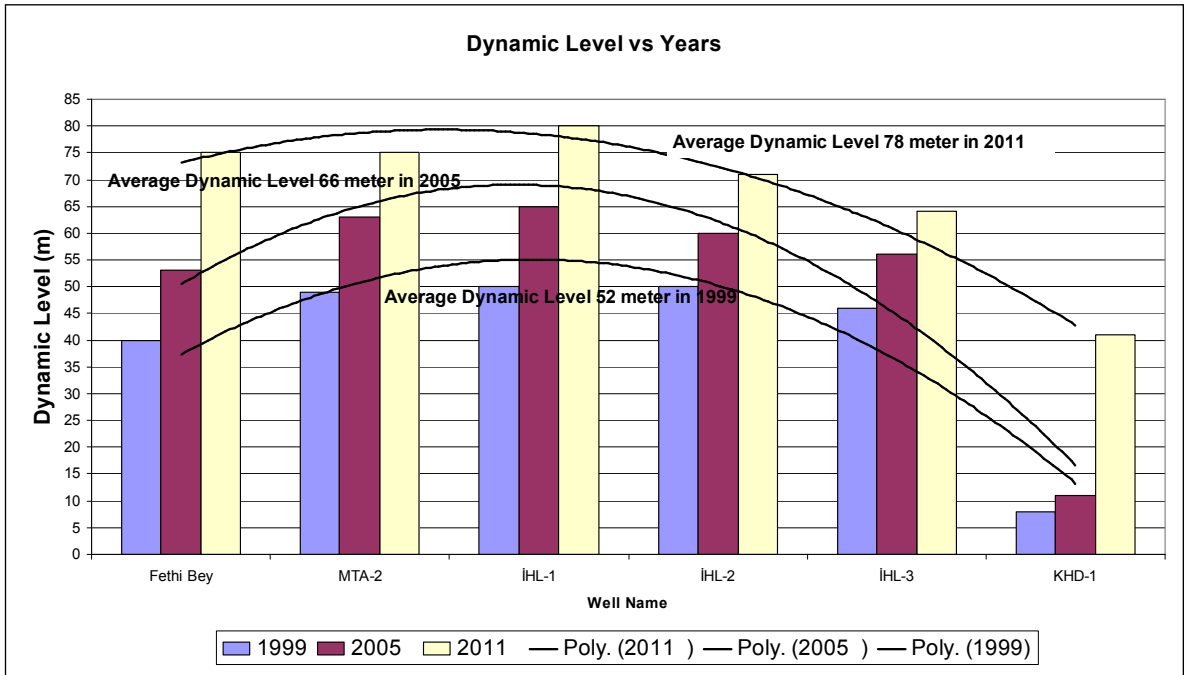
Figure 8.24 Kızılcahamam Geothermal Wells Bottom Hole Pressure History

The average water level was 52 meter in 1999. It is 66 meter in 2005 and this number will be 78 meter in 2011. It means that 141 kPa pressure decrease between 1999-2005 has occurred and, 120 kPa pressure decreases will occur up to 2011(Figure8.24).

8.5. Tracer Analysis

The tracer test results are given in Figure 8.25 through 8.35. As can be seen from these Figures the injected tracer reached to all wells including IHL-1 and IHL-3. This shows that all the wells in the field are connected to each other with a fracture system. Using the tracer breakthrough time obtained from this production well (Figure. 8.30) and the distance between the re-injection well (MTA-1) and IHL-1 (1400 m) the apparent velocity is calculated as 5.38 m/h. Table 8.3 gives apparent velocities calculated for each well. The highest apparent velocity is observed between MTA-1 and Fethibey. Tracer concentration of reinjection water which are produced from MTA-2, Fethibey is given in in figure 8.27. It means that we were injecting the tracer to the MTA-1 reinjection well. The tracer concentration amount which is injected is 4-18 ppb, so this value is very small so it is omitted for the EHTD model.
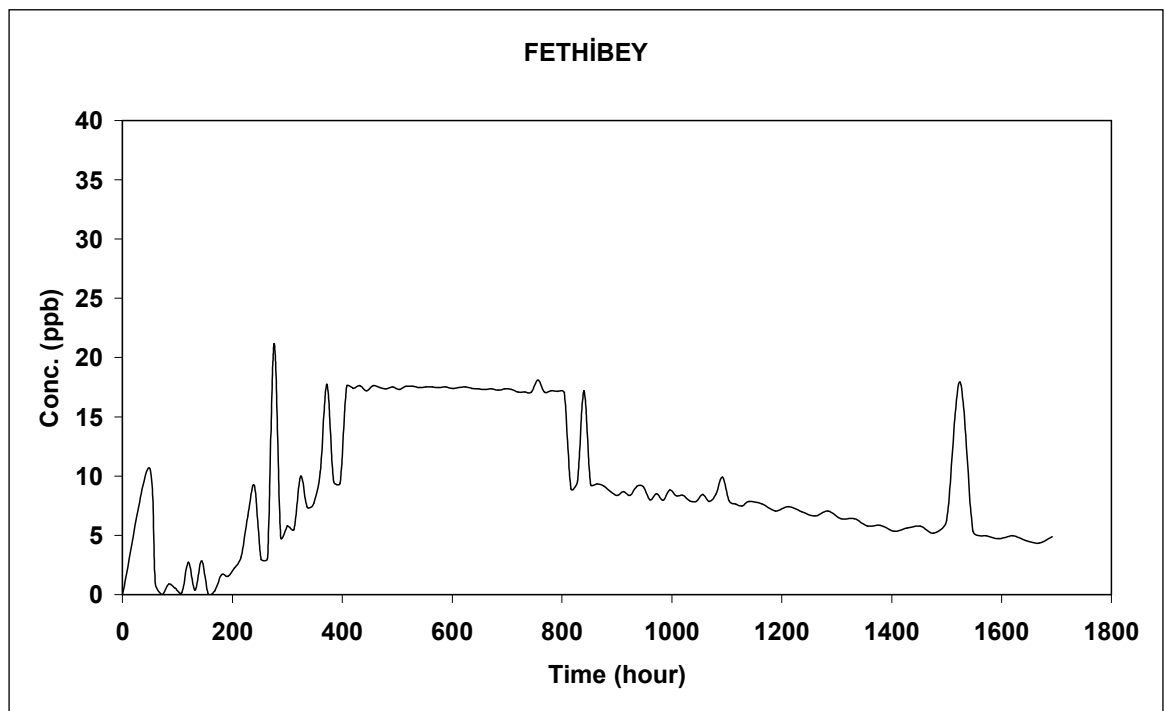
Figure 8.25 Fethi Bey Tracer Concentration vs Time

74
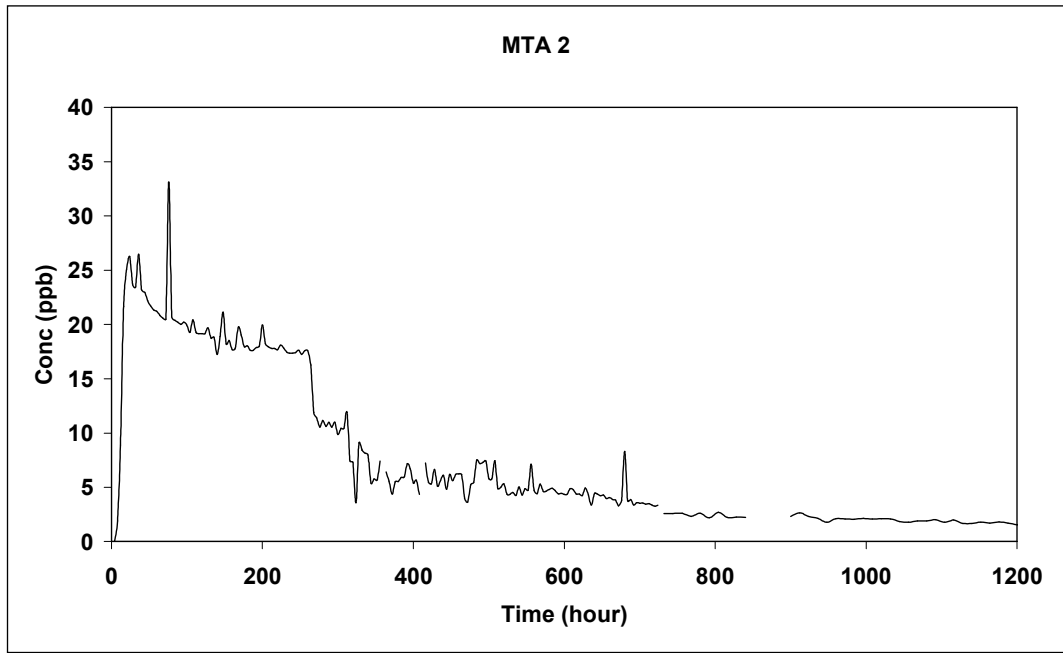
Figure 8.26 MTA-2 Tracer Concentration vs Time
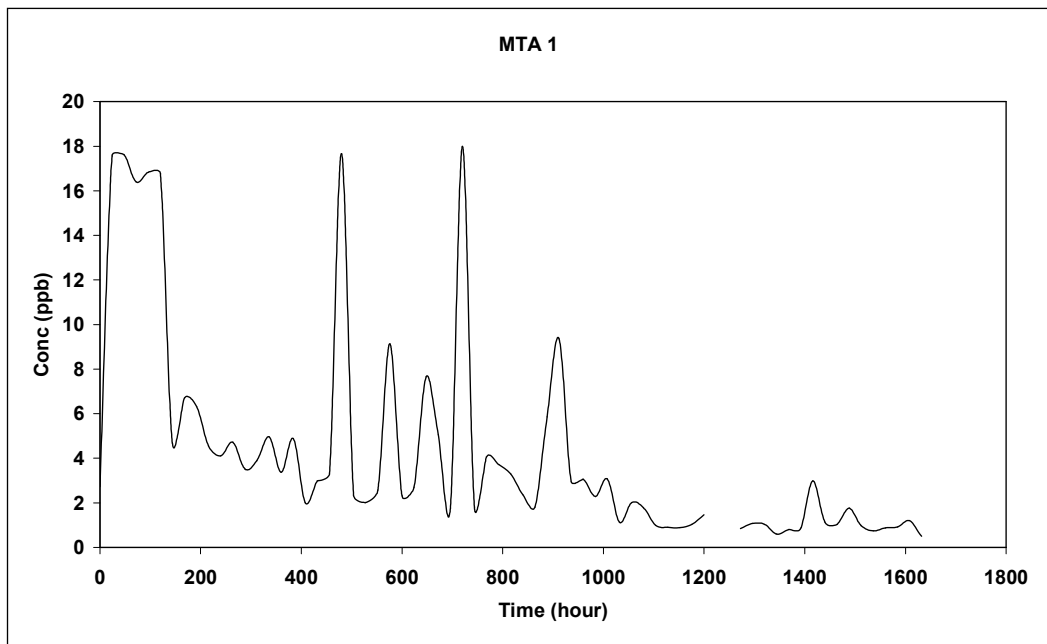
Figure 8.27 MTA-1 (reinjection water) Tracer Concentration vs Time
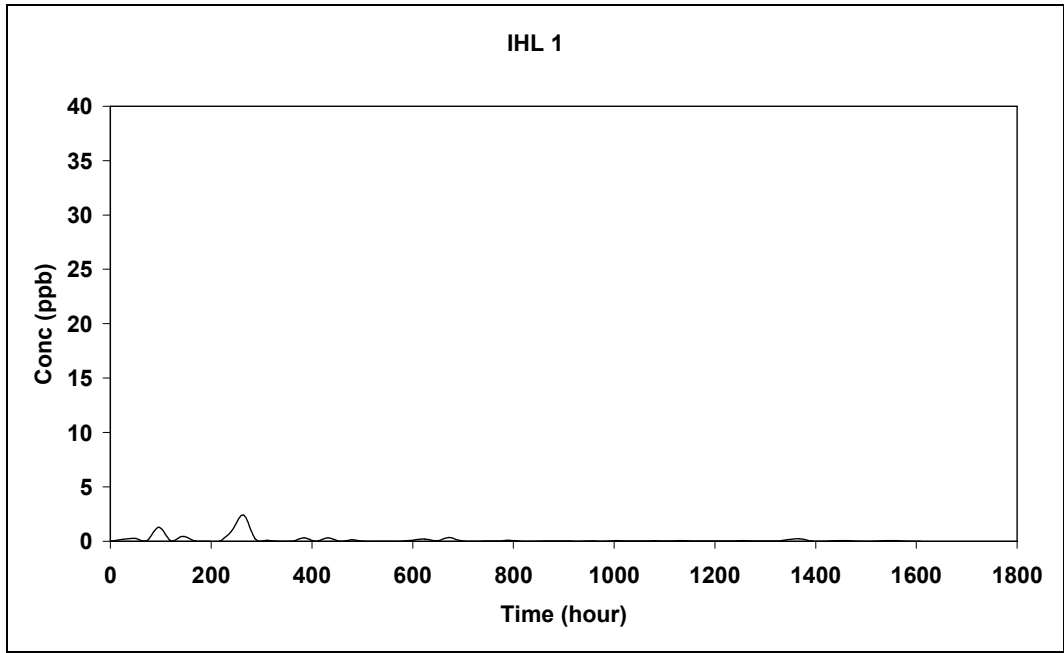
Figure 8.28 IHL-1 Tracer Concentration vs Time
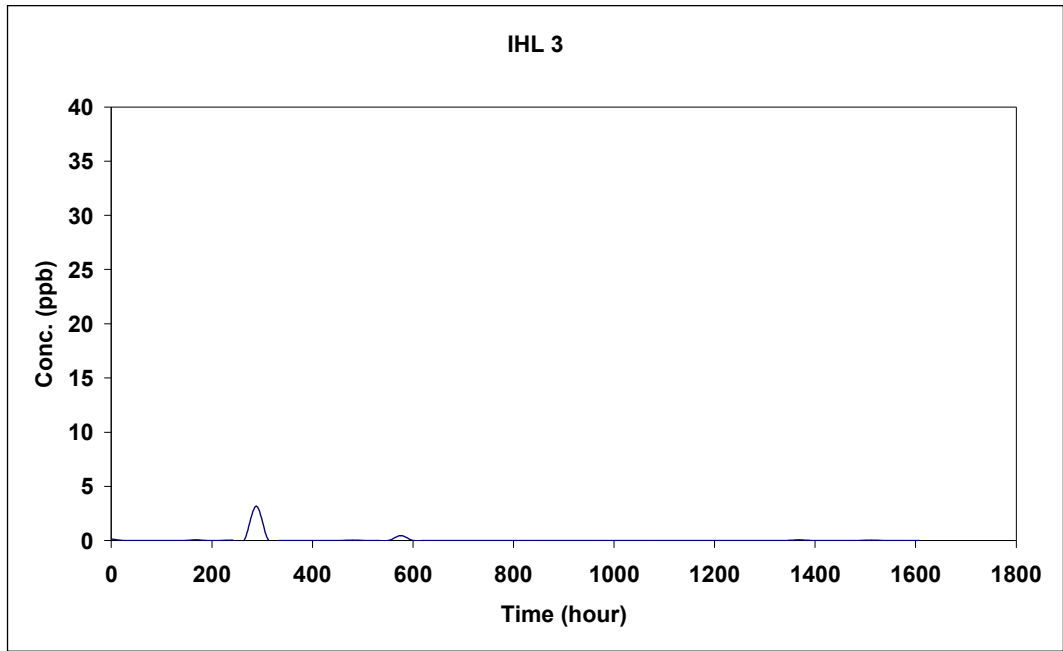
Figure 8.29 IHL-3 Tracer Concentration vs Time

Tracer concentration time plots were analyzed using the mathematical models given in Chapter 6 and the methodology reported in Chapter 7. Sum of squares residual values were used to identify the best matching model for the tracer return curves

reported for Fethibey and MTA-2 wells. The tracer data obtained from other wells were not analyzed as they are limited. The smallest sum of squares residuals was obtained using the multi-fracture model (Table 8.4) for both wells.

The uniform porous models were not as successful as the other models. Moreover, they are physically not representative of the Kızılcahamam field since the formation is believed to be fractured. Like wise double porosity models (i.e. double porosity cubes and slabs and double porosity pseudo steady state) and the fracture matrix models are physically not representative since they assume that flow occurs both in fracture and the matrix. However, as stated above, the producing formation in Kızılcahamam field is fractured and the matrix permeability is known to be very small [25].

In this regard, single fracture and multi-fracture models are the only models that physically represent the field. Of these models, single fracture model assumes that only one apparent fracture connects the injection well and the producing well. As can be seen since the sum of square residuals obtained using this model were not less than the ones obtained using the multi-fracture model, the multi fracture model is chosen as the best representing the fast flows occurring in the field. Beside the multi-fracture model second best models are double porosity cubes and double porosity slabs model. These three model can represent the flows in this field. These results show that Kızılcahamam field is not homogeneous field that can be represented using simple homogeneous models such as uniform porous models and single fracture model (Figure 8.32, Figure 8.33).
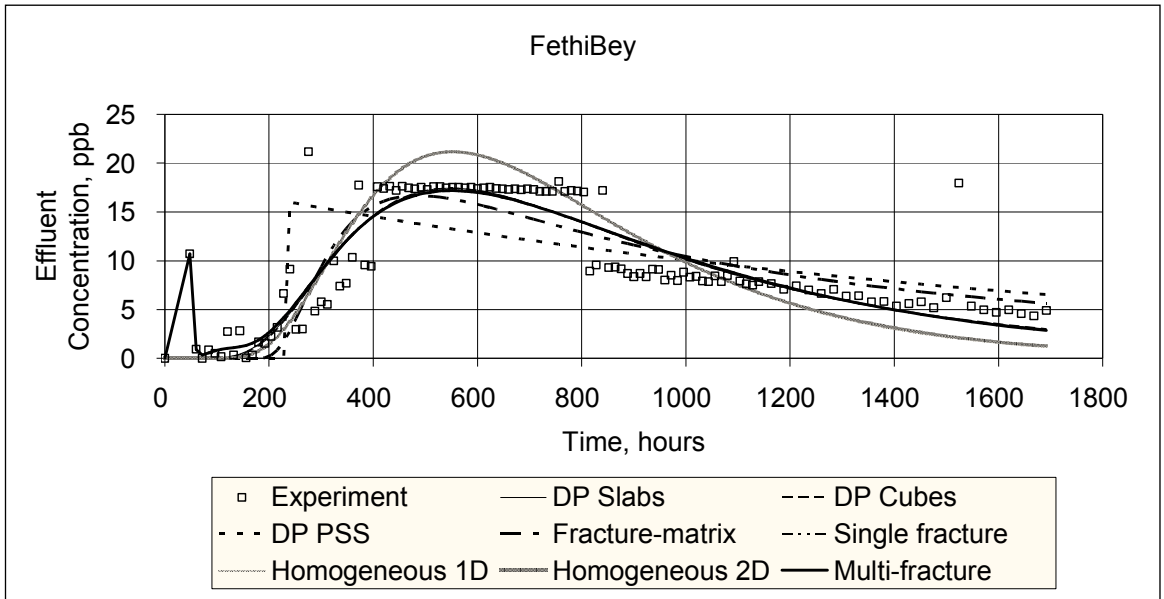
Figure 8.30 Fethibey Matching Model for the Tracer Return Curves
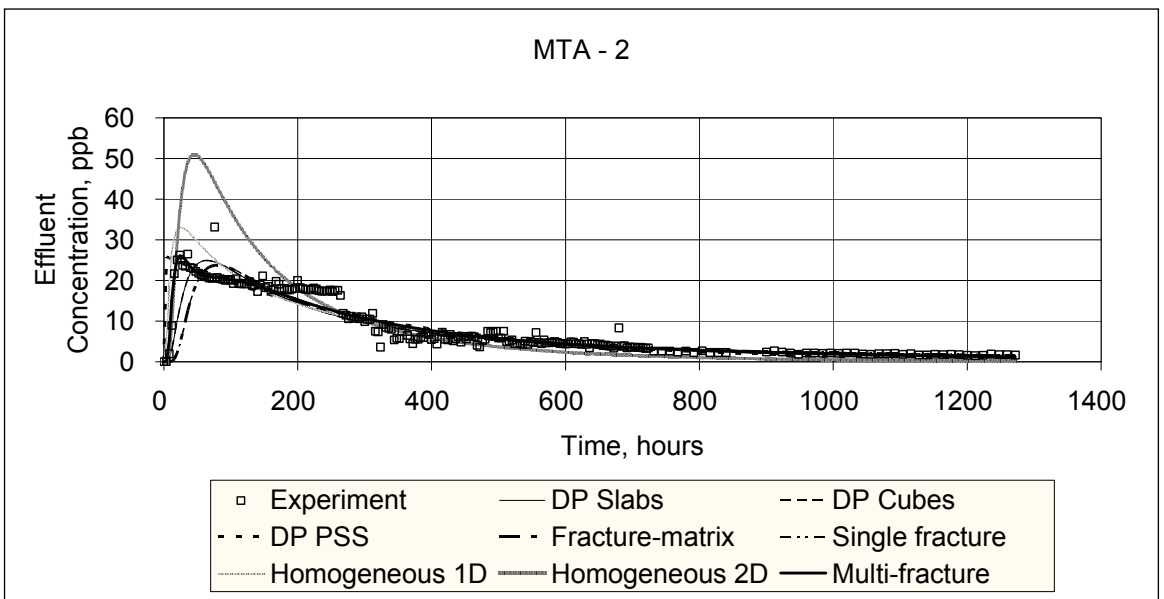
Figure 8.31 MTA-2 Matching Model for the Tracer Return Curves
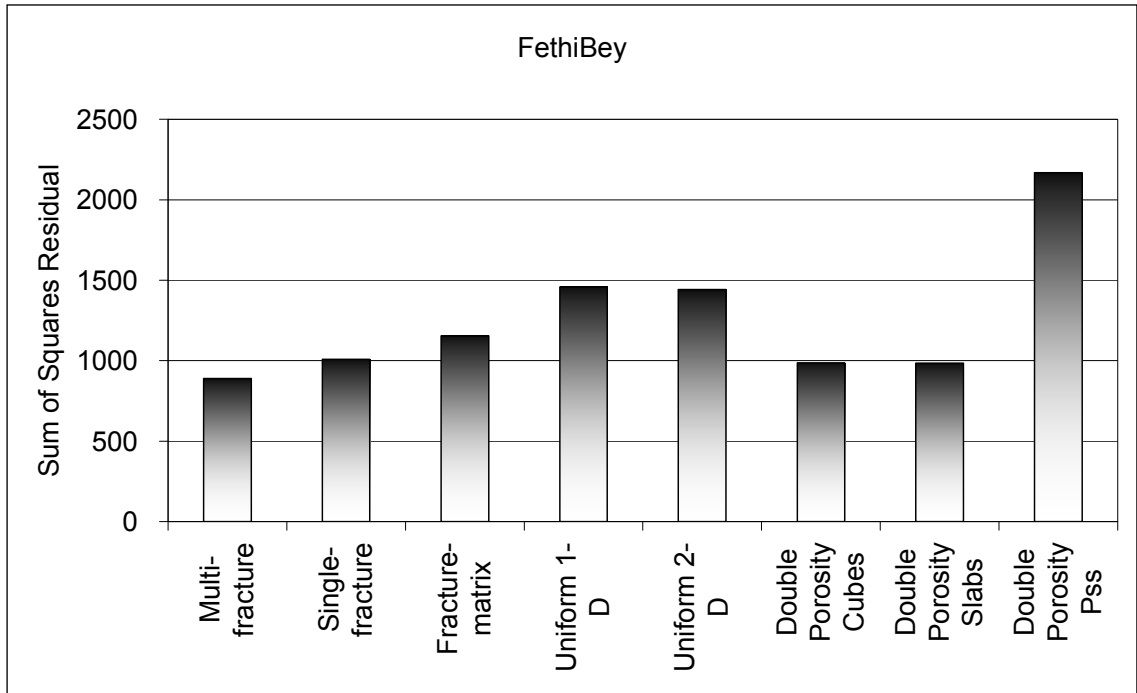
Figure 8.32 Comparison of analyzed data with mathematical models for Fethi Bey
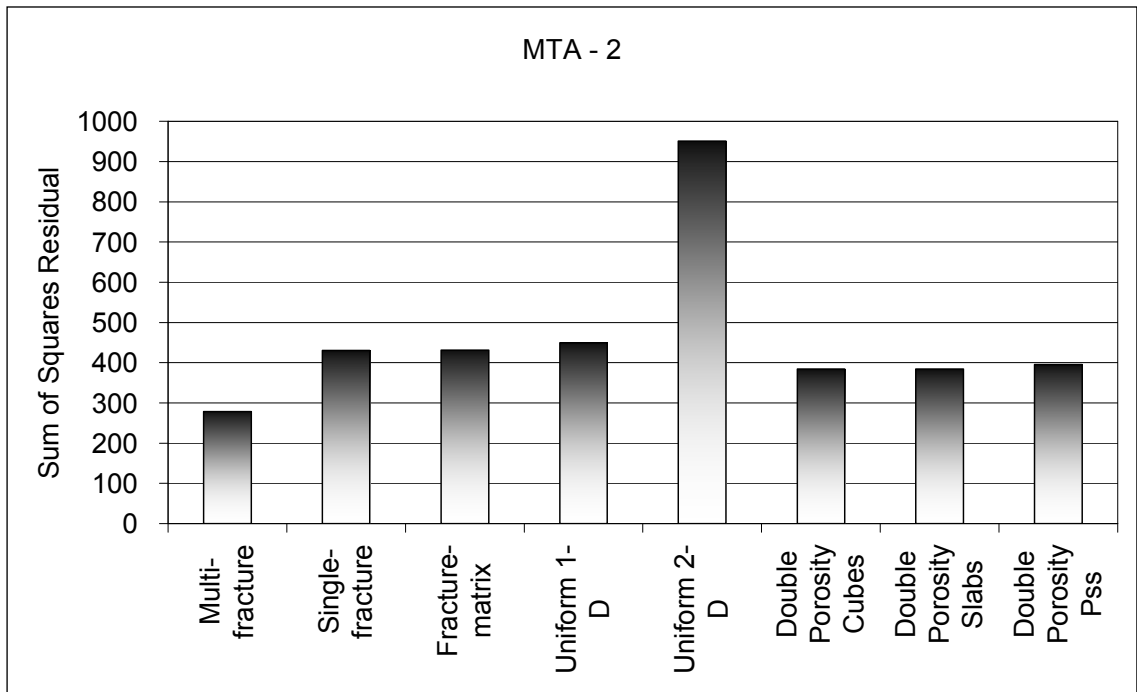
Figure 8.33 Comparison of analyzed data with mathematical models for MTA-2
Using the multi fracture model a detailed analysis will be reported. As can be seen in Figure 8.32 and 8.33 three apparent fractures represent the system. Lower number of fractures (i.e. 2 fractures) does not result in a better sum of squares residual.
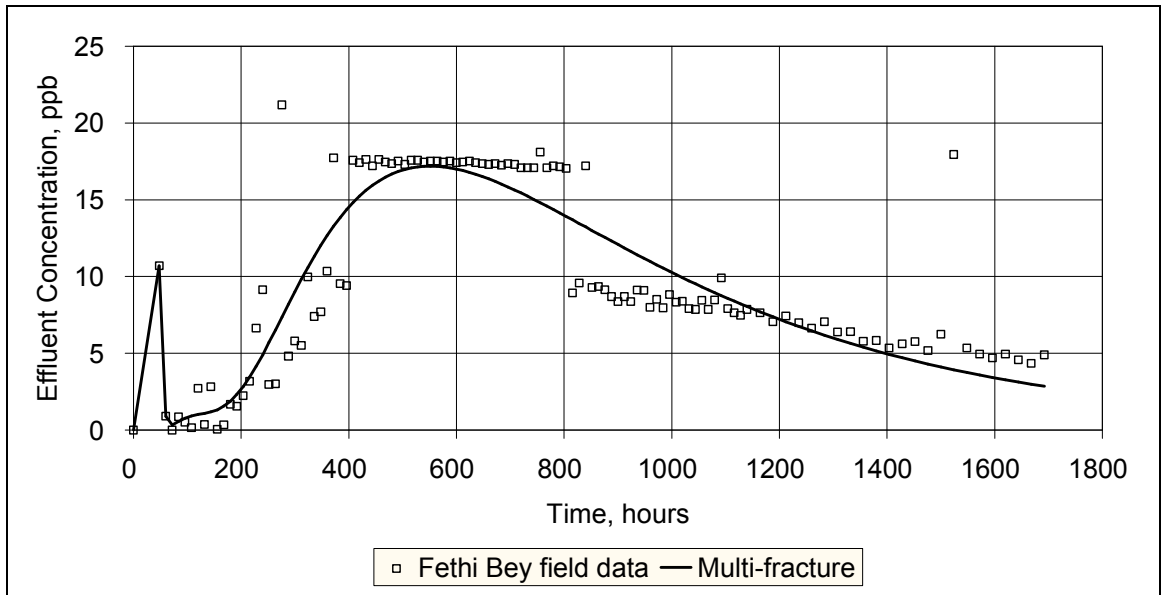
Figure 8.34 Fethibey Multi-fracture Model Curve
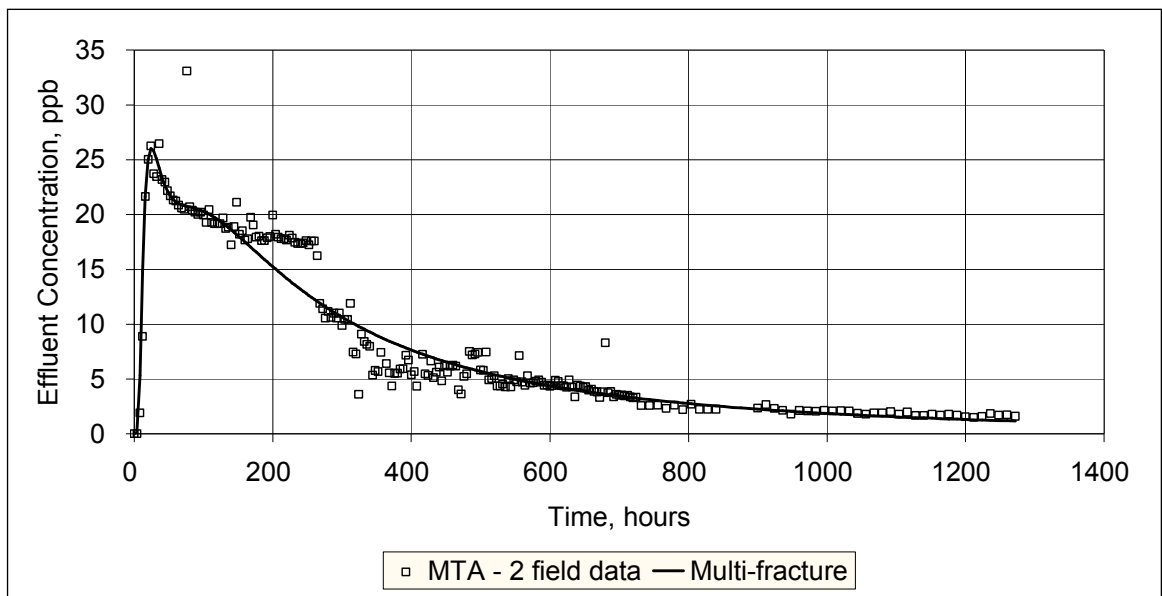
Figure 8.35 MTA-2 Multi-fracture Model Curve

On the other hand, it is possible to obtain a better match using larger number of fractures. However, the sum of squares residuals does not improve drastically. Thus, 3 fractures are enough to represent the system. (Appendix B) The multi-fracture model match parameters for Fethi Bey and MTA-2 wells are reported in Table 8.4 and 8.5.

Table 8.3 Apparent Velocity of Wells

Well Name	Surface Distance from MTA-1 (m)	Well bore Distance fromMTA-1 Well bore (m)	Breakthrou-gh Time (hour)	Apparent Velocity m/h
MTA-2	45	100	48	2,08
Fethi Bey	543	600	84	7,14
IHL-1	1400	1420	264	5,38
IHL-3	1045	1130	288	3,92

In Fethi Bey well there is a fast, thin and long hypothetical fracture with a small flow contribution (e=0.01), one medium velocity smaller fracture and one big aperture slow fracture. Peclet numbers in these fractures are 70.61, 15.2, and 5.44 respectively. The mean arrival times and dispersivities are also reported in Table 8.4.

Table 8.4 Fethi Bey matching parameters

W,Peclet number	L, Fracture Length(m)	t_m, hours mean arrival time	e, % dimensi-onless contribu-tion	m, ppb mass of tracer	D_l, m^2 longitudinal dispersivity	U, m/hour Fracture Velocity
70.61	7425.20	40.33	0.01	5728674.88	56.19	9.92
5.44	968.97	932.70	0.18	12949764.66	31.52	0.43
15.20	6.11	146.92	0.81	19399.08	71.64	2.72
						4,36

In MTA-2 well there is a fast, thin and long hypothetical fracture with a small flow contribution (e=0.07), one medium velocity smaller fracture and one big aperture slow fracture. Peclet numbers in these fractures are 50.92, 1.44, and 1.77 respectively. The mean arrival times and dispersivities are also reported in Table 8.5.

Table 8.5 MTA - 2 matching parameters

W,Peclet number	L, Fracture Length(m)	t_m, hours mean arrival time	e, % dimensionless contribution	m, ppb mass of tracer	D_l, m^2 longitudinal dispersivity	U, m/hour Fracture Velocity
50.92	0.41	46.24	0.07	395.13	0.38	0.65
1.44	529.47	624.59	0.10	11242242.88	1.00	0.05
1.77	49.73	89.93	0.83	362131.75	5.66	0.33
						0,35

When the average multi-fracture velocities of Fethi Bey (Table 8.4) and MTA-2 (Table 8.5) Wells are compared to their apparent velocities (Table 8.6) it can be seen that apparent velocities are more than the multi-fracture velocities for Fethi Bey and MTA-2 Wells. For the computation of apparent velocities tracer breakthrough times and the lengths between the wells are used. But the geothermal fluid probably flows through a

tortuous path rather than a straight line. Thus, due to tortuosity the length between the wells will be larger than the geographical length. Thus the velocities should be smaller. Therefore the tortuosity between MTA-1 and Fethi Bey is smaller (7.14/4.36=1.637) compared to tortuosity between MTA-1 and MTA-2 (2.08/0.35=5.943).Effect of the main fracture and secondary fractures (faults) can be seen on fracture velocities, dispersion and direction of tracer. The geological models for Kızılcahamam geothermal field proposed by Gevrek and Aydin [38] and Özbek [20]. confirm the multifracture model that we have studied.

Table 8.6 Comparison of Apparent Velocity and Fracture Velocities

Well Name	Apparent Velocity (m/h)	Fracture Velocity (m/h)
Fethi Bey	7,14	4,36
MTA-2	2,08	0,35

CHAPTER 9

CONCLUSIONS

The following conclusions can be drawn from the analysis of the results of this study:

1. Two wellbores in the field show temperature decline, MTA-1 and IHL-1. The decline in temperature in MTA-1 is the reinjection scheme applied in this wellbore. However, it is believed that a cold water zone encroachment is responsible due to cement failure or mechanical problems (casing failure) in the wellbore.

2. Although a reinjection scheme is applied in the Kızılcahamam geothermal field a decline in pressure is still observed while the temperature drop is insignificant.

3. The average water level was 52 meter in 1999 and 66 meter in 2005. It is estimated that it will drop to 78 meter in 2011. This means that there was 141 kPa decline in pressure between 1999-2005 and an additional 120 kPa drop in pressure is expected for the period of 2005-2011.

4. Total production to reinjection ratio was found as 3.2. This ratio is relatively high for a low temperature geothermal field and the consequence is that pressure decline is more than it should be.

5. The interpretation of tracer test shows that there is communication between reinjection well (MTA-1) and other wells in the field.

6. Production well are drilled only Kızılcahamam main and secondary fracture zone which is confirmed multifracture model in Kızılcahamam geothermal field for that reason production well effect each other.

7. Multifracture tracer model with three fractures is the most suitable model to describe the Kızılcahamam low temperature geothermal field. Beside the multi-fracture model second best models are double porosity cubes and double porosity slabs model.

8. Kızılcahamam field is not a homogeneous field that can be represented using simple homogeneous models such as uniform porous models and single fracture model.

9. Apparent velocities are more than the multi-fracture velocities for Fethibey and MTA-2 Wells.

10. Tortuosity between MTA-1 and FethiBey is smaller (7.14/4.36=1.637) compared to tortuosity between MTA-1 and MTA-2 (2.08/0.35=5.943).

11. Fethi Bey apparent velocity is 7.14 m/h and fracture velocity 4.36 m/h, MTA-2 apparent velocity is 2.03 m/h and fracture velocity is 0.35 m/h.

CHAPTER 10

RECOMMENDATIONS

The following points are recommended for further studies on the subject:

1. An extensive search should be carried out to find the reason of sudden cooling in IHL-1. If the reason is cold water encroachment due to casing failure as it was postulated in this study, a remediation job should be planned. It is also recommended to devise a procedure for casing material selection and cementation for new wellbores to be drilled in Kızılcahamam geothermal field.

2. The amount of reinjected fluid could be increased for pressure maintenance without having a cooling effect in the system. The ratio between production and reinjection wells which is 3.2 can be reduced to a smaller number (for example 1.5) for good pressure support and efficient management of the field.

3. Beside the MTA-1 well, KHD-1 well should be tested as reinjection well, Injectivity and tracer tests should be carried out in KHD-1 as reinejction well.

4. Monitoring of the geothermal wells which are well head pressures, well head temperatures, dynamic levels and chemistry of produced fluid should be done systematically.

REFERENCES

1. Dickson, M.H. and Fanelli, M.,1995, <u>Geothermal Energy</u>, Unesco Energy Engineering Series, John Wiley & Sons, New York.

2. Bertani,R., (2005) "World Geothermal Generation 2001-2005: State of the Art" Proc. World Geothermal Congress 2005, paper No: 0003 Antalya, Turkey, 24-29 April.

3. Lund, J.W., Freeston, D.H., and Boyd, T.L,2005, "World-Wide Direct Use of Geothermal Energy", Proc. World Geothermal Congress 2005, paper No: 0007 Antalya, Turkey, 24-29 April.

4. Simsek,S.,Mertoglu,O.,Bakir,N.,Akkus,I.,Aydogdu,O.,(2005)"Geothermal Energy Utulisation, Development and Projections-Country Update Report (2000-2004) of Turkey" Proc. World Geothermal Congress 2005, paper No: 0126 Antalya, Turkey, 24-29 April.

5. Garnish , J.D., ed., 1987. ''<u>Geothermal Hot-Dry Rock Technology</u>'', Proc. First EEC/US Workshop on, Geothermics 16, 323—461.

6. Dezayes,C., Genter,A., Hooijkaas,R.H., (2005), ''Deep-Seated Geology and Fracture System of the EGS Soultz Reservoir (France) based on a Recent 5km Depth Boreholes'' Proc. World Geothermal Congress 2005, paper No: 1612, Antalya, Turkey, 24-29 April.

7. Lindal, B., 1973. <u>Industrial and other applications of geothermal energy.</u> In: Armstead, H.C.H., ed., Geothermal Energy, UNESCO, Paris, pp.135—148.

8. Lund, J. W., and Freeston, D., 2001. World-wide direct uses of geothermal energy 2000. Geothermics 30, 29- 68.

9. Gudmunsson, J.S., 1988. The elements of direct uses. Geothermics, 17,119—136.

10. Sanner, B., Karaytsas, C., Mendrinos, D. and Rybach, L., 2003. Current status of ground source heat pumps and underground thermal energy storage. Geothermics, Vol.32, 579-588.

11. Rafeerty, K., 1997. An information survival kit for the prospective residential geothermal heat pump owner. Bull. Geo-Heat Center , 18, 2, 1—11.

12. Barbier, E. and Fanelli, M., 1977. Non-electrical uses of geothermal energy. Prog. Energy Combustion Sci., 3, 73-103.

13. Beall, S. E, and Samuels, G., 1971. The use of warm water for heating and cooling plant and animal enclosures. Oak Ridge National Laboratory, ORNL-TM-3381, 56 pp.

14. 8 th 5 Year Development Plan, 2000, Turkish Republic Prime Ministry State Planning Organization, Geothermal Report.

15. Preliminary Issue of Turkish Geothermal Association, 2005, The Importance of Geothermal Energy for Turkey and New Strategies for the Year 2005,

16. Simsek, S., Mertoglu, O., Kocak, Bakır,N, Akkus,I., Durak, S., Dilemre, A., Sahin, H., Akıllı, H., SUuluder, Y., Karakaya, C., Tan, E., State   Planning Organisation, 8th 5 Year Development   Plan, Geothermal Energy Report, 2001.

17. Mertoglu, O., N. Bakır, T. Kaya, 2003.”Geothermal Application Experiences in Turkey” , European Geothermal Conference, Szeged, Hungary.

18. Akkus. I., Geothermal Applications and MTA, JENARUM Summer School Proceedings, 2002, pp.1-32 (in Turkish).

19. Özbek, T.(1995):Termal Turizmde Ankara, TC Ankara Valiliği, İl Turizm Müdürlüğü yayınları, Ankara.

20. Özbek, T. (1989); Interpretation of Ankara-Kızılcahamam geothermal area. Seminar on New Devolopments in Goethermal Energy. United Nations Economic Commission for Europe. Ankara-Turkey..

21. Keskin, B. (1979) "Kızılcahamam Seyhamamı Bölgesinin Jeolojisi ve Jeotermal Enerji Olanakları", MTA, Ankara

22. Toker, M ve Durak S. (1990) "Kızılcahamam KHD-1 ve MTA-1 Kuyuları Test Raporu" MTA Ankara.

23. Koçak, A. (1989) "Kızılcahamam Kaplıcası Hidrojeoloji Etüdü", MTA Rap. No 8565, MTA, Ankara.

24. Ünlü R.M., ve Erişen B. (1980) "Ankara-Çubuk-Kızılcahamam-Kazan Alanının Jeolojisi ve Jeotermal Enerji Olanakları", MTA, Ankara.

25. Gevrek A.İ. (1989) "Ankara-Kızılcahamam Jeotermal Alanı Gradyan Sondajlarının (MTA-2, MTA-3, MTA-4, MTA-5, MTA-6) Kuyu Bitirme Raporu", MTA Rap No 8749, MTA, Ankara.

26. Ülker, İ. (1994); Sağlık turizmi, kaynaklar, planlama, tanıtım. Turizm bakanlığı yayını, Yorum matbaası, Ankara.

27. Akin, S.:"Analysis of Tracer Tests with Simple Spreadsheet Models" Computers
& Geosciences, 27, 2, 171-178, 2001.

28. Fossum, M.P. and Horne, R.N. 1982, Interpretation of tracer return profiles at Wairakei geothermal field using fracture analysis. Geothermal Resources Council, Transactions, (6), 261-264.

29. Bullivant, D.P. and O'Sullivan, M.J. 1989. Matching a field tracer test with some simple models. Water Resources Research, 25 (8), 1879-1891.

30. Sauty, J.P. 1980. An analysis of hydrodispersive transfer in aquifers. Water Resources Research, 6 (1), 145-158.

31. Kilpatrick ,F.A.,1993.Simulation of Soluble Waste Transport and Buildup in Surface Waters Using Tracers. Tech.Rep.Techniques of Water-Resources Investigations, Book 3,Chapter A20,37 p.,U.S.Geological Survey.

32. Field MS. A review of some tracer-test design equations for tracer-mass estimation and sample-collection frequency. ENVIRON GEOL 43 (8): 867-881 APR 2003.

33. Kilpatrick, F.A., Wilson,JR.,J.F., 1989. Measurement of Time of Travel in Streams by Dye Tracing Techniques. Rep.27 Techniques of Water-Resources Investigations of the U.S. Geological Survey,Book 3,Chapter A9,27 p.,U.S.Geological Survey.

34. Fylstra D, Lasdon L, Watson J, and Waren A. 1998. Design and use of the Microsoft Excel Solver. Interfaces 28: (5) 29-55.

35. Akin, S., and Demiral, B. 1998. Genetic algorithm for estimating relative permeabilities from displacement experiments. Computers & Geosciences, 24 (3), 251-258.

36. Güleç,N 1993. Geochemistry of thermal waters and its relation to the volcanism in the Kızılcahamam (Ankara) area, Turkey. Journal of Volcanology and Geothermal Research, 59 (1994) 295-312

37. Erol, O.1955. Köroğlu Işıkdağları volkanik kütlesinin orta bölümleri ile Beypazarı- Ayaş arasındaki Neojen havzasının jeolojisi hakkında rapor(in Turkish).MTA Report No:2299.

38. Gevrek,A.I and Aydın,S.N., 1988 Hydrothermal alteration studies in Kızılcahamam (Ankara) geothermal field and its evaluation on the development of this field .Proc. Int. Mediterranean Congress on Solar and Other New-Renewable Energy Resources 14-19 November, Antalya pp 609-616.

39. Kurtman, F., Samilgil,E. 1975 Geothermal Energy Possibilities, their exploration and evaluation in Turkey. Proc. Second U.N. Symposium on Geothermal Resources, San Francisco ,CA, PP 447-457

40. Simsek, S. and Okandan E., 1990 Geothermal Energy Development in Turkey, Geothermal Resources Council Trans.,14:257-266

APPENDIX A

TRACER-TEST DESIGN PROGRAM

```
*****************************************************************
*                                *
*          TRACER-TEST DESIGN PROGRAM            *
*          ------------------------         *
*                                *
*        LAST MODIFIED:        APRIL 03 2003    *
*                                *
*  EQUILIBRIUM MODEL FOR ROOTS AND NONLINEAR OPTIMIZATION    *
*  FOR TRACER MASS, TRACER RETARDATION, TRACER DECAY, INITIAL  *
*  SAMPLE COLLECTION TIME, AND SUBSEQUENT SAMPLING FREQUENCY   *
*                                *
*          MALCOLM S. FIELD            *
*          USEPA -- NCEA-W            *
*          WASHINGTON, DC  20460            *
*                                *
*                                *
*  DATA INPUT FILE:  khamam1.dat            *
*                                *
*****************************************************************
                INPUT DATA
          ==================================


       ALL DATA ARE IN "CONSISTENT UNITS"

         LENGTH [L]  (m)
         TIME  [T]  (h)
         CONC.  [M/T] (mg/m^3 = μg/L)
          ==================================

         PROJECT NAME AND TRACER-TEST CONDITIONS
====================================================================

            PROJECT NAME
     --------------------------------------------------
     KIZILCAHAMAM TRACER TEST DESIGN
-----------------------------------------------------------------
 FLOW TYPE    STATIONS    RELEASE MODE   RELEASE TIME
                    (h)
-----------------------------------------------------------------

   5      1     PULSE     4.0000E+00

RECIRCULATION TRACER TEST --- INJECTION/WITHDRAWAL WELLS
```

```
* STATION: MTA-1                          *
*                                *
*********************************************************************
```

TABLE 1.1. INPUT FACTORS THAT INFLUENCE TRACER-MASS ESTIMATION
===

MEASURED PARAMETERS OF INFLUENCE

DISCHARGE (m^3/h)	POROSITY (m)	THICKNESS (m)	X-DIST (m)	Y-DIST
1.4400E+02	8.00E-02	5.00E+01	1.00E+02	0.00E+00

INITIAL CONCENTRATION AND PRODUCTION PARAMTERS

INITIAL CONCENTRATION (µg/L = mg/m^3)	GAMMA1 (dimen.)	GAMMA2 (dimen.)
0.0000E+00	0.00E+00	0.00E+00

TRACER-REACTION FACTORS OF INFLUENCE

FACTOR	VALUE	LOWER BOUND	UPPER BOUND	ADJUSTABLE
RETARDATION	1.1000E+00	0.0000E+00	0.0000E+00	0
DECAY (1/h)	2.0000E-04	0.0000E+00	0.0000E+00	0

SET AVERAGE CONCENTRATION
(µg/L = mg/m^3)

2.50E+01
===

TRANSVERSE DISTANCE SET EQUAL TO 0.0 (DIST-Y = 0.0000E+00)

VELOCITY CALCULATED BY: [3.0 × DISCHARGE/(DISTANCE × THICKNESS × PI × POROSITY)]

VOLUME CALCULATED BY: [DISTANCE × PI × (THICKNESS/2)^2]

OPTIMIZATION RECOMMENDED FOR MODELING POROUS-MEDIA FLOW

WHEN RETARDATION > 1.0 OR DECAY > 0.0

OUTPUT DATA

ALL DATA ARE IN "CONSISTENT UNITS"

```
LENGTH [L]   (m)
TIME   [T]   (h)
CONC.  [M/T] (mg/m^3 = μg/L)
MASS   [M]   (mg, g, kg)
         =================================
```

TABLE 2.1.1. INITIAL ESTIMATED HYDRAULIC FACTORS
(NON-REACTIVE TRANSPORT = WATER)
===

ESTIMATED STATISTICAL TIMES OF TRAVEL

```
AVERAGE TIME   AVERAGE TIME   AVERAGE TIME    PEAK TIME
(INI. EST.)    (ADJ. EST.)     VARIANCE     (INI. EST.)
   (h)            (h)           (h^2)           (h)
---------------------------------------------------------------

 2.9089E+02     1.0137E+03     1.4398E+05     4.3633E+02
             |_____|   |_____|
                  |_____|
```

ESTIMATED TRANSPORT VELOCITIES AND DISCHARGE VOLUME

```
AVE. VELOCITY   AVE. VELOCITY   PEAK VELOCITY   SYSTEM VOLUME
 (INI. EST.)     (ADJ. EST.)     (INI. EST.)     (INI. EST.)
   (m/h)           (m/h)           (m/h)           (m^3)
---------------------------------------------------------------

 3.4377E-01      1.1586E-01      2.2918E-01      1.2566E+05
---------------------------------------------------------------
```

ESTIMATED DISPERSION PARAMETERS

```
 DISPERSION    PECLET NUMBER    DISPERSIVITY
  (m^2/h)        (DIMEN.)           (m)
---------------------------------------------------------------

 1.1196E+00     3.0704E+01      3.2569E+00
```
===

TABLE 2.1.2. FINAL ESTIMATED HYDRAULIC FACTORS WITH RETARDATION
(REACTIVE TRANSPORT: Rd = 1.10E+00
μ = 2.00E-04 1/h)
===

ESTIMATED STATISTICAL TIMES OF TRAVEL

```
 AVERAGE TIME     TIME VARIANCE     PEAK TIME
    (h)              (h^2)             (h)

 2.9089E+02       1.4398E+05       1.7453E+03
```

ESTIMATED TRANSPORT VELOCITIES AND DISCHARGE VOLUME

AVE. VELOCITY	PEAK VELOCITY
(m/h)	(m/h)
3.4377E-01	5.7296E-02

ESTIMATED DISPERSION PARAMETERS

| DISPERSION | PECLET NUMBER | DISPERSIVITY |
(m^2/h)	(DIMEN.)	(m)
1.1196E+00	3.0704E+01	3.2569E+00

===

RETARDATION EFFECT EQUIVALENT TO TRAVEL TIMES MULTIPLIED BY 1.10E+00

RETARDATION EFFECT EQUIVALENT TO TRANSPORT VELOCITY DIVIDED BY 1.10E+00

RETARDATION EFFECT EQUIVALENT TO DISPERSION DIVIDED BY 1.10E+00

TABLE 3.1. FINAL TRACER-MASS ESTIMATE CALCULATIONS
===

TRACER-MASS ESTIMATES

| TRACER MASS | TRACER MASS | TRACER MASS | TRACER MASS |
| (INI. EST.) | (ADJ. EST.) | (REA. EST.) | (FIN. EST.) |
(g)	(g)	(g)	(g)
3.6049E+03	1.5288E+03	---	1.5288E+03
ERROR CODE =>	2		2

FINAL TRACER-MASS REDUCTION FACTORS

| SYSTEM VOL. | DILUTION VOL. | RETARDATION | DECAY |
(m^3)	(m^3)	(DIMEN.)	(1/h)
4.6077E+04	9.2153E+04	1.1000E+00	2.0000E-04

TRACER CONCENTRATIONS

| SET CONC. | AVERAGE CONC. | PEAK CONC. |
(μg/L)	(μg/L)	(μg/L)
2.50E+01	2.5000E+01	1.5828E+01

94

TABLE 4.1. ESTIMATED SAMPLING FREQUENCY

==

SAMPLING TIME INTERVAL

EXACT (d)	CONVENIENT (d)

| 1.2499E+00 | 1. |

RECOMMENDED SAMPLING TIMES SINCE TRACER RELEASE

SAMPLE NUMBER	EXACT (d)	CONVENIENT (d)

1	2.4998E+00	2.
2	3.7497E+00	4.
3	4.9996E+00	5.
4	6.2496E+00	6.
5	7.4995E+00	7.
6	8.7494E+00	9.
7	9.9993E+00	10.
8	1.1249E+01	11.
9	1.2499E+01	12.
10	1.3749E+01	14.
11	1.4999E+01	15.
12	1.6249E+01	16.
13	1.7499E+01	17.
14	1.8749E+01	19.
15	1.9999E+01	20.
16	2.1248E+01	21.
17	2.2498E+01	22.
18	2.3748E+01	24.
19	2.4998E+01	25.
20	2.6248E+01	26.
21	2.7498E+01	27.
22	2.8748E+01	29.
23	2.9998E+01	30.
24	3.1248E+01	31.
25	3.2498E+01	32.
26	3.3748E+01	34.
27	3.4997E+01	35.
28	3.6247E+01	36.
29	3.7497E+01	37.
30	3.8747E+01	39.
31	3.9997E+01	40.
32	4.1247E+01	41.
33	4.2497E+01	42.
34	4.3747E+01	44.
35	4.4997E+01	45.
36	4.6247E+01	46.

37	4.7497E+01	47.
38	4.8746E+01	49.
39	4.9996E+01	50.
40	5.1246E+01	51.
41	5.2496E+01	52.
42	5.3746E+01	54.
43	5.4996E+01	55.
44	5.6246E+01	56.
45	5.7496E+01	57.
46	5.8746E+01	59.
47	5.9996E+01	60.
48	6.1246E+01	61.
49	6.2495E+01	62.
50	6.3745E+01	64.
51	6.4995E+01	65.
52	6.6245E+01	66.
53	6.7495E+01	67.
54	6.8745E+01	69.
55	6.9995E+01	70.
56	7.1245E+01	71.
57	7.2495E+01	72.
58	7.3745E+01	74.
59	7.4995E+01	75.
60	7.6244E+01	76.
61	7.7494E+01	77.
62	7.8744E+01	79.
63	7.9994E+01	80.
64	8.1244E+01	81.

```
*****************************************************************
*                                    *
*   CALCULATED TRACER-MASS:        1.529E+00 kg         *
*                                    *
*                  1.529E+03  g        *
*                                    *
*                  1.529E+06 mg          *
*                                    *
*****************************************************************
*                                    *
*   RECOMMENDED TRACER-MASS:       1.529E+00 kg         *
*                                    *
*                  1.529E+03  g        *
*                                    *
*                  1.529E+06 mg          *
*                                    *
*                                    *
*                                    *
*   INJECTION CONCENTRATION:      2.654E+03 mg/m^3       *
*                                    *
*   INJECTION VOLUME:        5.760E+02 m^3        *
*                                    *
*   INJECTION RATE:         1.440E+02 m^3/h       *
*                                    *
*****************************************************************
```

TRACER-TEST DESIGN PROGRAM RESULTS AS OF: 10/16/2004
10:49:58:71 am

Table B-1 Fethi Bey Well Matching Tracer Test Data With Some Simple Models

Multi Fracture Model - Fossum & Horne 1982			
Experiment	Fethi Bey		
	Derived Values		
m_1=	5728674,9	**D_{tr3}=**	71,643749
m_2=	12949765	**u_1=**	9,9192184
m_3=	19399,078	**u_2=**	0,428863
D_{tr1}=	56,18915	**u_3=**	2,7226454
D_{tr2}=	31,516755		
	Fracture 1	**Fracture 2**	**Fracture 3**
w=	70,61	5,44	15,20
L=	7425,20	968,97	6,11
t_m=	40,33	932,70	146,92
e=	0,01	0,18	0,81-1,00
q=	144	**R=**	400,00
Input Data		Optimized Parameters	S=888,4748
Time (hrs)	Cexp (ppb)	C_{model} (ppb)	(Canal-Cexp)²
0,001	0	0,00	0
48	10,7	10,70	8,30777E-07
60	0,92	0,90	0,000553595
72	0	0,34	0,114993183
84	0,87	0,56	0,096293663
96	0,52	0,78	0,065799294
108	0,17	0,93	0,578322331
120	2,73	1,03	2,902201117
132	0,36	1,10	0,543916766
144	2,83	1,19	2,702367407
156	0,05	1,33	1,639790267
168	0,34	1,56	1,484802297
180	1,68	1,89	0,042255214
192	1,55	2,32	0,586896682
204	2,24	2,85	0,367068318

Table B-1 (continued)

Input Data		Optimized Parameters	
Time (hrs)	Cexp (ppb)	C_{model} (ppb)	(Canal-Cexp)² S=
216	3,18	3,46	0,080954623
228	6,64	4,16	6,160303664
240	9,14	4,91	17,88960027
252	2,97	5,71	7,482236816
264	3,01	6,53	12,37072084
276	21,17	7,36	190,6779857
288	4,82	8,19	11,39034471
300	5,8	9,02	10,3474339
312	5,52	9,82	18,46682886
324	9,97	10,59	0,383061258
336	7,4	11,33	15,40909812
348	7,69	12,02	18,76759992
360	10,35	12,68	5,408497972
372	17,73	13,28	19,77165974
384	9,54	13,84	18,52692243
396	9,41	14,36	24,47744083
408	17,57	14,82	7,545845187
420	17,4	15,24	4,658930423
432	17,62	15,61	4,023994279
444	17,2	15,94	1,583156088
456	17,62	16,23	1,942109463
468	17,46	16,47	0,980657774
480	17,36	16,67	0,471099196
492	17,51	16,84	0,448679796
504	17,3	16,97	0,107993214
516	17,57	17,07	0,250646132
528	17,57	17,14	0,188206042
540	17,46	17,17	0,081864712
552	17,51	17,18	0,105964263
564	17,51	17,17	0,115658402
576	17,46	17,13	0,10754091
588	17,51	17,07	0,191197717
600	17,41	16,99	0,173339773
612	17,46	16,90	0,317562371
624	17,51	16,78	0,528901669
636	17,41	16,65	0,571611545

Table B-1 (continued)

Input Data		Optimized Parameters	
Time (hrs)	Cexp (ppb)	C_{model} (ppb)	(Canal-Cexp)² S=
708	17,3	15,64	2,763884557
648	17,36	16,51	0,7199706
660	17,3	16,36	0,889858308
672	17,36	16,19	1,367145731
684	17,25	16,01	1,525552165
696	17,36	15,83	2,340547747
720	17,09	15,44	2,729145799
732	17,09	15,23	3,450536511
744	17,09	15,02	4,277960052
756	18,1	14,81	10,84737967
768	17,09	14,59	6,262491438
780	17,2	14,37	8,034699016
792	17,14	14,14	8,994638607
804	17,04	13,91	9,769357379
816	8,94	13,69	22,52911719
828	9,57	13,46	15,11351003
840	17,2	13,23	15,77511388
852	9,29	13,00	13,75432292
864	9,35	12,77	11,6922129
876	9,15	12,54	11,4965637
888	8,69	12,31	13,12464536
900	8,36	12,09	13,88361938
912	8,69	11,86	10,05359312
924	8,36	11,64	10,73887378
936	9,12	11,42	5,267584263
948	9,1	11,20	4,389955473
960	8	10,98	8,865425311
972	8,51	10,76	5,071778498
984	7,96	10,55	6,703311435
996	8,83	10,34	2,276007936
1008	8,33	10,13	3,243127691
1020	8,39	9,93	2,358791275
1032	7,92	9,72	3,253050466
1044	7,86	9,52	2,769863685
1056	8,45	9,33	0,770705049
1068	7,86	9,13	1,624321629

Table B-1 (continued)

Input Data		Optimized Parameters	
Time (hrs)	Cexp (ppb)	C_{model} (ppb)	(Canal-Cexp)² S=
1080	8,47	8,94	0,2247703
1092	9,91	8,76	1,329965024
1104	7,91	8,57	0,43889113
1116	7,63	8,39	0,57958278
1128	7,48	8,21	0,53759969
1140	7,86	8,04	0,031761447
1164	7,65	7,70	0,002256909
1188	7,06	7,37	0,095544809
1212	7,42	7,05	0,134780016
1236	7	6,75	0,063179543
1260	6,63	6,46	0,030210844
1284	7,05	6,18	0,765187643
1308	6,39	5,91	0,234689392
1332	6,4	5,65	0,56731736
1356	5,78	5,40	0,145417099
1380	5,84	5,16	0,461266008
1404	5,34	4,93	0,16566939
1428	5,61	4,71	0,801470288
1452	5,77	4,51	1,598131636
1476	5,18	4,31	0,764103578
1500	6,23	4,11	4,475144489
1524	17,94	3,93	196,2372283
1548	5,35	3,76	2,539241854
1572	4,95	3,59	1,851935501
1596	4,71	3,43	1,640583405
1620	4,95	3,28	2,80154577
1644	4,58	3,13	2,102317419
1668	4,34	2,99	1,821420787
1692	4,9	2,86	4,174031404

Table B-2 MTA-2 Well Matching Tracer Test Data With Some Simple Models

Multi Fracture Model - Fossum & Horne 1982			
Kızılcahamam:	MTA 2		
	Derived Values		
m_1=	395,12757	D_{tr3}=	5,6615403
m_2=	11242243	u_1=	0,6488093
m_3=	362131,75	u_2=	0,0480317
D_{tr1}=	0,3822742	u_3=	0,3336025
D_{tr2}=	0,9979092		
	Fracture 1	**Fracture 2**	**Fracture 3**
w=	50,9171	1,4440	1,7677
L=	0,4061	529,4654	49,7315
t_m=	46,2386	624,5881	89,9274
e=	0,0743	0,0957	0,8300-1,00
q=	144	R=	30,00
Input Data		Optimized Parameters S=278,44124	
Time (hrs)	Cexp (ppb)	C_{model} (ppb)	(Canal-Cexp)²
0,001	0	0,00	0
4	0	0,11	0,10664535
8	1,9	5,31	3,41272484
12	8,9	14,85	5,952394879
16	21,65	21,65	1,41028E-05
20	25,04	24,98	0,060212661
24	26,26	26,02	0,239663203
28	23,72	25,84	2,116655749
32	23,45	25,11	1,664077513
36	26,47	24,24	2,230860065
40	23,19	23,41	0,215664527
44	22,97	22,70	0,274772454
48	22,18	22,13	0,050636399
52	21,7	21,70	3,07939E-06
56	21,33	21,39	0,056206847
60	21,22	21,16	0,056807306
64	20,85	21,01	0,157044577
76	33,1	20,75	12,34993638
80	20,69	20,69	4,18123E-05
84	20,38	20,63	0,248074138
88	20,22	20,56	0,339317909

Table B-2 (continued)

Input	Data	Optimized	Parameters
Time (hrs)	Cexp (ppb)	C_{model} (ppb)	Time (hrs)
92	20,01	20,48	0,470322904
96	20,22	20,39	0,169042977
100	19,95	20,28	0,33442166
104	19,26	20,17	0,90612909
108	20,43	20,03	0,395643696
112	19,26	19,89	0,629656593
116	19,16	19,73	0,572824652
120	19,16	19,56	0,40480566
124	19,16	19,39	0,226627742
128	19,69	19,20	0,490647435
132	18,73	19,00	0,27403985
136	18,84	18,80	0,038277502
140	17,25	18,59	1,343389735
144	18,89	18,38	0,510023734
148	21,12	18,16	2,957644109
152	18,2	17,94	0,258661601
156	18,52	17,72	0,802331191
160	17,67	17,49	0,177971696
164	17,78	17,27	0,514963696
168	19,74	17,04	2,702746688
172	19,05	16,81	2,240815775
176	17,94	16,58	1,358718088
180	18,04	16,35	1,686049111
184	17,62	16,13	1,492449007
188	17,62	15,90	1,717599034
192	17,89	15,68	2,211218098
196	17,99	15,46	2,53305948
200	19,95	15,24	4,71290775
204	18,2	15,02	3,180575893
208	17,94	14,80	3,135902627
212	17,78	14,59	3,188749939
216	17,78	14,38	3,399000801
220	17,67	14,17	3,496557089
224	18,1	13,97	4,131337668
228	17,83	13,77	4,063276649
232	17,46	13,57	3,8923218

102

Table B-2 (continued)

Input	Data	Optimized	Parameters
Time (hrs)	Cexp (ppb)	C_{model} (ppb)	Time (hrs)
236	17,36	13,37	3,988433104
248	17,62	12,80	4,818920233
252	17,25	12,62	4,633096803
256	17,57	12,44	5,13428079
260	17,57	12,26	5,312481844
264	16,25	12,08	4,167714885
268	11,91	11,91	5,45129E-07
272	11,4	11,74	0,340640871
276	10,55	11,57	1,024179001
280	11,15	11,41	0,260584804
284	10,61	11,25	0,639825529
288	11	11,09	0,091866188
292	10,55	10,94	0,3866699
296	11	10,78	0,215801812
300	9,86	10,63	0,774411265
304	10,42	10,49	0,067268269
308	10,42	10,34	0,077272513
312	11,89	10,20	1,689253451
316	7,45	10,06	2,611282603
320	7,29	9,92	2,634292467
324	3,58	9,79	6,209732772
328	9,09	9,66	0,567560076
332	8,41	9,53	1,117730981
336	8,14	9,40	1,26020222
340	7,97	9,27	1,304930746
344	5,36	9,15	3,791873803
348	5,77	9,03	3,26098899
352	5,67	8,91	3,24223432
356	7,42	8,80	1,375568264
360		8,68	8,680949794
364	6,41	8,57	2,15833842
368	5,56	8,46	2,89769422
372	4,36	8,35	3,988977862
376	5,5	8,24	2,742150629
380	5,53	8,14	2,607174434
384	5,91	8,03	2,124011835

Table B-2 (continued)

Input	Data	Optimized	Parameters
Time (hrs)	Cexp (ppb)	C_{model} (ppb)	Time (hrs)
388	5,93	7,93	2,002626041
392	7,17	7,83	0,662980926
396	6,7	7,74	1,035041029
400	5,38	7,64	2,25877156
404	5,66	7,54	1,884138399
408	4,34	7,45	3,111108097
420	5,48	7,18	1,701309846
424	5,33	7,09	1,764369784
428	6,64	7,01	0,368875263
432	5,12	6,92	1,804796767
436	5,63	6,84	1,21210541
440	6,09	6,76	0,670772929
444	4,82	6,68	1,860771676
448	6,18	6,60	0,422074604
452	5,61	6,52	0,914655263
456	6,16	6,45	0,288487785
460	6,25	6,37	0,123546877
464	6,16	6,30	0,139807808
468	3,99	6,23	2,237246399
472	3,63	6,16	2,525839013
476	5,23	6,09	0,855562543
480	5,48	6,02	0,536394404
484	7,49	5,95	1,541687482
488	7,18	5,88	1,298704694
492	7,28	5,82	1,464678324
496	7,43	5,75	1,679628986
500	5,8	5,69	0,113576829
504	5,79	5,62	0,166541544
508	7,44	5,56	1,878542377
512	4,9	5,50	0,60040186
516	5,02	5,44	0,420272784
520	5,3	5,38	0,081052425
524	4,35	5,32	0,97272322
528	4,35	5,27	0,915268003
532	4,52	5,21	0,688669996
536	4,25	5,15	0,902912796

Table B-2 (continued)

Input	Data	Optimized	Parameters
Time (hrs)	Cexp (ppb)	C_{model} (ppb)	Time (hrs)
540	5,02	5,10	0,077980373
544	4,28	5,04	0,763857055
548	4,9	4,99	0,090527522
552	4,74	4,94	0,197976798
556	7,13	4,89	2,243809759
560	4,72	4,84	0,115153536
564	4,4	4,78	0,384852688
568	5,29	4,74	0,554725988
572	4,62	4,69	0,066404127
576	4,65	4,64	0,011770052
580	4,8	4,59	0,20926132
584	4,91	4,54	0,366082192
588	4,7	4,50	0,202244906
592	4,4	4,45	0,052238568
596	4,44	4,41	0,03264348
600	4,34	4,36	0,023097499
604	4,37	4,32	0,0505497
608	4,87	4,28	0,593596038
612	4,76	4,23	0,526052238
616	4,38	4,19	0,187928793
620	4,36	4,15	0,209235968
624	4,24	4,11	0,12998381
628	4,92	4,07	0,85018215
632	4,28	4,03	0,24984061
636	3,36	3,99	0,631031394
640	4,44	3,95	0,487575355
644	4,36	3,91	0,44566988
648	4,22	3,88	0,343261013
652	4,29	3,84	0,450357401
656	3,96	3,80	0,156967508
660	4,06	3,77	0,293099625
664	3,87	3,73	0,138761866
668	3,81	3,70	0,113962181
672	3,3	3,66	0,361291648
676	3,83	3,63	0,203008003
680	8,31	3,59	4,716868601

Table B-2 (continued)

Input	Data	Optimized	Parameters
Time (hrs)	Cexp (ppb)	C$_{model}$ (ppb)	Time (hrs)
684	3,74	3,56	0,180297458
688	3,87	3,53	0,343301739
692	3,37	3,49	0,124111537
696	3,59	3,46	0,128064506
700	3,52	3,43	0,089836605
704	3,54	3,40	0,141211362
708	3,44	3,37	0,072195246
712	3,51	3,34	0,172794597
716	3,36	3,31	0,053015627
720	3,27	3,28	0,007135574
724	3,33	3,25	0,082346964
728		3,22	3,218530908
732	2,57	3,19	0,619763454
744	2,58	3,11	0,525533447
756	2,59	3,02	0,434299514
768	2,32	2,95	0,625923928
780	2,6	2,87	0,270276723
792	2,18	2,80	0,617235183
804	2,69	2,73	0,03668337
816	2,22	2,66	0,438511684
828	2,24	2,59	0,352616458
840	2,23	2,53	0,298899579
852		2,47	2,46726814
864		2,41	2,407634114
876		2,35	2,349914053
888		2,29	2,294028804
900	2,33	2,24	0,09009675
912	2,64	2,19	0,452533931
924	2,31	2,14	0,173350496
936	2,13	2,09	0,042610849
948	1,77	2,04	0,269623768
960	2,12	1,99	0,126704914
972	2,09	1,95	0,141652361
984	2,06	1,90	0,155271395
996	2,13	1,86	0,267612345
1008	2,07	1,82	0,248723183

Table B-2 (continued)

Input	Data	Optimized	Parameters
Time (hrs)	Cexp (ppb)	C_{model} (ppb)	Time (hrs)
1020	2,1	1,78	0,318649662
1032	2,08	1,74	0,337435431
1044	1,85	1,70	0,145122155
1056	1,77	1,67	0,101749621
1068	1,9	1,63	0,267355835
1080	1,9	1,60	0,301977124
1092	2,01	1,56	0,445648219
1104	1,77	1,53	0,238402338
1116	1,98	1,50	0,48027127
1128	1,67	1,47	0,201285442
1140	1,67	1,44	0,231473992
1152	1,78	1,41	0,370864836
1164	1,7	1,38	0,319484723
1176	1,8	1,35	0,447359298
1188	1,71	1,33	0,384513156
1200	1,54	1,30	0,240969891
1212	1,48	1,27	0,206752147
1224	1,58	1,25	0,331881662
1236	1,84	1,22	0,616379312
1248	1,71	1,20	0,510265153
1260	1,73	1,18	0,553558455
1272	1,59	1,15	0,436277744